Author Manuscript
Author Manuscript
Author Manuscript
Author Manuscript

HHS Public Access
Author manuscript
Curr Med Chem. Author manuscript; available in PMC 2017 September 01.

Published in final edited form as:
Curr Med Chem. 2016 ; 23(18): 1818–1869.

Considerations in the Development of Reversibly Binding PET Radioligands for Brain Imaging

Victor W. Pike*
Molecular Imaging Branch, National Institute of Mental Health, National Institutes of Health, Rm. B3C346A, 10 Center Drive, Bethesda, MD 20892, United States

Abstract

The development of reversibly binding radioligands for imaging brain proteins *in vivo*, such as enzymes, neurotransmitter transporters, receptors and ion channels, with positron emission tomography (PET) is keenly sought for biomedical studies of neuropsychiatric disorders and for drug discovery and development, but is recognized as being highly challenging at the medicinal chemistry level. This article aims to compile and discuss the main considerations to be taken into account by chemists embarking on programs of radioligand development for PET imaging of brain protein targets.

Keywords

PET; radioligand; molecular imaging; positron-emitter; carbon-11; fluorine-18; efflux transporter; blood-brain barrier

1. INTRODUCTION

A strong premise in modern medicine is that neurochemical dysfunctions underpin many neuropsychiatric disorders. Indeed, the majority of drugs that are available for treating such disorders exert their effects through binding to one or more proteins within the brain [1]. Targeted proteins are commonly neurotransmitter transporters, receptors, ion channels, or enzymes (Table 1). Few techniques are available for investigating brain disorders at the molecular level through measurement of specific protein-ligand or protein-drug interactions *in vivo*. Positron emission tomography (PET) and single photon emission computed tomography (SPECT) have unrivaled sensitivity for this purpose when used with biochemically-specific radioligands. Proteins present in brain at very low regional concentrations (~ nM) may be detected and measured, albeit with a spatial resolution that is

*Address correspondence to this author at the Molecular Imaging Branch, National Institute of Mental Health, National Institutes of Health, Rm. B3C346A, 10 Center Drive, Bethesda, MD 20892, USA; Tel.: 301 594 5986; Fax: 301 480 5112; pikev@mail.nih.gov.

DISCLAIMER
Although this article was written as part of Dr Pike's official duties as a government employee, the views expressed in this article do not necessarily represent those of NIMH, NIH, HHS, or the United States Government.

SUPPLEMENTARY MATERIALS
Supplementary material is available on the publisher's web site along with the published article.

CONFLICT OF INTEREST
The author confirms that this article has no conflict of interest.

Author Manuscript Author Manuscript Author Manuscript Author Manuscript

limited to a few millimeters. An ability to make such measurements allows the roles of brain proteins in the unfolding of neuropsychiatric disorders to be investigated [2–4]. Moreover, the interactions of drugs or experimental therapeutics with brain proteins may be assessed. Therefore, these molecular imaging techniques have become integral to CNS drug discovery and development programs [5–8], and are also important for monitoring the neurochemical effects of drug treatments or therapies [8].

Key to further exploiting the potential utility of SPECT and PET in neuropsychiatric research is the development of useful radioligands. Primarily, because of the requirement for facile entry from blood into brain (see Section 8), suitable radioligands are based on low molecular weight drug-like molecules. Radioligands for use with SPECT are mostly labeled with γ-emitting iodine-123 ($t_{1/2}$ = 13.2 h). Only rarely has technetium-99m ($t_{1/2}$ = 6.0 h) been applied with some success [9, 10]. Both iodine-123 and technetium-99m are available commercially. A radioligand for use with PET must be labeled with a positron-emitter, which is nearly always carbon-11 ($t_{1/2}$ = 20.4 min) or fluorine-18 ($t_{1/2}$ = 109.8 min). The short half-lives of these positron-emitters require that they are produced close to or at the site of use. Nowadays, dedicated biomedical cyclotrons are invariably used to produce these PET radionuclides, whereby they are obtained in very simple chemical forms, such as [^{11}C]carbon dioxide, [^{11}C]methane or [^{18}F]fluoride ion. Ensuing transformations of these radionuclide sources into radioligands for human use is complex and resource-demanding. PET is therefore more expensive and more logistically demanding than SPECT. However, PET has no need for physical collimation in order to achieve optimal spatial resolution, and therefore has far greater sensitivity for radiation detection than SPECT (Fig. 1). Moreover, small drug-like molecules offer more opportunities for labeling with either carbon-11 or fluorine-18 than with any of the heavier single γ-emitter options. PET, because of these advantages, has now emerged as far preferable to SPECT for brain molecular imaging.

Expansion of the biomedical scope of PET is primarily determined by the range of effective radiotracers that can become available. The development of PET radioligands for imaging proteins in brain is an especially challenging area, because the design of any single radioligand needs to satisfy a wide array of chemical, biochemical and pharmacological requirements. Over recent decades, the assorted properties to be sought in candidate PET radioligands for brain imaging have been surveyed occasionally, but at varying levels of detail [11–19]. This article revisits this topic taking into account new developments and findings, and is mainly intended to be a useful primer for chemists entering this research area. The following discussion is confined to radioligands that bind reversibly to their protein targets because these radioligands represent the vast majority in use for brain protein quantification. Nonetheless, the reader will readily appreciate that many of the considerations that apply to reversibly-binding PET radioligands apply just as well to SPECT and irreversible radioligands.

Author Manuscript Author Manuscript Author Manuscript Author Manuscript

2. PRINCIPLES UNDERLYING BRAIN PROTEIN MEASUREMENTS WITH REVERSIBLY BINDING PET RADIOLIGANDS

Fundamentally, PET has the capability to provide quantitative measures of radioactivity distribution in living subjects, ranging from small animals (*e.g.,* mouse, rat, cat, pig and dog) through to non-human primates (NHPs) and humans. Researchers in neurology and psychiatry aim to exploit this capability with suitable radioligands to derive *quantitative* information on the distribution of proteins of interest in living brain, and on how these distributions are changed in neuropsychiatric disorders, or by attempts at their treatment. Furthermore, drug developers can use target-specific radioligands to *measure* the extent of engagement of the target by established therapeutics or experimental drugs and so arrive at safe and effective dosage regimens in clinical practice or preceding clinical trials.

Before starting to discuss general considerations with regard to PET radioligand development, it is pertinent to provide a simple background on how reversibly binding radioligands serve to quantify the density of a specific brain protein of interest, since in turn this will start to define the properties that will be desirable in such radioligands. In reality, the derivation of output measures of protein density from PET imaging with reversibly binding radioligands constitutes a challenging scientific task - and one that remains an active area of methodological research. Readers are therefore directed to expert reviews of this area for more details [20, 21]. Here, only some of the bare essentials of major approaches to quantification of protein density are outlined as an aid to understanding the remainder of this article.

High-affinity reversible binding of a radioligand (R*) to a target protein (P) is at the foundation of the majority of PET methods for quantifying brain proteins (Equation 1).

$$\mathrm{R}*+\mathrm{P}\underset{k_{\mathrm{off}}}{\overset{k_{\mathrm{on}}}{\rightleftharpoons}}\mathrm{R}*\mathrm{P} \qquad \text{Equation 1}$$

The rate of protein-radioligand association, k_{on} is a second order rate constant having units of $nM^{-1}min^{-1}$, whereas the rate of dissociation k_{off} is a first order rate constant having units of min^{-1}. The equilibrium dissociation constant K_D is simply defined as k_{off}/k_{on}. Importantly, it should be noted that the K_D value of a ligand for binding to a particular protein actually corresponds to the concentration of radioligand needed to bind half the available concentration of protein. The inverse of K_D defines the strength of ligand binding, and in fact ligand affinity ($1/K_D$) relates to the Gibbs free energy of binding (ΔG^O) by Equation 2:

$$\Delta G^{O}=-RT\ln K_{\mathrm{D}} \qquad \text{Equation 2}$$

in which R is the gas constant and T is the absolute temperature. According to this relationship a radioligand with a K_D of 1 nM for a target protein has a binding energy of 53

Author Manuscript Author Manuscript Author Manuscript Author Manuscript

kJ/mol, which is much lower than that of a typical covalent bond (*e.g.,* ~ 430 kJ/mol for a C-H bond).

For brain protein imaging with PET to be successful, the concentration of bound radioligand ([R*P]) will clearly need to be high relative to unbound radioligand concentration [R*], which implies that numerically k_{on} should be high and k_{off} relatively low. Consequently, successful PET radioligands usually have affinities represented by K_D in the low nM or, in some cases, sub-nM range.

The concentration of the target protein, often called B_{max}, is a further vital consideration. Application of the Law of Mass Action to the simple theoretical equilibrium shown in Equation 1 can be used to derive Equation 3, which relates the concentration of bound protein B to both B_{max} and K_D.

$$B=([\mathrm{R}*]\times B_{\max})/(K_{\mathrm{D}}+[\mathrm{R}*]) \quad \text{Equation 3}$$

[R*] represents the concentration of free radioligand, which includes any non-radioactive counterpart, known as *carrier*. As [R*] increases, B asymptotically approaches B_{max}. However, under conditions where [R*] is much less than K_D, Equation 3 approximates to:

$$B=([\mathrm{R}*]\times B_{\max})/K_{\mathrm{D}} \quad \text{Equation 4}$$

If the ratio of B to free radioligand concentration ([R*]) under these conditions is defined as binding potential (BP) [22], then:

$$BP=B/[\mathrm{R}*]=B_{\max}/K_{\mathrm{D}} \quad \text{Equation 5}$$

BP is seen to be the product of the target protein density (B_{max}) and the affinity ($1/K_D$) of the radioligand. Therefore, for radioactivity measured in brain with PET to be dominated by radioligand that is not free but specifically bound to target protein, B_{max} should well exceed the K_D of the radioligand when these are measured in the same units, typically chosen as nM. This is a very important guideline for a successful PET radioligand. Considerations surrounding this guideline are expanded on later (Section 5).

The preceding theoretical discussion pertains to radioligand binding to a target protein at equilibrium *in vitro*. In PET experiments, the conditions ([R*] $\ll K_D$) required for Equation 4 to be applicable are usually met with PET radioligands administered along with only low amounts of carrier *i.e.*, administered at high specific radioactivity, where specific radioactivity is the ratio of ligand radioactivity (Bq) to the total amount of ligand (radioactive plus non-radioactive; mol).

Some PET radioligands are administered intravenously by a bolus injection followed by constant infusion in order to achieve equilibrium conditions over the time-course of

Author Manuscript Author Manuscript Author Manuscript Author Manuscript

scanning. Under these conditions, one version of binding potential is simply the concentration of target-bound radioligand in the brain tissue of interest (C_S) divided by the total concentration of radioligand in blood plasma (free and bound to blood proteins) (C_P). By a quite recent expert consensus [23], this version is termed BP_P, with the subscript P denoting plasma. On the assumption that the K_D of the radioligand for binding to the target protein is constant across brain *in vivo*, BP_P gives a measure that is directly proportional to the target protein density *available in vivo*, known as B_{avail}. In most circumstances, B_{avail} will be less than the actual B_{max} value because *in vivo* protein targets are often partially occupied by their endogenous ligands and/or by other molecular entities, or may be only partially accessible to radioligand.

Other versions of BP pertaining to radioligand binding *in vivo* are BP_F and BP_{ND} [21, 23]. BP_F is the ratio at equilibrium of the brain receptor-bound radioligand concentration to that of *free* radioligand in brain tissue. The latter concentration at equilibrium is assumed to equal that which is free in plasma for a radioligand that only crosses the blood-brain barrier (BBB) by passive diffusion in either direction. Analogously, BP_{ND} is the ratio at equilibrium of receptor-bound radioligand concentration to that of *non-displaceable* radioligand concentration in tissue, where the non-displaceable radioligand is the sum of free and nonspecific components. BP_{ND} may be shown to relate to B_{avail}, the K_D of the radioligand *in vivo*, and f_{ND}, the fraction of free ligand in target-free tissue (the non-displaceable compartment) by the equation:

$$BP_{ND} = f_{ND} \times (B_{avail}/K_D) \quad \text{Equation 6}$$

The other two versions of binding potential are also directly proportional to B_{avail}/K_D, and are mathematically defined as follows:

$$BP_F = B_{avail}/K_D \quad \text{Equation 7}$$

$$BP_P = f_P \times (B_{avail}/K_D) \quad \text{Equation 8}$$

Equations 6–8 may be appreciated graphically in terms of radioligand distribution in blood and brain at equilibrium (Fig. 2).

An important assumption underlying measurement of any kind of binding potential is that the radioactivity measured in brain tissue with PET is composed solely of unchanged radioligand; that is without contamination by any radiometabolite. Experimental radioligands may fail to be useful if they generate radiometabolites in brain. The vast majority of PET radioligands are found to metabolize extensively in periphery (see Section 12). Except in some modeling approaches mentioned later, estimation of an output parameter, such as a binding potential, requires determination of the unchanged radioligand concentration in plasma. Analyses are usually performed by separating plasma from arterial

Author Manuscript Author Manuscript Author Manuscript Author Manuscript

blood, removal of proteins by precipitation, and finally chromatographic separation of parent radioligand from circulating radiometabolites. Methods avoiding need for precipitation of proteins from plasma have also been brought into recent practice.

Usually PET radioligands are administered as brief bolus injections, and the time-courses of radioactivity concentrations in brain regions are measured with PET. For many radioligands, the time-course of exposure of the brain to unchanged radioligand in plasma must also be determined, if quantitative output measures are to be obtained from a PET experiment. For this purpose, blood must be sampled at several time-points throughout the scanning period and analyzed for the concentration of unchanged radioligand in plasma to provide the 'metabolite-corrected arterial input function'. Compartmental modeling [20, 21] may then be applied to the PET and plasma data in order to derive output measures reflecting target protein densities. Mostly, two types of compartmental model are in use, a one-tissue compartmental model (1-TCM), in which brain is considered to be one compartment, and a two-tissue compartmental model (2-TCM) in which brain is considered to have kinetically distinguishable specific and non-displaceable compartments (Fig. 3).

In practice, an important output parameter is the total volume of distribution, V_T. Essentially, V_T is defined as the ratio of the concentration of the non-metabolized radioligand in the tissue of interest (C_T) to that in plasma at equilibrium (C_P), *i.e.*

$$V_T = C_T / C_P \quad \text{Equation 9}$$

For a 1-TCM, it follows that V_T also equals K_1/k_2.

V_T is derived from PET measurements that have a mm-order of spatial resolution. Consequently, each image voxel (volume element) contains radioligand that is: i) free in water space, ii) nonspecifically bound to tissue, and iii) specifically bound to the target protein. (In reality, each voxel also contains radioactivity in blood, but this is sometimes neglected, as blood accounts for only about 5% of human brain volume, or is otherwise accounted for by a fixed or fitted correction). Thus, V_T is the sum of three components, the volume of distribution of radioligand that is: i) free in tissue water (V_F), ii) nonspecifically bound (V_{NS}), and iii) specifically bound (V_S), *i.e.*

$$V_T = V_F + V_{NS} + V_S \quad \text{Equation 10}$$

Because only specifically bound radioligand can be displaced by a competing ligand, the sum of V_F and V_{NS} is termed the volume of distribution for 'non-displaceable' binding, V_{ND}, *i.e.*

$$V_T = V_{ND} + V_S \quad \text{Equation 11}$$

Author Manuscript Author Manuscript Author Manuscript Author Manuscript

V_{ND} is usually considered to be constant across brain. Thus, normally, both V_T and V_S reflect the available concentration of unbound target protein, B_{avail}. In fact, V_S is the *same* as BP_P. However, V_{ND} must be determined to obtain V_S. V_T has special importance as a useful output measure for PET studies when V_{ND} estimates are not easily accessible, as is often the case for human subjects. Clearly, radioligands that give high V_S in one or more target-rich regions relative to V_{ND}, and hence a high V_T value, are most sensitive to target protein density and will tend to be the most useful in practice. Thus, minimizing V_{ND} among a series of candidate PET radioligands can be a key component for achieving success in a search for an effective radioligand (see Section 11). It should be noted that with respect to a 2-TCM (Fig. 3), V_{ND} is simply the ratio of K_1 to k_2, *i.e.*

$$V_{ND}=K_1/k_2 \quad \text{Equation 12}$$

The binding potential most often measured with PET is BP_{ND}, which may be expressed in terms of volumes of distribution, as follows:

$$BP_{ND}=(V_T-V_{ND})/V_{ND}=(V_T-V_{ND})-1 \quad \text{Equation 13}$$

V_T/V_{ND} is sometimes called the distribution volume ratio or *DVR*, and hence:

$$BP_{ND}=DVR-1 \quad \text{Equation 14}$$

Measurement of a metabolite-corrected arterial input function requires arterial cannulation of the subject. Avoiding the need for arterial sampling is preferable, if possible, to reduce risk and, more importantly, to reduce resource requirements and simplify methodology. For a few radioligands, the radioligand concentration in blood may be followed with PET at the same time as brain imaging, to provide an ‘image-derived input function’ (IDIF). An example is [^{11}C](*R*)-rolipram [24], a slowly metabolized radioligand for the phosphodiesterase subtype-4 (PDE4) enzyme. Even so, IDIF still requires a few blood samples to be taken - to ‘calibrate’ the PET measurements on blood.

For certain radioligands, a sizeable region within the brain is known to be devoid of the target protein. Because V_{ND} is usually quite uniform across brain regions, uptake of radioactivity in this region may be taken to represent non-displaceable binding. This concept underpins useful approaches to quantification of target protein density with PET radioligands without the need for arterial cannulation, such as the ‘simplified reference tissue model’ (SRTM) [25, 26].

Other useful biomathematical approaches have also been developed for deriving quantitative output measures. These include the popular ‘Logan graphical analysis’, which also gives V_T as an output measure [27–29].

Author Manuscript Author Manuscript Author Manuscript Author Manuscript

Simultaneous PET measurements of both B_{avail} and K_D are possible. One approach is based on 'Scatchard analysis', as often performed *in vitro*. The radioligand is administered serially with different amounts of carrier to the same subject and the ratio of bound to free radioligand concentration is plotted against bound radioligand concentration. B_{avail} and K_D are given by the intercept on the X-axis, and the negative magnitude of the inverse of slope, respectively (Fig. **S1**). Such measurements have been performed with PET in rat [30], NHPs [31], and occasionally in human [32–34]. They are quite logistically demanding because of the necessity for more than one radioligand injection. Hence, only two injections are normally performed for this type of analysis. B_{avail} and K_D may also be determined from a single radioligand injection [35]. Generally, however, radioligand affinity is assumed to be constant *in vivo* and the V_T value, obtained from a single radioligand injection, is taken as the index of target density.

The foregoing discussion on the quantification of PET radioligand binding to brain proteins already alludes to the many properties to be sought in candidate radioligands, as highlighted in former reviews. These include a high ratio of target protein B_{avail} to radioligand K_D in target brain regions, selectivity for the target versus off-target sites, ability to penetrate the BBB following intravenous injection, low nonspecific binding, lack of brain-penetrant radiometabolites, and amenability to labeling with carbon-11 or fluorine-18. Subsequent sections of this article now expand discussion on these and other important considerations in PET radioligand development.

3. REGIONAL TARGET PROTEIN DENSITY

In any program aimed at developing a PET radioligand for a protein target that has not previously been imaged, prior knowledge of the expected concentration of the target is a primary concern. Based on Equation 6, the lower the target density (B_{avail}) the higher must be the affinity ($1/K_D$) of a radioligand for successful imaging to be possible.

A priori considerations are whether the imaging target is already expressed in normal human brain, and whether the density is expected to increase or decrease in one or more regions during the progression of a disease of interest. Most proteins that have been targeted for PET imaging have presence and function in normal brain; they include, for example, neurotransmitter transporters, receptors and enzymes. Through the use of PET radioligands, many of these targets have been found to show density changes in the progression of certain neuropsychiatric disorders [2]. Often, these changes are reductions in density rather than increases, and often they are relatively small. The direction of a small change may remain unclear, even after many PET studies as, for example, has been noted for serotonin subtype-1A (5-HT_{1A}) receptors in depression [36]. The development of higher-performing radioligands may help to resolve such lingering uncertainties, and presents an ongoing challenge to chemists within this field. Gender differences in protein density and also changes with age, usually a progressive decline, are not uncommon [2]. For some other protein targets, substantial increases in density over low basal levels occur with progression of disease. Prominent examples are Aβ plaque in Alzheimer's disease [37, 38] and the translocator protein 18-kDa (TSPO) in various neuroinflammatory disorders [39–42].

Author Manuscript Author Manuscript Author Manuscript Author Manuscript

A further consideration is that not all subjects may present the same version of the imaging target. In particular, recent studies of radioligands for imaging TSPO highlight how human genetic variation can be an important factor in PET radioligand performance and utility. Thus, the radioligand [^{11}C]PBR28 succeeds in imaging brain TSPO in only about 90% of human subjects of European ancestry [43]. The failure in 10% of subjects stems from a codominant rs6971 single nucleotide polymorphism (SNP) that causes a non-conservative threonine-to-alanine substitution at position 147 of TSPO protein [44, 45]. This SNP results in three subject groups: homozygous for threonine-147, homozygous for alanine-147, and heterozygous. The relative prevalence of these three groups is about 49: 9: 42 for subjects of Caucasian ancestry. TSPO having alanine in position 147 has very low affinity for PBR28 [46], and this explains why the approximately 10% of individuals that are homozygous for this SNP cannot be imaged with [^{11}C]PBR28 (Fig. 4). Heterozygous individuals do give PET images, but their binding potentials are effectively about half those of threonine-147 homozygous individuals [45]. The three groups are now dubbed high-affinity binders (HABs), low-affinity binders (LABs) and mixed-affinity binders (MABs), respectively. LABs are readily excluded from PET studies with [^{11}C]PBR28 by their inability to give an image of TSPO. However, if MABs are not excluded by genotyping, their presence may reduce the power of PET studies that compare TSPO in diseased and normal brain [45]. Many alternative TSPO radioligands, including those in other structural classes, show some genotype sensitivity and therefore have this issue in common with [^{11}C]PBR28 [47–49].

Considerable evidence exists for genotype sensitivity among radioligands for some other imaging targets, but as yet this evidence is not as comprehensive as for TSPO radioligands. Notably, Willeit and Praschak-Rieder [50] have reviewed the apparent influence of polymorphisms on radioligand binding to sites involved in brain monoaminergic neurotransmitter systems. They found strong evidence for the influence of the triallelic 5-HTTLPPR *LA* allele on increasing [^{11}C]DASB binding to the serotonin transporter (SERT), and also for the influence of the D2Ta11 A1allele carriers on decreasing the binding of [^{11}C]raclopride to dopamine D_2-like receptors.

Some protein targets are diffusely distributed across human brain, such as the PDE4 enzyme, the cannabinoid subtype-1 (CB_1) receptor, and the metabotropic glutamatergic subtype-5 (mGlu5) receptor. They provide no clear opportunity to use a single region as a target-devoid tissue in PET imaging with a convenient SRTM. Other protein targets, such as dopamine subtype-2 (D_2), serotonin subtype-1A (5-HT_{1A}) and μ-opiate receptors, and the dopamine transporter (DAT), are more discretely located in one or more sizeable brain regions, and do provide opportunities to apply SRTM. Thus, knowledge of human brain regional target distribution, if only qualitative, is valuable upon entering into a PET radioligand development program.

All too often information on target protein density in normal or diseased human brain is lacking or difficult to obtain. This may be because of a scarcity of suitable post mortem human brain tissue or an absence of a suitable radioligand for *in vitro* measurements, or both. Ideally, the target protein density across normal human brain regions will have been estimated ahead of PET radioligand development through quantitative brain autoradiography [51–55], or through a binding assay on brain tissue with a selective radioligand [56].

Author Manuscript Author Manuscript Author Manuscript Author Manuscript

Usually, such measurements are performed with radioligands having a high specific activity tritium or radioiodine label, but they are also sometimes feasible with a radioligand having a carbon-11 [54] or fluorine-18 [55] label.

Protein densities determined *in vitro* are often cited in units of fmol/g of brain tissue or fmol/mg of protein. For proposed radioligands, B_{max} values are usefully expressed in units of nM for direct estimation of the *in vitro BP* (*i.e.*, B_{max}/K_D) values. Generally, brain is assumed to contain 100 mg of protein per g of wet tissue [57], in which case 1 fmol/g of brain tissue simply equates to 1 nM and 1 fmol/mg protein to 0.1 nM. The range of normal human brain protein densities that has been imaged with PET spans more than two orders of magnitude, for example from about 0.5 nM for the $\alpha_4\beta_2$ subtype of nicotinic acetylcholine receptors ($\alpha_4\beta_2$nACh) receptors [58, 59] in cortex to over 150 nM for dopamine subtype-1 (D_1) receptors in striatum [60] (Table 2). Estimates of human protein target density are recognized to vary considerably with the type of measurement (*e.g.,* autoradiography *in vitro*, membrane assay *in vitro*, or PET) and the choice of radioligand [60]. Therefore, *in vitro* estimates of binding potentials that are to be expected from PET studies may not be reliable and must be treated cautiously.

Data on target protein distribution and regional densities are of course more readily accessible from animals than from human subjects. These data must also be used cautiously because major species differences may exist. Such variations should be considered in selecting animal species for the pre-clinical evaluation of prospective radioligands with PET. Ideally, a species with a target density similar to or greater than that in human would be chosen. For example, the density of mGlu5 receptors is much higher in rhesus monkey or human cerebellum than in rat cerebellum [75], and hence monkey is preferred over rat for the evaluation of experimental mGlu5 receptor radioligands. The density of TSPO in normal rhesus monkey brain is at least an order of magnitude higher than in normal human brain, and therefore PET signals obtained with [^{11}C]PBR28 in human are not as strong as those seen in monkey [80]. Nonetheless, rhesus monkey has regularly served as a useful animal model for the pre-clinical evaluation of candidate TSPO radioligands.

The form of the target protein that is possible to measure *in vitro* may not correspond to what is intended to be imaged *in vivo*. For example, consider targets that are G-protein-coupled receptors (GPCRs). Measurement of target density *in vitro* with an antagonist radioligand will measure the density of all available target receptors, regardless of the proportion that is present in the G-protein coupled state at any instant. This information will be most relevant to the development of PET radioligands that are themselves antagonists, but will be less relevant to the development of agonist radioligands intended to bind only to the sub-population of a GPCR target that is actually coupled to G-protein. Brain cryosections that are used for *in vitro* autoradiography represent a quasi-physiological environment, as do membranes and cells in binding assays [81]. Consequently, these techniques also offer opportunities for identifying proteins in active functional states, such as GPCRs interacting with second messenger systems. Clearly, wherever possible, the measurement of target density *in vitro* should be relevant to the form of the protein that is intended to be measured *in vivo* with PET. Other examples of situations in which this consideration would become relevant are in PET imaging of an open channel version of a precursor protein (*e.g.,* the open

Author Manuscript Author Manuscript Author Manuscript Author Manuscript

N-methyl-D-aspartate (NMDA) receptor). However, the expected prevalence of a sub-population of an imaging target relative to the full population is often uncertain because of the absence of *in vitro* estimates or because of difficulties in making such estimates.

In a few cases, the targeted binding site may only be truly accessible in post mortem brain tissue from human subjects. A pertinent example occurs in the development of radioligands intended to image Aβ plaques in AD. Notably, the use of artificial plaques generated *in vitro*, and also of plaques generated in transgenic rodents, frustrated early pre-clinical efforts to develop PET radioligands, because of the lack of correspondence in radioligand binding site architecture in these models to that in human brain [82].

A further consideration is that a single target protein may contain more than one type of radioligand binding site. Aβ plaques are again an important example; they present at least three distinct binding sites, which may be classed on the basis of their strong interactions with particular ligand types, namely Congo Red, thioflavin T and FDNNP [82]. Some GPCRs, such as mGlu5 receptors, and also ion channels, such as NMDA receptors, present allosteric as well as orthosteric binding sites, and, in principle, either may be exploited for PET quantification of the target protein.

GPCRs and many other proteins would be expected to have the same number of allosteric and orthosteric binding sites for antagonist radioligands. However, some proteins are known to offer different B_{max} values for different ligand classes. Aβ plaques are again a notable example [82].

Finally, radioligands that succeed for delineating protein distribution and density in autoradiography or in membrane assays will not necessarily succeed *in vivo* where confounding effects of poor delivery, metabolism and unacceptable nonspecific binding may readily occur. PET may be thought of as '*in vivo* autoradiography'. Radioligands that fail autoradiography *in vitro* are virtually certain to fail *in vivo*.

4. RADIOLIGAND AFFINITY

The foregoing discussion has already raised the importance of radioligand affinity for successful imaging of a protein target. By Equation 6 binding potential (BP_{ND}) is proportional to affinity ($1/K_D$). Estimates of ligand affinities for a particular protein are generally derived from an *in vitro* radioligand competition binding assay employing a reference radioligand, R*, that binds tightly but reversibly to the target protein. Essentially, the test ligand is incubated at different concentrations in the assay medium along with the radioligand and target protein. The binding of the radioligand to the protein is determined at equilibrium at each test ligand concentration, resulting in a competition binding curve (Fig. **S2**). Assays are designed to provide the protein in a particular biological matrix, which may be tissue homogenate, isolated membranes, or intact cells [81, 83]. Cells may be produced to over-express the target protein of interest to provide an adequate concentration for use in the assay. In many cases, the human target protein may be usefully expressed in such a manner. The radioligand is generally labeled in high specific activity with a β-emitting radionuclide, often tritium ($t_{1/2}$ = 12.32 y), but sometimes radioiodine (*e.g.,* ^{125}I; $t_{1/2}$ = 59.4 d).

Author Manuscript Author Manuscript Author Manuscript Author Manuscript

Occasionally, a radioligand labeled with a short-lived positron-emitter (^{11}C or ^{18}F) has been deployed [84, 85]. The output of these assays is an IC_{50} value, which is the concentration inhibiting 50% of the specific binding of the reference radioligand. Assuming that the K_D value of the reference radioligand is known, for example, from a self-competition assay, the inhibition constant, K_I, for a test ligand can be estimated according to Equation 15, where [R*] is the total concentration of reference radioligand in the assay:

$$K_I = IC_{50}/(1+([R*]/K_D)) \quad \text{Equation 15}$$

Consequently, if [R*] is much less than K_D, then K_I approximates to the IC_{50} value. K_I and IC_{50} values can be used as surrogates for K_D to rank the binding affinities in a series of test ligands for the target protein, with their inverses representing binding affinity (as earlier explained for $1/K_D$). Equation 15 is a version of the well-known Cheng-Prusoff equation [86], originally developed with regard to enzyme-inhibitor interactions. For inhibitors binding to enzymes, the concentration causing 50% inhibition is analogously termed the EC_{50} value.

Binding affinities determined from competition binding assays may vary with various parameters, including not only the protein matrix, but also temperature and buffer composition [87]. Assays are typically run at 4 or 20 °C. As a result, binding affinities may be unpredictably different from those occurring at mammalian physiological temperature (37–39 °C) in PET experiments. For example, the benzodiazepine receptor radioligand, [^{11}C]flumazenil, has five-fold lower affinity at 37 °C than at 4 °C. This finding partially explained an earlier apparent discrepancy between *in vitro* and *in vivo* measures of binding affinity [67]. Similarly, the radioligand [^{18}F]fallypride was found to have about five-fold lower affinity for rat D_2 receptors at 37 °C than at 22 °C [88]. By contrast, only one of four tested PET radioligands for SERT, showed a significant decrease in affinity between 22 and 37 °C [14].

Attention to buffer compositions is particularly important when testing agonists, if binding affinity values relevant to conditions *in vivo* are to be obtained. Given these considerations, binding affinities determined at different laboratories often vary considerably, sometimes by an order of magnitude or so. Replications of determinations in the same laboratory by the same methodology may also show some variation due to intrinsic errors in determining inhibition curves. These curves are conveniently plotted as in Fig. (**S2**), as % inhibition *versus* log of the test ligand concentration, with concentration typically varied over several decades to obtain the full binding curve. The IC_{50} value representing 50% inhibition will be at the inflexion in this log-linear curve and may not always turn out to have the desired precision. Possible uncertainty in binding affinity is an important consideration to take into account when selecting candidate PET radioligands for evaluation given that binding potential is *linearly* proportional to binding affinity, and not to its logarithm. Nonetheless, because binding affinities may occur over a wide range of values, they are often conveniently recorded as the negative logarithm to base 10 of the measured affinity parameter, *e.g.,* as pK_D, pK_I, or pIC_{50}.

Author Manuscript Author Manuscript Author Manuscript Author Manuscript

GPCRs are often targets for new therapeutics and for PET radioligand studies. GTPγS binding assays have gained popularity for assessing ligand potency and efficacy at GPCRs [89]. These assays are based on assessing the influence of the test ligand on the binding of either [^{35}S]GTPγS or Eu-GTPγS to GPCRs in tissue. For antagonists, GTPγS binding assays can provide K_D values. For agonists and inverse agonists, data on the concentrations giving maximal effect and half maximal response may be obtained. It should be noted that such functional assays do not give direct estimates of agonist binding affinity. This is because the receptor response depends on both the occupancy of the receptor by the agonist and the efficacy of the generated receptor-agonist complex. Also, in some cases, full occupancy of the receptor by an agonist may not be necessary to elicit full receptor response, whereas some agonists may show lower potencies than expected from their affinities as determined in competition binding assays. Other functional assays are also available for GPCRs [90], such as the Ca^{2+} flux assay, which is especially useful for high throughput ligand screening, but again much less so for predicting radioligand affinity. Technology for performing receptor-ligand binding assays also continues to advance, driven by needs for high throughput screening, and includes several non-radiometric methods [91].

It is not unusual for ligand binding affinities to vary considerably across species, particularly for those between rodents and NHPs. Binding assays for a wide range of protein targets are now offered to investigators by the NIMH-sponsored Psychoactive Drug Screening Program (PDSP; https://pdspdb.unc.edu.pdsweb), and also by commercial entities. Assays offered by PDSP are mainly based on recombinant human receptors.

The affinities of PET radioligands for their targets have kinetic consequences. In general, the higher the affinity of the radioligand (with all other factors being equal), the slower will be the brain kinetics following a bolus injection, as represented by a slower peak radioactivity in a target-rich brain region and a slower washout. This is due to the longer time needed to reach a transient equilibrium between radioligand association and dissociation, as has been shown by simulation [14]. Over-slow kinetics is undesirable because of the consequent need for a long PET scan duration to acquire sufficient data to generate robust quantitative outputs. Studies on radioligands for D_2-like receptors illustrate this point. [^{11}C]Raclopride (K_D = 3.89 nM) has long been used to measure D_2-like receptors in human striatum. The structurally related benzamide [^{11}C]FLB 457 has much higher affinity (K_D = 20 pM) for D_2-like receptors, and is suitable for measuring the much lower densities of these receptors in extrastriatal regions [92]. Transient equilibrium occurs within ten minutes of scanning after bolus radioligand administration. However, kinetics in receptor-rich striatum are very slow such that transient equilibrium is not reached, even after more than one hour of scanning, thus precluding their robust measurement. Slow kinetics has been notably problematic in the development of high-affinity radioligands for sparse $\alpha_4\beta_2$nACh receptors [93].

5. BINDING POTENTIAL

Earlier, a simple theoretical basis was given for requiring *in vitro* estimates of binding potential ($BP = B_{max}/K_D$) to well exceed unity in order for a PET radioligand to be successful. In practice, BP values predicted from *in vitro* measurements of B_{max} and K_D that are greater than 5, or even much higher, are generally found to be needed (Table 2). This

Author Manuscript Author Manuscript Author Manuscript Author Manuscript

may be appreciated by comparing the data presented in Tables 2 and 3 for [^{3}H/^{11}C]flumazenil, [^{3}H/^{11}C]SCH23390, [^{3}H/^{11}C]raclopride, and [^{3}H/^{11}C]diprenorphine for benzodiazepine (Bz), D_1, D_2-like, and opiate receptor targets, respectively. The complexity of the environment *in vivo* relative to the highly controlled and simpler environment used for measurements *in vitro* account for such differences. In particular, the tissue free fraction in brain (f_{ND}) is a major factor in determining BP_{ND}, the ratio of specific to non-displaceable binding at equilibrium *in vivo*. In fact, BP_{ND} is proportional to f_{ND} as earlier defined by Equation 6, and illustrated in Fig. (2).

Ordinarily, f_{ND} is not directly measureable. However, the non-displaceable volume of distribution V_{ND} is frequently measureable, especially in animal PET experiments where specific binding of the radioligand has been prevented by a competing non-radioactive ligand (blocking agent) given at a target-saturating dose. With respect to a 2-TCM, V_{ND}, earlier defined as K_1/k_2 (Equation 16), may also be expressed simply as the ratio of f_P to the brain free fraction (f_{ND}), for a radioligand that crosses the BBB by passive diffusion only, *i.e.*

$$V_{ND}=f_P/f_{ND} \quad \text{Equation 16}$$

Consequently, BP_{ND} may also be defined according to the equation:

$$BP_{ND}=(f_p \times B_{avail})/(V_{ND} \times K_D) \quad \text{Equation 17}$$

This equation theoretically implicates three radioligand properties in determining the magnitude of $BP_{ND,}$ namely affinity *in vivo* ($1/K_D$), non-displaceable binding (V_{ND}), and plasma free fraction (f_P). As will be discussed later (Section 10), the latter parameter tends to increase with radioligand lipophilicity, as does f_{ND}. However, for individual radioligands, f_P and f_{ND} may differ widely because of the different chemical make-ups of blood and brain tissue environments. Data from Guo *et al.* [99] for the f_P and f_{ND} values for 28 radioligands in pig clearly illustrate this lack of correspondence (Fig. 5).

The influence of f_p and f_{ND} on PET BP_{ND} has been well exemplified by considering the binding of [^{11}C]PIB to Aβ plaques in AD [16]. BP_{ND} for this radioligand from PET studies is about 2, whereas *in vitro* the radioligand K_D is about 2 nM and the B_{max} is estimated to be 1–2 μmol, giving a B_{max}/K_D value of 500–1000. f_p is known to be < 0.01. By Equation 6, it may be deduced that f_{ND} is also extremely low (< 0.005), thereby accounting for the several hundred-fold mismatch between B_{max}/K_D and measured binding potential. Several candidate PET radioligands have likely failed because of the marked effect of low f_{ND} on BP_{ND}, even where the *in vitro* B_{max}/K_D value appears substantially above unity [16].

In practice, in addition to low f_{ND}, other factors may also act to decrease apparent BP_{ND} *in vivo*, for example, undesirable nonspecific binding from radiometabolites [100], and for brain regions that are quite small relative to the spatial resolution of the PET camera leading to a ‘smearing’ of the radioactive signal through a ‘partial volume effect’.

Author Manuscript Author Manuscript Author Manuscript Author Manuscript

6. SELECTIVITY FOR TARGET

Clearly, an ideal PET radioligand would bind only to the target protein in brain. Nevertheless, in practice some radioligands show an appreciable affinity for one or more off-target sites, in addition to an inevitable component of nonspecific binding. This raises the question: what level of selectivity for the target site is required in a PET radioligand? There are two main considerations in answering this question. The first is the anatomical location of the competing 'off-target site'. If this is distinct and distant from the target site, a lack of selectivity may be tolerable. Thus, the D_1 receptor radioligand, [^{11}C]NNC 112, also has high affinity for 5-HT_{2A} receptors. This is problematic for imaging D_1 receptor in cerebral cortex where about 25% of specific binding is to prevalent 5-HT_{2A} receptors. This radioligand is nonetheless useful to measure D_1 receptor in striatum, because of their high density relative to the low density of 5-HT_{2A} receptors [101].

If the off-target site and the target site are found in the same region of interest, binding of the radioligand to the off-target site relative to that of the target site must be considered. The BP_{ND} measured with PET will be the sum of the binding potentials at each site. On the basis of Equation 6, this sum may be expressed as:

$$BP_{ND} = {}^{O}f_{ND}({}^{O}B_{avail}/{}^{O}K_{D}) + {}^{T}f_{ND}({}^{T}B_{avail}/{}^{T}K_{D}) \quad \text{Equation 18}$$

in which the prefixed superscripts ^{O} and ^{T} denote parameters for the off-target site and target site, respectively. By the likely reasonable assumption that the same free fraction of radioligand (f_{ND}) is available to each type of site, Equation 18 simplifies to:

$$BP_{ND} = f_{ND}({}^{O}B_{avail}/{}^{O}K_{D} + {}^{T}B_{avail}/{}^{T}K_{D}) \quad \text{Equation 19}$$

Therefore, the relative B_{avail}/K_D values of the radioligand for the target and off-target site need to be considered, usually on the basis of *in vitro* estimates of B_{max}/K_D.

An example of two target proteins that have been of interest for PET imaging and that show overlapping anatomical distribution are DAT and SERT. Both DAT and SERT are expressed in the striatum, but DAT is by far the more abundant. Consequently, DAT can be imaged with PET by using radioligands that have quite low affinity and quite low selectivity for binding to DAT versus SERT. However, by contrast, the imaging of SERT requires a radioligand with both high binding affinity and very high SERT selectivity [102].

Recent efforts to develop radioligands for neurofibrillary tangles (NFTs) in tauopathies provide another interesting example. Here it is important that the radioligand is selective for binding to NFTs versus Aβ plaques, which may also be present in these and other neurodegenerative disorders at greater abundance than NFTs. By considering density estimates of these proteins, Schafer *et al.* [103] estimated that a useful NFT-selective radioligand would need to show more than 20-fold greater affinity for NFTs than for Aβ

Author Manuscript Author Manuscript Author Manuscript Author Manuscript

plaques. Radioligands that show selectivity for imaging NFTs over Aβ-amyloid plaque are now beginning to emerge.

Given that the monoamine transporters, DAT, SERT and NET share a high degree of structural homology, it is not surprising that the development of selective high-affinity radioligands has been a challenging task. Likewise, both NFTs and Aβ plaques display extensive β-sheet structures that are important for ligand binding, and hence this similarity is a challenge in developing selective radioligands. More surprising is the lack of selectivity of some high-affinity ligands for binding to structurally dissimilar proteins. For example, some high-affinity ligands for the CB_1 receptor, a seven transmembrane domain GPCR, were also found to bind strongly to TSPO, a channel composed of five subunits [104]. Despite the strong structural dissimilarity in these proteins, their pharmacophore requirements appear to be quite similar with regard to the gross distribution of H-bonding and lipophilic groups.

The initial assessment of radioligand selectivity is usually made on the basis of *in vitro* screening for affinities against a broad battery of receptors and binding sites, as offered by PDSP and commercial entities. The selectivity of a radioligand may also be checked with PET in a suitable living animal model, preferably NHP. Challenge of the PET signal by simultaneous or preceding administration of the non-radioactive ligand in high dose is sometimes very useful to show whether appreciable specific binding of any kind is occurring in brain. Such experiments should be done rigorously to account for possible differences in brain exposure to radioligand in plasma, for example, by application of compartmental modeling with a metabolite-corrected arterial input function to determine any changes in V_T, or preferably V_T/f_P, under baseline and challenge conditions. Such an experiment leaves open the question of whether any observed specific binding is associated only with the target binding site. To answer this question, a compound which is known to be selective for the target site should be given at high dose before the radioligand. This compound should ideally belong to a different structural class, be safe for administration at high dose, and be expected to occupy all target sites at the time of radioligand injection. In some cases this type of administration may increase the peak uptake of radioactivity seen in brain, because blockade of peripheral target of the same type as the brain target may increase radioligand availability in plasma. This is commonly the case for experiments performed with TSPO-selective radioligands [48, 105, 106], and also for SERT radioligands which, may have avid binding in lung. When it is important to check that the radioligand is not binding to a particular off-target site, the PET signal may be challenged with a ligand that is selective for that off-target site. An alternative to administering challenge ligands preceding radioligand administration is to perform a displacement experiment, in which the challenge agent is given after the radioligand, and to observe whether radioactivity is then more rapidly cleared from target regions or not. For example, the selectivity of the radioligand [^{18}F]FIMX for binding to mGlu1 versus mGlu5 receptors has been checked in this manner (Fig. 6) [107].

7. LIGAND EFFICACY (INTRINSIC ACTIVITY)

The concept of ligand efficacy (intrinsic activity) is at the core of pharmacology. As a recap there are various classes of ligand efficacy. Ligands that bind to receptors may elicit a full pharmacological effect and are termed full agonists. Those that fully occupy receptors

Author Manuscript Author Manuscript Author Manuscript Author Manuscript

without eliciting a full pharmacological effect are termed partial agonists. Ligands that diminish the agonist-independent activity of a receptor, or that reverse a pharmacological effect either fully or partially to another type, are full or partial inverse agonists, respectively. Ligands that bind to the receptors without eliciting any function and which are capable of blocking the effect of all types of agonists are termed antagonists. These various terms may be exemplified by the pharmacological actions of various ligands for brain $GABA_A$ (Bz) receptors [108] (Fig. 7). Antagonists, such as flumazenil (Ro-15-1788), are without pharmacological effects, whereas full agonists, such as diazepam, cause sedation, and full inverse agonists, such as Ro-19-4603, cause seizures. Partial agonists, such as bretazenil (Ro-16-6028), are anticonvulsant, and partial inverse agonists, such as sarmazenil (Ro-15-3505), are anxiogenic [109]. It is important to note that ligands may not display the same type of efficacy in all situations *in vitro*. Moreover, many ligands that have originally presented as antagonists have turned out to be inverse agonists on deeper investigation [110]. Nor does ligand efficacy relate to ligand affinity; for example some partial agonists may have higher binding affinities than full agonists.

A high proportion of PET radioligand development for brain imaging has been directed at GPCRs and other functional neurotransmitter receptors. Leads for such radioligand development have frequently emerged from medicinal chemistry efforts to develop either agonists or antagonists as drugs. Before proceeding to discuss how radioligand efficacy at GPCRs affects PET radioligand imaging performance it is useful to give some background with regard to how GPCRs are now thought to function. Some of the earliest models with utility for understanding GPCR function are so-called ‘general two-state models’, in which a GPCR is considered to be in equilibrium between non-activated (Re) and activated states (Re*) [111] (Fig. 8). In such models, an agonist (Ag) binds with these forms of the receptor to alter the position of equilibrium towards Re* and thereby generate a cellular response. Inverse agonists are considered to shift the equilibrium away from Re*. In a further refinement of this model, known as the ‘extended ternary complex model’, it is considered that both Re* and the complex with agonist AgRe* must become bound reversibly to G-protein to generate a cellular response (Fig. 8). According to such models, agonists bind with high affinity to Re*G, the G-protein coupled form of Re*, and with lower affinity to the non-G-coupled form Re. In relatively early studies, ratios of affinity for the G-protein-coupled state ($1/K_D$high) to affinity for the uncoupled state ($1/K_D$low) *in vitro* were found to correlate well and linearly with ligand efficacy (E%) at several GPCRs, such as $5\text{-}HT_{1A}$ [112,113], $5\text{-}HT_{2A}$ [114], $5\text{-}HT_{2C}$ [114], CB_1 [115], and D_2 receptors [116]. A low E% value would correspond to a partial agonist and 100% efficacy to a full agonist. In these studies, full agonists showed affinity ratios that depended on the particular GPCR, and they ranged from 11.7 for serotonin at $5\text{-}HT_{2A}$ receptors to 238 for dopamine at D_2 receptors.

Evidence that has been accumulated from studies of GPCR functional selectivity, biophysics and crystal structures now shows that the early models of GPCR function are too simple. GPCRs are now known to adopt a variety of interconverting conformational states, whether free or bound to ligand or to a G-protein or both [117–119]. Each conformational state is associated with a particular free energy. This gives rise to the notion of an energy landscape relating all free and bound forms of the receptor. Conformational intermediates that are involved in receptor activation or deactivation can be regarded as wells in the energy

Author Manuscript Author Manuscript Author Manuscript Author Manuscript

landscape, and the deeper any particular well the more stable is the conformation. Ligand structure determines the particular make-up of the conformational ensemble that will be bound, and therefore these ensembles vary from ligand to ligand. Ligand efficacy for different signaling pathways derives from the ligand stabilization of particular conformational ensembles that interact with specific effectors. Thus, agonists are considered to bind with high affinity to only a sub-set of relatively high-energy receptor conformations. Such binding lowers the energies of the bound conformations and increases their relative concentrations. The energy landscape concept has become especially helpful in understanding how GPCRs may recruit different G-proteins for activation of different pathways that lead ultimately to different cell responses. This concept also helps to explain the basal or constitutive activity of most GPCRs. Thus, GPCRs are no longer viewed as simple 'two-state switches', but more like 'molecular rheostats' that present an array of conformations with relatively close energy differences.

Overall, antagonists have been the most productive leads for developing effective PET radioligands for GPCRs. This is at least partially explicable on the basis that the density of a protein target (B_{avail}) that is available to an antagonist will be at least as high as that for an agonist because antagonists bind with similar affinity to all versions of the target receptor in both G-protein coupled and non-coupled states. The history of PET radioligand development for brain 5-HT_{1A} receptors illustrates how ligand efficacy may influence the ability of radioligands to image GPCRs. Many early efforts preceded the development of high-affinity antagonist radioligands for 5-HT_{1A} receptors and therefore were obliged to be based on agonists or partial agonists. Despite the availability of agonist leads with very high affinity [120], effective PET radioligands giving high specific to nonspecific binding signals in rodents or NHPs failed to emerge. Only upon the development of antagonist radioligands based on the 'silent' high-affinity antagonist WAY-100635 were 5-HT_{1A} receptors first imaged and quantified effectively in human brain [120–124].

For further illustration, Fig. (9) plots pA (negative $\log_{10}$ of affinity, where A is IC_{50}, K_I or K_D) versus lipophilicity, as represented by clogD$^{7.4}$, for a set of radioligands that have been evaluated for imaging brain 5-HT_{1A} receptors with PET in rodents or monkeys. Antagonists are plotted as green symbols and non-antagonists as red symbols. Antagonists in the top left-hand sector of Fig. (9) bound by pA > 8.5 and clogD$^{7.4}$ < 3.5 give sizeable receptor-specific PET signals. Many of these have progressed to regular use for PET imaging in human subjects, including [^{11}C]WAY-100635, [^{11}C]DWAY, [^{18}F]FCWAY, and [^{18}F]MPPF. By contrast, non-antagonist radioligands with very similar parameters fail to give sizeable PET signals. The enantiomer pair, [^{11}C](R)-RWAY and [^{11}C](S)-RWAY, provide an especially interesting comparison. They have similar affinities, identical lipophilicities and virtually identical nonspecific binding levels in receptor-poor cerebellum. The R-enantiomer, an antagonist, gives a sizeable receptor-specific signal in monkey, whereas the somewhat higher affinity S-enantiomer, a partial agonist, gives a much lower signal [127]. Absent or low PET signals from non-antagonists compared to those from antagonists with comparable affinity and lipophilicity supports the notion that only relatively small sub-populations of 5-HT_{1A} receptors are available for binding to non-antagonists. In this regard, it is interesting to note that the proportion of 5-HT_{1A} receptors that exists in either a high-affinity G-protein coupled

Author Manuscript Author Manuscript Author Manuscript Author Manuscript

state or a low-affinity G-protein uncoupled state in rat hippocampal membranes is about the same [128].

A further consideration is that the binding of an agonist radioligand to a GPCR target in a G-protein coupled state *in vivo* might well be transient, as agonist binding is generally expected to decouple the G-protein rapidly and to generate a target protein conformation with lower affinity [117–119]. Nonetheless, considerable efforts continue to be expended on attempts to develop full agonist-type PET radioligands for two main reasons. Firstly, such radioligands might image only sub-populations of the target receptor that are in functional G-protein-coupled states. Secondly, agonist radioligand binding is expected to be more sensitive to the synaptic concentration of endogenous agonist. Thus, true full agonist-type radioligands might be more selective than antagonist-type radioligands for investigating pharmacological and other influences on neurotransmission.

Continuing efforts to develop agonist radioligands for imaging the high-affinity G-protein-coupled states of the 5-HT_{1A} receptor have so far met with limited success. For a time, the most promising of these radioligands appeared to be [^{11}C]CUMI-101 [129], but on deeper investigation this radioligand is now considered to be an antagonist in native rat brain tissue [130] and in primate brain [131]. [^{11}C]Raclopride has long served as an effective antagonist radioligand for imaging D_2-like receptors. Extensive efforts have also been directed at the discovery of agonist-type PET radioligands for D_2-like receptors in order to explore dopaminergic neurotransmission. [^{11}C]MNPA has become the preferred and most prominently explored agonist radioligand for this purpose [132]. This radioligand appears to be more sensitive than [^{11}C]raclopride to displacement by endogenous dopamine [133]. However, it is not yet conclusively demonstrated that [^{11}C]MNPA specific binding *in vivo*, or that of any other agonist PET radioligand, is to high-affinity states of the D_2-receptor [132–135]. In one PET study, an agonist-type radioligand [^{11}C]NPA and an antagonist radioligand, [^{11}C]raclopride, showed similar B_{avail} values for D_2-like receptors in baboons [136]. A similar result was found in cat when comparing the agonist radioligand [^{11}C](+)PHNO with [^{11}C]raclopride [137]. In this regard, Seeman [138] has argued that [^{11}C](+)PHNO, likely reports ‘low-affinity’ G-protein uncoupled states *in vivo*, because agonist binding to the receptor results in very rapid sub-second dissociation of the G-protein followed by a not so fast reversion of the receptor to the low affinity state while the agonist remains bound. Therefore, considerable uncertainty surrounds the identity of conformational ensembles that may be imaged with non-antagonist PET radioligands for GPCRs. Different PET radioligands may be imaging different conformational ensembles, and these ensembles may well be mainly composed of non G-protein coupled conformations.

Notwithstanding considerations with regard to agonist radioligands for 5-HT_{1A} and D_2-like receptors, some agonist radioligands for other GPCRs have been found effective, including, for example, [^{11}C]carfentanil for imaging μ-opioid receptors [139]. The inverse agonist [^{18}F]FMPEP-d_2 has also been used successfully for imaging abundant brain cannabinoid subtype-1 (CB_1) receptors [140]. The conformational ensembles being imaged by such agonist or partial agonist radioligands again however remains open to question. Some non-antagonist radioligands are also used successfully for PET imaging of non-GPCRs, such as the partial inverse agonist [^{11}C]Ro-15-4513 for $GABA_A$ receptors [141].

Author Manuscript Author Manuscript Author Manuscript Author Manuscript

The majority of PET radioligands for imaging proteins interact at sites that bind the endogenous ligand and these are termed orthosteric sites. Radioligands may also be developed to interact with sites that are remote from the orthosteric site, termed allosteric sites. Ligands binding to allosteric sites are also classified according to their effects on the action of endogenous ligand. Positive allosteric modulators (PAMs) potentiate response to the endogenous agonist, negative allosteric modulators (NAMs) inhibit response, and silent (or neutral) allosteric modulators (SAMs) are without effect and also block the actions of PAMs and NAMs. The earlier mentioned ligands for $GABA_A$ receptors (Fig. 7) bind to allosteric sites. Allosteric binding sites are often less structurally conserved than orthosteric sites among closely related receptor subtypes, and have become attractive targets for the development of drugs with high binding selectivity [142, 143]. Similarly, they have become of increased interest for developing target subtype-selective PET radioligands. The recent successful development of selective radioligands for PET imaging of mGlu5 receptors [144] and also of very structurally related mGlu1 receptors [107], each based on subtype-selective allosteric modulators, exemplifies the value of this approach.

Finally, a major consideration in the use of an agonist radioligand is its pharmacological action. The mass doses of carrier that are co-administered with such radioligands often need to be limited for subject safety. Antagonist radioligands generally avoid pharmacological concerns.

8. ABILITY TO PASS THE BLOOD-BRAIN BARRIER

Self-evidently, PET radioligands administered intravenously for imaging proteins within the brain must be able to penetrate the BBB and have a high peak uptake that allows for accurate radioactivity measurement. A useful parameter for quantifying radioactivity concentrations in regions of brain or other organs after administration of a PET radioligand is the standardized uptake value (SUV), which normalizes measured concentrations (Bq/g) for injected dose (Bq) and subject body weight (g). SUV may be defined as follows:

$$\mathrm{SUV} = [\%\,\text{injected dose per g} \times \text{body weight (g)}]/100 \quad \text{Equation 20}$$

An SUV value of 1 in a particular organ or tissue corresponds to the radioactivity concentration that would be expected if administered radioactivity were evenly distributed throughout the subject. Higher SUV values therefore indicate an enrichment of radioactivity concentration above the overall average. The SUV parameter usefully enables comparisons of the radioactivity uptake between different tissues, organs and species. For example, assuming that a typical laboratory mouse weighs 40 g, a radioactivity concentration of 5% injected dose per g of brain would be 2 SUV. For a laboratory rat weighing 400 g, a radioactivity concentration of only 0.5% injected dose per g of brain gives the same SUV value. Successful PET radioligands mostly exhibit peak brain radioactivity values in the range 2–10 SUV (Table 4). A major hurdle to achieving such concentrations of radioligands in brain can be the BBB.

Author Manuscript Author Manuscript Author Manuscript Author Manuscript

The BBB is a complex structure that operates at the capillary level to separate circulating blood from brain extracellular fluid in the CNS. The BBB protects the brain from infectious agents (*e.g.,* bacteria, viruses) and possibly harmful exogenous substances, which may also include small drug-like molecules and radiotracers [177]. The capillary walls of the BBB are formed from endothelial cells that form very tight junctions (Fig. 10). These cells are mainly composed of phospholipid bilayers, having hydrophilic phosphate heads and lipophilic tails (Fig. 11). Consequently, the membrane is generally impervious to passive diffusion by charged or highly polar species, but not to relatively lipophilic species. Free diffusion across the BBB is mainly limited to small molecules. Some small polar species may cross the BBB by an intercellular pathway at the tight junctions, but this pathway is usually negligible. In general, charged molecules are excluded from passage across the BBB, except those needed by the brain for which there are specific transporter proteins, such as those known for essential amino acids and nucleosides. In addition to having these transporter proteins for delivery of specific compounds to the brain, the BBB contains efflux transporter proteins, which actively exclude many unwanted compounds. Many drug-like molecules that might be expected to cross the BBB by passive diffusion, including experimental therapeutics and candidate PET radioligands, are in fact prevented from doing so by the action of efflux transporters, as is discussed later (Section 9). For radioligands that are not substrates for efflux transporters, peak uptake in brain is influenced by many factors, some that stem from the physicochemical properties of the radioligand, but also by others of which the most important is the arterial plasma input of the radioligand. The latter is influenced by peripheral metabolism and by plasma free fraction. The propensities of the radioligand to bind in brain and/or periphery, either specifically and/or nonspecifically, are also other important factors.

Methods for predicting the ability of a radioligand to enter brain from knowledge of molecular structure alone are keenly sought in order to avoid wasted efforts on candidate radioligand synthesis and evaluation. Developers of drugs for CNS disorders have a similar need for methods to predict BBB penetration. Hence, numerous studies have attempted to identify molecular parameters that may be key to attaining a high equilibrium ratio of the concentration of a compound in brain to that in plasma, which is termed BB or K_p, and often discussed as logBB. BB values have been readily obtained in rodents. Generally, a K_p value of > 2, corresponding to logBB > 0.3, has been sought in CNS drug development. Before considering the influence of efflux transporters, it is valuable to consider the many possible molecular factors that may influence the ability of a compound to traverse the BBB by passive diffusion alone.

Parameters that have been considered for predicting BB values are numerous but often related to compound size (MWt), lipophilicity indexes ($logD^{7.4}$ or logP*,* computed or measured), charge (pK_a), molecular volume (V_x), shape (cross-sectional area or principal axes ratio), polarity [*e.g.,* topological polar surface area (TPSA)], and hydrogen bonding capability [hydrogen bond donors (HBDs), hydrogen bond acceptors (HBAs), and/or total heteroatom count]. Some of these parameters are clearly inter-dependent, for example MWt and V_x, or total heteroatom count and TPSA. A few of these parameters are readily calculated from simple 2-dimensional representations of molecular structure plus, in some cases, the use of readily available software packages (*e.g.,* for calculating lipophilicity or

Author Manuscript Author Manuscript Author Manuscript Author Manuscript

TPSA). A myriad of other parameters has also been considered for 'in silico' prediction of compound ability to penetrate the BBB, but the estimation of these parameters is computationally more demanding.

Several 'rules or thumb' have been proposed for predicting compound penetration of the BBB on the basis of the more simply acquired molecular data. Examples are specified at the foot of Table 4. These rules highlight the importance of molecular weight, lipophilicity, absence of charge and low HBD capacity. Table 4 shows the maximal uptakes of 20 PET radioligands in rhesus monkey brain and human brain as SUV, as measured in our laboratory, along with many of their properties that may be used to predict BBB penetration by the listed simple 'rules of thumb'. Inspection of this dataset shows that the majority of radioligands comply with the following criteria:

MWt < 500 Da

$clogD^{7.4}$ > 1 and < 5

logP < 5

pK_a of most basic site < 9.5

HBDs < 3

TPSA < 90 $Å^2$

These criteria quite closely correspond to those that were concluded to be acceptable in another recent survey of 77 CNS PET radioligands [175]. An understanding of why such criteria show importance may be gained from numerous experimental studies that are exemplified as follows.

The criterion for MWt < 500 Da reflects the difficulty for large molecules to pass through the tight junctions of the BBB [177]. In this regard, Gleeson [174] reported on logBB for 3,059 diverse molecules from a GlaxoSmithKline database. LogBB declined almost linearly with MWt. Molecules with MWt < 300 Da had a mean BB value of 2.2 compared to 0.1 for molecules with MWt > 700 Da.

The criteria for logP, pK_a, and $logD^{7.4}$ reflect the inability of charged and hydrophilic molecules to readily undergo passive diffusion across the BBB. LogP values represent the partition coefficients for neutral compounds between an organic phase, *n*-octanol, and water. Ligand uptake into brain from plasma is expected to increase as logP increases. However, binding to blood proteins will also be expected to increase, eventually restricting entry into brain from plasma. Notionally, therefore, moderate lipophilicity is desirable for adequate brain entry. A preponderance of CNS drugs and brain PET radioligands either do not ionize or are basic amines. Highly basic compounds with pK_a > 9.5 will be almost fully protonated at the pH of blood (7.4) and mostly incapable of crossing the BBB. $LogD^{7.4}$ represents the distribution of the fraction of uncharged species between *n*-octanol and pH 7.4 buffer. For strong and moderately strong bases, $logD^{7.4}$ values are generally much lower than logP values, as may be seen in Table 4. Because charged species are well excluded from entering brain from plasma (pH 7.4), $logD^{7.4}$ is preferable to logP for assessing the influence of radioligand lipophilicity on brain uptake. A $logD^{7.4}$ value >1, showing preference of a

Author Manuscript Author Manuscript Author Manuscript Author Manuscript

compound for organic phase over aqueous phase, may be rationalized as clearly desirable for easy brain entry.

Considering only the lipophilicity parameter logP, Waterhouse [178] observed an approximately parabolic relationship between logP and rat whole brain uptake for a set of 43 candidate and 7 effective PET radioligands, with a peak in the range 2–3 for logP. However, whether such a parabolic relationship holds generally is perhaps uncertain: plots of peak uptake in monkey brain versus computed logP or measured $\log D^{7.4}$ for the 20 radioligands listed in Table 4 do not show a similar relationship, only tendencies for peak brain uptake to decrease slightly with increasing lipophilicity (Fig. 12). Peak brain uptakes are however strongly correlated between monkey and human (Fig. 13).

Norinder and Haeberlein [172] considered both MWt and logP parameters and found the following simple but strong relationship (r^2 = 0.89) with logBB for a set of 20 compounds:

$$\log BB = -0.00116 MWt + 0.272 \log P - 0.088 \quad \text{Equation 21}$$

This equation also predicts positive logBB for 19 of the 20 the brain-penetrant radioligands in Table 4, with [^{11}C]CUMI-101 as the only exception.

The listed criteria for HBDs and TPSA reflect the recognized detrimental effect of high hydrogen bonding capacity on brain penetration [173, 179]. The high energy cost of compound desolvation is considered to be the reason why a high HBD number disfavors ready passive diffusion across the BBB. TPSA often strongly reflects the total number of HBDs, and is rapidly computable from two-dimensional structure with commercial software [180], such as ChemDraw. Clark [181] found the following relationship (r^2 = 0.79) between logBB, and the two parameters clogP and PSA (polar molecular surface area, which may be regarded as similar to TPSA) for 55 compounds:

$$\log BB = 0.152 \text{clog}P - 0.0148 PSA + 0.139 \quad \text{Equation 22}$$

Moreover, Rishton *et al.* [182] found a very similar strong relationship (r^2 = 0.79) for 207 compounds:

$$\log BB = 0.155 \text{clog}P - 0.0100 PSA + 0.164 \quad \text{Equation 23}$$

Decreasing the number of HBDs and/or decreasing TPSA have been found effective strategies for enhancing compound brain uptake in several studies [173]. Consistent with the criteria for lack of charge, lack of HBDs and hydrophobicity, certain polar structural features have been observed as detrimental to successful brain entry and include sulfonamido, sulfone, tetrazole, carboxylic acid or *N*-oxide groups [173].

Strenuous efforts have been made to move beyond simple rules-of-thumb to derive strong computational methods for predicting compound brain penetration. For example, Gerebtzoff

Author Manuscript Author Manuscript Author Manuscript Author Manuscript

and Seelig [183] closely studied the effects of drug charge and molecular shape on brain entry. For a set of 43 compounds, they computed molecular cross sectional areas (A_D) for the calculated conformation with strongest amphiphilicity, which they considered to be the membrane-binding conformation. They concluded that a ligand cross-sectional area of less than 70 $Å^2$ is required to allow brain entry. Use of this criterion gave 83% success in predicting brain penetration for a separate set of 42 compounds. However, lack of availability of the software for the computational procedures restricts wider testing of this promising but computationally challenging method.

Adenot and Lahana [184] investigated several models for their ability to predict BBB penetration for a set of 1,595 drugs. Overall, 67 variables were considered. This study exposed some simple yet powerful approaches to predicting BBB penetration, of which two are especially worthy of mention. Thus, by reference to Lipinski's rules [170], Adenot and Lahana [184] derived a composite parameter C_{diff} based on five parameters (1–5), namely MWt (1), clogP (2), HBDs (3), HBAs (4), and TPSA (5), respectively. C_{diff} was defined as a pseudo-continuous variable ranging from 0 to 1 by the following equation:

$$C_{\mathrm{diff}}=\sum_{i=1,5} S(i)/5^2 \quad \text{Equation 24}$$

in which $S(i)$ is a scaling function for the ith parameter. Each function was characterized by its respective slope a_i and lower and upper thresholds, t_i and t_i' respectively, with the following values: $a_1 = -6.7 \times 10^{-3}$, $t_1 = 0$, $t_1' = 800$; $a_2 = 0.4$, $t_2 = -2.5$, $t_2' = 5$; $a_3 = -1$, $t_3 = 0$, $t_3' = 5$; $a_4 = -0.5$, $t_4 = 0$, $t_4' = 10$; $a_5 = -0.02$, $t_5 = 0$, $t_5' = 250$. C_{diff} above 0.4 correctly classified 95% of brain-penetrant compounds and 93% of non-penetrant compounds among the large training set. Similar performance was achieved on an external set of 82 compounds. An attractive feature of C_{diff} is its simple computation from 2-dimensional molecular structure.

Among the multitude of variables examined by Adenot and Lahana [184], a remarkably high performer was found to be the total number of heteroatoms (defined as O, S, N, P, and halogen), which correctly predicted 94% of brain-penetrant compounds and 72% of non-penetrant compounds, when the criterion for brain entry was set at less than 9 heteroatoms. Thus, simple heteroatom-counting performed almost as well as any of the numerous computationally more demanding methods for predicting BBB penetration. All radio-ligands in Table 4 meet this simple requirement.

The parameter logBB, although frequently used as an index of brain penetration, really represents the distribution of compound between plasma and brain where the compound is able to diffuse passively across the BBB in either direction [179, 185]. This parameter is strongly criticized as an index of compound brain penetration [186]. For example, logBB takes no account of ligand binding to proteins in plasma or to tissue in brain, whereas it is generally considered that only free ligand in plasma is available for brain entry. The rate constant K_1 (Fig. 3) more truly reflects the degree to which a compound is able to diffuse passively across the BBB.

Author Manuscript Author Manuscript Author Manuscript Author Manuscript

Guo *et al.* [99] used an *in-silico* method to predict K_1 (mL/cm^3/min) from perfusion (f; mL/cm^3/min), compound permeability (P′; cm/min), and capillary surface area (S; cm^2/cm^3), as follows:

$$K_1 = f \times (1 - e^{-P' S/f}) \quad \text{Equation 25}$$

Perfusion and capillary surface area are known physiological parameters. P′ was calculated from computed lipophilicity (clogD$^{7.4}$) and molecular volume (V_x), according to the relationship:

$$\log P' = 0.121(\text{clogD}^{7.4} - 2.298)^2 - 2.544\log(V_x^{1/3}) - 2.525 \quad \text{Equation 26}$$

The coefficients of this parabolic relationship between P′ and clogD were derived empirically from 30 putative non-efflux transporter (P-gp) substrates. The parabola has an optimum at a clogD$^{7.4}$ value of 2.3, and shows a quite strong correlation with the empirical data (r^2 = 0.58). The Pearson coefficient (r) for the correlation between predicted K_1 and that measured in pig with PET was nonetheless quite low at 0.402. Three of these compounds have very low brain penetration and may be considered as outliers (perhaps due to efflux transporter action). Curve-fitting of the dataset excluding these 3 outliers shows a maximum for K_1 at a clogD$^{7.4}$ value of about 2 (Fig. 14).

In view of the Guo *et al.* study [99], and of the earlier mentioned studies, candidate PET radioligands should probably be sought with clogD$^{7.4}$ in the range 1 to 4, and optimally about 2.2, for the purpose of achieving adequate brain penetration. In addition, as listed previously, MWt should preferably be < 500 Da, the pK_a of the most basic site < 9.5, HBDs < 3, TPSA < 90 Å^2, and heteroatom count < 9.

Finally, it should be noted that commercial software is now available to predict compound logBB, such as that from ACD/Labs. This program correctly classifies 92% of the large dataset of Adenot and Lahana [184], as either brain-penetrant or non-penetrant [187], after removing compounds that are putative P-gp substrates from the dataset.

9. EFFLUX TRANSPORTER ACTION

The preceding discussion on PET radioligand penetration of the BBB does not take into account the influence of efflux transporters. Brain efflux transporters are responsible for the inability of a high proportion of small molecules, including experimental therapeutics, to access brain. Of primary consideration and seemingly most relevant to PET radioligand development are transporters of the adenosine triphosphate binding cassette (ABC), which has 48 identified members. These include P-glycoprotein (P-gp; MDR1/mdr-1a; ABCB1), breast cancer resistant protein (BCRP; ABCG2), and multidrug resistance associated protein (MRP1; ABCC1) [188]. These are each expressed on the luminal (blood facing) side of the BBB (Fig. 10).

Author Manuscript Author Manuscript Author Manuscript Author Manuscript

P-gp is less abundant than BCRP in human brain [179], but has been by far the most studied. Considerable species differences in the expression levels of these two transporters have been noted [179]. For example, the order of brain expression of P-gp is mouse > human > cynomolgus monkey, and for BCRP, cynomolgus monkey > human > mouse. Moreover, there exist considerable species differences in the sequence homologies of P-gp. Thus, guinea pig, rat, mouse, dog, rhesus monkey and chimpanzee share 82, 85, 87, 87, 93, and 97% homology with human P-gp, respectively [179]. Given these variations in P-gp expression level and in sequence, compounds may show considerable species differences in P-gp substrate behavior [189, 190]. Thus, Xia *et al.* [189] found appreciable differences in the affinities of 21 substrates for P-gp between beagle dog, rhesus monkey and human. Some PET radioligands show adequate brain uptakes (> 2 SUV) in human subjects, but markedly lower brain uptakes in rodents, perhaps suggesting a role for efflux transporters in rodents.

For many radioligands, it has been noted that genetic or pharmacological knockout of either P-gp (Table 5) or BCRP (Table 6) results in globally increased brain uptake of radioactivity *in vivo*. However, conclusions from such studies that a particular PET radioligand is indeed a substrate for P-gp or BCRP must be treated with some caution, because of other possible explanations. Thus, increases in the uptakes of PET radioligands into brain following pharmacological inhibition of P-gp have been ascribed to increases in radioligand f_P, in at least two cases, namely [^{11}C]RWAY in monkey [198], and [^{18}F]MPPF in baboon [194]. In many other studies, full compartmental modeling with correction for radioligand f_P has been impractical or has not been applied.

The behavior of [^{11}C](*R*)-RWAY exemplifies how species differences in efflux transporter action may dramatically affect radioligand performance. This radioligand readily enters rhesus monkey and human brain; and has found application in studies requiring brain 5-HT_{1A} receptors to be measured in rhesus monkey [154, 155]. However, P-gp greatly prevents appreciable uptake of this radioligand into rodent brain [198]. As a general observation, species differences in efflux transporter action between NHPs and humans have seldom been observed, unlike those between rodents and primate.

Some radioligands that do show adequate uptake in human brain for target quantification are nonetheless possibly weak substrates for efflux transporters. The substrate behavior of some PET radioligands towards human efflux transporters has been tested with *in vitro* assays, making use of cells expressing human P-gp [197] (Tables 5 and 6). However, investigation *in vivo* is difficult because of a paucity of efflux transporter inhibitors that may be given effectively and safely to human subjects. Currently, tariquidar seems most promising for inhibiting P-gp in human subjects to test for PET radioligand substrate behavior [207]. In this regard, the 5-HT_{1A} receptor radioligand [^{18}F]FCWAY has recently been identified as a weak substrate of P-gp in human subjects by using tariquidar to inhibit P-gp [192].

Considerable efforts have been made to identify structural features or molecular properties that may impart the presence or absence of P-gp substrate behavior [208, 209]. Gleeson [174] found that compound susceptibility to P-gp efflux increased markedly over the MWt range 300–700 for 1975 diverse molecules. Among this large set of compounds ionization

Author Manuscript Author Manuscript Author Manuscript Author Manuscript

was found to play a minor role in extent of P-gp efflux. Compounds with logP between 3 and 5 were more prone to P-gp efflux than compounds with lower or higher logP. The effect of lipophilicity was independent of MWt. Earlier in this article, it was argued that moderate lipophilicity is desirable for facile radioligand penetration of the BBB. Thus, it is desirable for a radioligand to have moderate lipophilicity without efflux transporter substrate behavior, and to identify molecular criteria that might achieve this aim.

Seelig *et al.* [210, 211] proposed that P-gp substrate behavior was conferred if a molecule contained two or three HBAs separated by 2.5 or 4.6 Å. Hitchcock [212] reviewed the structural features that alter compound P-gp efflux susceptibility and suggested that susceptibility is minimized in compounds that have < 2 HBDs, and TPSA < 90 $Å^2$, with a preferred value of < 70 $Å^2$. From an analysis of 2000 compounds at Eli Lilly, Desai *et al.* [213] found that compounds with TPSA < 60 $Å^2$ and with pK_a calculated to be < 8 exhibited a much lower likelihood of being a P-gp substrate (6%) than those with parameters outside these limits (75%). From this dataset, a QSAR model was developed that predicted both P-gp substrates and non-substrates with 80% success. Didziapetris *et al.* [214] proposed that molecules with MWt < 400 Da, with < 7 nitrogen plus oxygen atom HBAs, and having a basic pK_a of < 8 are unlikely to be P-gp substrates. This became dubbed the ‘rule of 4’ and compliance with this rule appears to be a useful strategy for avoiding efflux transporter substrate behavior [182].

In summary, the suggested criteria for MWt, TPSA, pK_a and HBD for avoiding liability to efflux transporter substrate behavior are within the limits that were earlier considered desirable for facile penetration of the BBB by passive diffusion. However, it is clear that whether a particular PET radioligand will be a substrate for efflux transporters in any particular species is still not easily predictable. Currently, data on the efflux transporter susceptibility of PET radioligands for brain imaging are sparse, and accumulation of more data are needed to have a deeper understanding of this area.

10. ADEQUATE AND MEASUREABLE FREE FRACTION IN PLASMA

The free fraction of a radioligand in plasma (f_P) is an important parameter because it is assumed that only radioligand that is free in plasma may cross the BBB for binding in brain. f_p may vary appreciably between subjects and between different experimental scenarios, such as between baseline and target blocking conditions. Ideally, comparisons of V_T values should be corrected for significant differences in f_P under compared conditions *i.e.*, it is generally preferable and more rigorous to compare V_T/f_p values than V_T values. Equilibrium dialysis of the non-radioactive tracer is regarded as the ‘gold standard’ method for f_p determination [215, 216], but is relatively slow and inapplicable to PET experiment settings. For PET experiments, f_P is usually measured by a rapid ultrafiltration technique with the radioligand preparation, using blood sampled from the subject of study [217]. Where f_P measurements are used, they need to be accurate and precise. Experimentally, this is more easily achieved when the f_p value itself is substantial.

Author Manuscript Author Manuscript Author Manuscript Author Manuscript

In general, f_p tends to decrease with increasing lipophilicity, but not linearly so. Zoghbi *et al.* [176] generated the parameter ${}^{m}\log D_{pr/pl}$ which is the measured logarithm of the distribution of radioligand between plasma protein and plasma, where

$$D_{pr/pl}=(1-fp)/fp \quad \text{Equation 27}$$

For a set PET radioligands ${}^{m}\log D_{pr/pl}$ was linearly related to measured logD value by the following equation for human:

$${}^{m}\log D_{pr/pl}=0.733\,{}^{m}\log D-0.651\ (r^2=0.738) \quad \text{Equation 28}$$

and for monkey:

$${}^{m}\log D_{pr/pl}=0.780\,{}^{m}\log D-1.15\ (r^2=0.832) \quad \text{Equation 29}$$

The strong dependency of f_P on compound lipophilicity has also been noted in other reports [174, 218]. Generally, the following trend in f_P has been observed: acids > neutrals > zwitterions > bases [178]. From equations 28 and 29, a radioligand that has a logD of about 2.2 may be considered appropriate for achieving acceptable passage of the BBB, and would be expected to have f_P values of about 0.10 and 0.21 in human and monkey, respectively. These values would be easily measurable with accuracy and precision.

11. LOW NONSPECIFIC BINDING (OR LOW NON-DISPLACEABLE BINDING)

All radioligands for PET imaging of brain proteins display accompanying nonspecific binding. Excessive nonspecific binding masks any specific binding and so can render a radioligand of little or no utility. An overall objective in developing a PET radiotracer for brain imaging is therefore to achieve a high signal-to-noise ratio, as represented by a high ratio of V_T to $V_{NS,}$ where V_{NS} is V_{ND} minus V_F (Equation 11). For a radioligand which crosses the BBB by free passive diffusion only, V_F is simply $1/f_{ND}$. Hence, in such cases, it follows that V_{NS}/f_P is proportional to V_{ND}/f_P according to Equation 30:

$$V_{NS}/f_P=V_{ND}/f_P-1 \quad \text{Equation 30}$$

Recalling Equation 12 for radioligands that cross the BBB by passive diffusion only, nonspecific binding (V_{ND}) theoretically equates to the ratio of plasma free fraction (f_P) to brain free fraction (f_{ND}). V_{ND} measurements from PET and f_p and f_{ND} data from equilibrium dialysis provide experimental support for the validity of this relationship in pig [219]. In this study of 36 PET radioligands, V_{ND} varied from 0.23 to 29.7. Radioligands with unexpectedly low V_{ND} values were considered likely to be efflux transporter substrates. Moreover, in another study, f_P values have been found to be highly correlated across three

Author Manuscript Author Manuscript Author Manuscript Author Manuscript

species (rat, pig and human ($r^2 > 0.81$, $n = 21$), so indicating relatively uniform microenvironments for ligand binding in different species of brain tissue [220]. Brain has an overall different composition to plasma. The lipid content of brain (11% by volume) is 20-fold higher than that of plasma whereas plasma has twice as much protein as brain [221]. Therefore, it is unsurprising that f_{ND} is often very different to f_p for particular radioligands.

Because of the high lipid content of brain, it is generally expected that nonspecific binding in brain will increase with radioligand lipophilicity. Some authors have attempted to relate surrogate parameters of non-specific binding and $\log D^{7.4}$ for PET radioligands. For example, Andersson *et al.* [222] reported a weak linear correlation ($r^2 = 0.50$) between radioactivity in cerebellum at 60 min, assumed to be nonspecific and non-displaceable binding, and $\mathrm{clog}D^{7.4}$ over a narrow range for 8 experimental 5-HT_{1B} receptor radioligands in cynomolgus monkey. However, possibly more meaningful relationships between V_{NS} or V_{ND} and $\mathrm{clog}D^{7.4}$ were not tested. Assmus *et al.* [223] found a good correlation ($r^2 = 0.88$) between $\log V_{NS}/f_P$ values determined with PET in human and estimates of log partition coefficients between brain tissue and water at pH 7.4 ($\log D_{brain}$). These $\log D_{brain}$ estimates were obtained in a lipid membrane binding assay for a small set ($n = 6$) of well-known PET radioligands that were considered non-efflux transporter substrates. Assmus *et al.* also found only a very poor correlation between radioligand $\log D^{7.4}$ and the log of nonspecific binding ($\log NSB$) estimated from *in vitro* autoradiography. However, the estimates of logNSB were not strictly controlled for factors affecting nonspecific binding in autoradiography, such as the ligand concentration to which tissue was exposed, which ranged widely (0.08–23.5 nM). Correlations were much stronger for logNSB versus $\log D_{brain}$. Gleeson [174] found that compound binding to brain tissue had a similar dependence on lipophilicity as plasma protein binding in an analysis of over 986 diverse compounds from a GlaxoSmithKline database. This correlation was largely independent of ligand molecular weight. Also in this study, binding to brain tissue was not as greatly affected by ligand ionization state as was plasma protein binding.

The identification of possible mechanisms underpinning nonspecific binding beyond hydrophobic interactions has received little attention. Rosso *et al.* [224] applied quantum mechanical modeling to show a correlation between estimates of the energies of drug molecule-lipid molecule interactions with *in vivo* nonspecific binding as estimated by PET for a small set of radioligands. The P-gp efflux radiotracer [^{11}C]loperamide is moderately basic ($pK_a = 7.3$) and has been shown to accumulate in acidic lysosomes (pH ~ 5.5) due to entrapment of its protonated form [225]. Lysosomes appear to have quite high capacity for such entrapment [225], and therefore conceivably similar ionic entrapment might contribute to the 'nonspecific' binding of radioligands or their radiometabolites with similar pK_a.

Nonspecific binding (V_{ND}) is quite readily determined in animal PET experiments as being equivalent to the V_T in experiments where radioligand specific binding has been completely prevented pharmacologically (as earlier illustrated for [^{18}F]FIMX [107] (Fig. 6). Moreover, a 'Lassen plot', which in its simplest and original form is a plot of brain regional V_T in a baseline experiment ($V_{ND} + V_S$) *versus* the regional reductions in V_T in a partial target block experiment, provides V_{ND} as the Y-axis intercept [226]. This type of plot, and its more recent variations [227], are useful even in the absence of a target-free reference region and

Author Manuscript Author Manuscript Author Manuscript Author Manuscript

can enable measurement of drug occupancy at the target in response to variation of administered dose. Determinations of V_{ND} in human subjects are not always accessible in this manner, because of the absence of a known blocking agent with adequate brain penetration and safety. An interesting approach to overcome this obstacle is a modified Lassen plot in which the brain regional expression of target mRNA is used as a surrogate for V_S on the Y-axis. This approach worked satisfactorily for determining the human V_{ND} for [^{18}F]FIMX [228]. It may be noted that because of gross interspecies similarities in brain compositions, V_{ND} is not expected to vary greatly between species, and particularly between primates. Brain regional variations in V_{ND} also appear rare.

12. LACK OF ACCUMULATION OF RADIOME-TABOLITES IN BRAIN OR SKULL

A PET camera is unable to assign detected radioactivity to particular molecular sources, and therefore is simply unable to distinguish parent radioligand from radiometabolites. For brain imaging with PET, the radioactivity in brain is ideally ascribable to parent radioligand alone [19, 100]. If this is not the case, then radiometabolites in brain may distort or confound attempts at quantifying radioligand-target protein interactions, for example, by contributing erroneously to radiotracer V_T and V_{ND} estimates derived from compartmental models. The time-stability of these estimates may also be imperiled by brain radiometabolites. Where radiometabolites also show specific binding, V_s can also be affected. Radiometabolites in brain also decrease the 'signal-to-noise' ratios, *i.e.* the V_S/V_{ND} value. Only in relatively few cases, such as for [^{18}F]altanserin, where either a constant infusion paradigm [229] or a reference tissue model [230] can be reliably applied, are brain radiometabolites of less concern. In these cases, it has to be assumed that radiometabolites contribute solely to nonspecific binding in a uniform manner across brain.

The vast majority of PET radioligands do undergo rapid and extensive metabolism over the time-spans of PET scanning sessions. This metabolism may occur in periphery and/or brain [100]. For reversibly binding PET radioligands for brain imaging, such metabolism is ideally confined to the periphery. Some radioligands produce radiometabolites in the periphery that are more lipophilic than the parent radioligand, and this can be especially problematic as the radiometabolites may have enhanced entry into brain. An example comes from a DAT radioligand, [*O-methyl*-^{11}C]β-CIT, which produces the more lipophilic and brain-penetrant [*O-methyl*-^{11}C]*nor*-β-CIT as a radiometabolite [231]. For most radioligands, however, peripheral metabolism results in radiometabolites showing lower lipophilicity than the parent radioligand. In such cases, the blood-brain barrier may often serve beneficially to preclude extensive entry of circulating radiometabolites into brain. This is an important consideration in the design of any brain radioligand, particularly with respect to selecting the molecular position for the label. As a caution, although peripheral radiometabolites that are less lipophilic than the parent radioligand are generally considered to have much less ability to cross the BBB, this cannot always be assumed. Thus, in the example of [^{18}F]altanserin, a significant radiometabolite is the less lipophilic alcohol, [^{18}F]altanserol, generated from reduction of its ketone moiety, which does enter brain [232].

Author Manuscript Author Manuscript Author Manuscript Author Manuscript

An often favored position for a carbon-11 label is in an aryl *O*-methyl group, as seen in [^{11}C]raclopride, [^{11}C]PBR28, [^{11}C](*R*)-rolipram, [^{11}C]RX-1, [^{11}C]Me-PPEP, [^{11}C]CUMI-101 and [^{11}C]RWAY (Table 4). Such groups are often susceptible to demethylation in the periphery to generate [^{11}C]formaldehyde, which is further oxidized to [^{11}C]carbon dioxide with negligible radioactive contamination of brain. A radioligand with a carbon-11 label in a secondary *N*-methyl-amino position may be metabolized similarly and therefore just as benignly. However, a radioligand with a carbon-11 label in a tertiary *N,N*-dimethylamino group has a risk of being cleaved by monoamine oxidase within the brain to release [^{11}C]dimethylamine, which then becomes protonated and unable to leave brain [233], or of being metabolized to the radioactive secondary methylamine, which may well enter brain and in some cases show some specific binding to the target or other proteins. A notable exception is the SERT radioligand, [^{11}C]MAD-AM, which performs acceptably well with the carbon-11 label in its dimethylamino position [234].

Tolyl compounds are known to be susceptible to oxidative metabolism to the corresponding aryl hydroxymethyl compounds and then through to the aryl carboxylic acid. A radioligand having a tolyl group has a risk of producing the radioactive hydroxymethyl compound and thenceforth the radioactive aryl carboxylic acid. An example is [^{11}C]PE2I, for which the radioactive hydroxymethyl metabolite is brain-penetrant in rat [235], and also possibly in human [236]. Although aryl methyl groups are amenable to labeling with carbon-11, caution is clearly warranted with regard to considering an aryl methyl group as a prospective site for a carbon-11 label.

Labeling with carbon-11 in an aryl *O*-methyl position is not guaranteed to avoid issues from radiometabolites, because metabolic transformations at other sites in such a radioligand may be significant and result in metabolites that retain the radiolabel. The 5-HT$_{1A}$ receptor radioligand, [*O-methyl*-^{11}C]WAY-100635, provides a classic example. In primates, including human, this radioligand is predominantly metabolized by amide hydrolysis to give a brain-penetrant and pharmacologically active amine radiometabolite, known as [^{11}C]WAY-100634 (Fig. 15) [237]. Although [*O-methyl*-^{11}C]WAY-100635 provided the first images of 5-HT$_{1A}$ receptor in human brain [121], the same ligand when labeled in the amide carbonyl position gave images with much lower nonspecific binding in cerebellum and hence higher contrast for receptor-rich regions [122]. For the carbonyl-labeled ligand, amide hydrolysis results in [*carbonyl*-^{11}C]cyclohexane-carboxylic acid and not [*O-methyl*-^{11}C]WAY-100634 as the radiometabolite [238]. The radioactive acid has poor ability to enter and accumulate in brain, and consequently nonspecific binding is decreased. Labeling on the carbonyl side of a metabolically vulnerable amide bond can therefore be an effective strategy to avoid extensive brain-penetrant radiometabolites. A similar strategy can be effective for metabolically vulnerable esters, as exemplified by the 5-HT$_4$ receptor radioligands, [^{11}C]RX-1 and [^{18}F]RX-2 [152].

A useful test of whether radiometabolites contaminate the PET signal seen in brain is whether placement of a radiolabel in another molecular position of the same ligand results in the same signal. Identical signals provide some assurance that radiometabolites are not an issue, whereas different uptakes indicate brain contamination by radiometabolite for at least one version of the radioligand. Thus, [^{11}C]flumazenil and [^{18}F]flumazenil have highly

Author Manuscript Author Manuscript Author Manuscript Author Manuscript

comparable human brain kinetics, thereby indicating that brain-penetrant radiometabolites are not an issue for either of these radioligands [239]. ^{11}C-Labeled methyl esters are readily prepared and have been explored as prospective radioligands. An example is the DAT radioligand [^{11}C]LBT-999. Aside from expected hydrolysis by widespread esterases, [^{11}C]LBT-999 is susceptible to metabolism by cytochrome P450 enzymes through tolyl group oxidation, *N*-dealkylation and tropane ring dehydrogenation [240]. LBT-999 labeled with fluorine-18 in its *N*-fluorobut-2-enyl group gave very different signal to [^{11}C]LBT-999 in baboon brain [241]. Neither radioligand was advanced to evaluation in human in anticipation of metabolism likely confounding quantification of radioligand-DAT interaction. In the studies of LBT-999, incubations in rat and liver microsomes with subsequent LC-MS-MS, and also radio-HPLC analysis of radiometabolites from excised rat brain, and of rat and human plasma following radioligand administration, were some of the techniques used to elucidate metabolic pathways.

Whereas radioanalytical methods can be applied to identify and measure radiometabolites in rodent brain following radioligand administration, this is clearly not so for human brain. Inspection of the stability of a quantitative outcome measurement, such as V_T, with respect to the duration of imaging data used to make the measurement may give some indication of whether radiometabolites enter brain or not. Highly unstable V_T values are indicative of radiometabolite contamination in brain, and stable values indicative of a lack of significant contamination. Generally, V_T values that stabilize within 10% of a terminal value are considered acceptable. Many such examples have been reported for stable V_T in monkey and in human. One radioligand showing exceptionally stable V_T in human is [^{18}F]FPEB [242].

The 5-HT$_{1A}$ receptor radioligand [*O-methyl*-^{11}C](*R*)-RWAY [127] was designed as a more easily labeled alternative to [*carbonyl*-^{11}C]WAY-100635, with an expected lower susceptibility to amide hydrolysis as a result of having a reversed amide bond direction. This radioligand was found to perform well in rhesus monkey, as judged by V_T stability [154]. However, this radioligand failed to give adequately stable V_T in human, likely because of increased generation and brain ingress of a moderately lipophilic radiometabolite that appears to correspond to that seen in monkey [156]. Hence, effective application of this radioligand has been confined to studies in monkey [155]. Findings with this radioligand affirm that even subtle species differences in extent or nature of metabolism may be critical to radioligand performance. In detailed studies, species differences in metabolic pathways and the rates of radiometabolite generation are invariably observed [232, 243, 244]. Generally, metabolism tends to be faster in experimental animals, especially rodent and pig, than in human subjects. Possible adverse metabolic effects therefore pose uncertainty when advancing an experimental radioligand to human evaluation following encouraging findings in animals.

Labeling with carbon-11 in the *N*-methyl position of a secondary amide has also proven to be effective in several instances, as for example in [^{11}C](*R*)-PK11195, [^{11}C]ER176, and [^{11}C]NOP-1A (Table 4). However, radioligands with a carbon-11 label in a tertiary di-methylamido group would be potentially susceptible to demethylation to give a brain-penetrant radiometabolite, as exemplified by the P-gp efflux transporter radiotracer [^{11}C]loperamide, which demethylates to [^{11}C]desmethyl loperamide ([^{11}C]dLop) [245].

Author Manuscript Author Manuscript Author Manuscript Author Manuscript

[^{11}C]dLop is in fact preferred as a radiotracer for the study of P-gp efflux transporter function, because of its less troublesome radiometabolite profile [246].

^{18}F-Labeled ligands raise their own specific concerns, of which susceptibility to radiodefluorination is paramount. Peripheral radiodefluorination of a radioligand will produce [^{18}F]fluoride ion in plasma which will then be taken up in bone, including skull. High radioactivity in skull compromises accurate measurement of radioactivity in brain regions near the skull, such as in neocortex, because of 'spill-over' effects. Table 7 summarizes observations on the susceptibility of ^{18}F-labeled sub-structures to radiodefluorinate in human subjects. In general, ^{18}F-fluorine atoms bound to carbons in homoaromatic groups (entries 1–6) and in substituted pyridinyl moieties (entries 7–13) show strong resistance to metabolic defluorination. [^{18}F]SP203 (entry 14) shows extensive radiodefluorination in rat and monkey but not in human, although there is moderate accumulation of radioactivity in skull [166]. This skull radioactivity is considered to be radioactivity in red marrow rather than in bone itself, based on the whole body radioactivity distribution showing high uptake in bone structures with high red marrow content, such as lumbar vertebrae [259]. Thus, species differences in the susceptibility of radioligands to radiodefluorination can occur.

Fluorine-18 present at the terminus of a straight saturated alkyl chain of two or more carbons appears quite resistant to defluorination in human subjects (entries 15, 19–28, 30, 31, 33). However, fluorine-18 at the terminus of the unsaturated carbon chain of [^{18}F]LBT-999 is highly susceptible to defluorination (entry 39), as is fluorine-18 attached to the secondary carbon in [^{18}F]FCWAY (entry 32). The severe radiodefluorination of [^{18}F]FCWAY that leads to very high uptake of radioactivity in human skull can be countered by pre-inhibition of the enzyme identified as being responsible, namely CYP2E1; the required inhibition is simply achievable with a single oral dose of Antabuse (disulfiram) [284]. Because peripheral radiodefluorination is inhibited, the radioligand is more available for brain entry and therefore enhanced images are obtained in the absence of appreciable skull radioactivity. Inhibition of metabolic enzymes has wider applicability for enhancing radioligand performance. Thus, inhibition of cytochrome CYP1A2 by fluvoxamine has been suggested for reducing the metabolism of the A1 adenosine receptor PET radioligand, [^{18}F]CPFPX (entry 37) [285]. Also inhibition of catechol *O*-methyl transferase with tolcapone has been proposed for avoiding a troublesome radiometabolite from the D_1 receptor agonist radioligand, (*R*)-[^{11}C]SKF 82957 [286]. A recently developed 5-HT_{1A} receptor radioligand, [^{18}F]Mefway, overcomes the defluorination issue seen with *trans*-[^{18}F]FCWAY by attaching fluorine-18 to a primary alkyl carbon (entry 33).

Radioligands labeled with fluorine-18 in aryl methoxy groups are well-known to be susceptible to radiodefluorination. Dideuteration of the methoxy group may reduce this susceptibility through an isotope effect, as for [^{18}F]FMPEP-d_2, [^{18}F]MENER-d_2, and [^{18}F]SPA-RQ (entries 16–18). As dideuteration is easily achievable, this has become virtually standard practice for this mode of labeling.

Aside from radiodefluorination, ^{18}F-labeled prosthetic groups in PET radioligands may present other issues. Thus, the *N*-[^{18}F]2-fluoroethyl group in [^{18}F]FECNT (entry 35) is

Author Manuscript Author Manuscript Author Manuscript Author Manuscript

susceptible to oxidative metabolism from liver cytochrome P-450 enzymes to produce [^{18}F]2-fluoroacetaldehyde, which may metabolically interchange with [^{18}F]2-fluoroethanol and [^{18}F]fluoroacetate. These two-carbon radiometabolites are able to traverse the BBB to confound brain radioligand quantification [167]. Other candidate radioligands, having an *N*-[^{18}F]2-fluoroethyl group, such as [^{18}F]FAMV for imaging vesicular acetylcholine transporter, also have limited utility because they likely produce [^{18}F]fluoroacetate as a brain-penetrant radiometabolite [287]. [^{18}F]Fluoroacetate itself may also be defluorinated within the brain. By contrast [^{18}F]FBR (entry 34), which has an [^{18}F]fluoroacetamido group, shows little tendency to radiodefluorinate, as do the [^{18}F]*N*-3-fluoropropyl groups in [^{18}F]CPFPX (entry 37) and [^{18}F]FPCIT (entry 38).

Finally, it should be noted that rapid peripheral metabolism of a radioligand to non brain-penetrant radiometabolites can be helpful rather than detrimental to radioligand performance, by decreasing radioligand in plasma and thereby free and nonspecifically bound radioligand in brain, which are all ideally in rapid equilibrium.

13. AMENABILITY TO ACCURATE QUANTIFICATION

Important questions with regard to the performance of a PET radioligand for brain imaging are not only the signal-to-noise ratio but also the utility of the radioligand for accurate quantification of the imaging target. The desirability of reliable and robust output measures, such as V_T, V_T/f_P, or BP_{ND}, was discussed above with regard to these measures being free of influences from radiometabolites in brain. As earlier mentioned, radioligands giving output measures that persistently stay within about 10% of the terminal value are usually regarded as adequately amenable to accurate quantification. The ability to derive stable measures is also dependent on the kinetics of the radioligand. Generally, PET radioligands intended to quantify brain proteins through reversible high-affinity binding should have sufficiently fast kinetics to show both accumulation and washout of radioactivity from the brain during the period of scanning [14]. Ideally, peak radioactivity in brain will occur relatively early so that the scanning session may be reasonably short and logistically acceptable to both subject and investigator. Data from the washout phase need to be adequate for accurate identifiability of kinetic parameters in the applied biomathematical model. For this purpose, it is typically desirable to acquire data covering more than 25% of the decline in radioactivity within brain.

14. AMENABILITY TO LABELING WITH ^{11}C OR ^{18}F

Research on developing methods for labeling compounds with carbon-11 or fluorine-18 to generate PET radiotracers has intensified over the last four decades, and has now resulted in an impressive arsenal of methods that renders most small drug-like molecules amenable to labeling in at least one molecular position. This methodology has been frequently reviewed at varying depths and from various perspectives, for example, either generally [288, 289], or with focus on either carbon-1l [290–293] or fluorine-18 [294–300]. Only a brief survey of this methodology is given here from the narrow perspective of developing reversibly binding brain PET radioligands.

Author Manuscript Author Manuscript Author Manuscript Author Manuscript

A primary requirement of any reversibly binding PET radioligand for imaging a protein target within the brain is for the carrier accompanying the radioligand to not cause appreciable occupancy of the available protein, and thereby invalidate the tracer assumptions underlying common quantification methods. In general, it is considered that any target occupancy should be kept below 5% [301]. Imaging targets are almost invariably present at very low densities (Tables 2 and 3), and therefore reversibly binding PET radioligands must be produced with low amounts of carrier that correspond to high specific activities. This is especially true for experiments in small animals [302, 303]. These specific activities are typically required to be greater than 40 GBq/μmol at time of administration to human, and even higher specific activities are always desirable.

The requirement for high specific activity imposes restrictions on the types of radiochemistry that can be used for preparing radioligands. Generally, reactions involving isotope exchange are ruled out because these will inevitably introduce carrier. Methods for producing the radionuclide, either carbon-11 or fluorine-18, must be no-carrier-added (NCA), and preferably very high yielding from modern medium-energy biomedical cyclotrons. Ideally, labeling procedures need to involve as few steps as possible, and be efficient and fast, to conserve activity as well as specific activity. The importance of the position of label for radioligand efficacy has already been stressed in this review. Hence, radiochemistry methods need to be available for labeling candidate PET radioligands at a position of choice. Carbon-11 and fluorine-18 pose different radiochemical challenges and possibilities, as summarized below.

14.1. Carbon-11

For carbon-11, the requirement for production at high yield and specific activity is well satisfied by the $^{14}N(p,\alpha)^{11}C$ reaction on nitrogen gas [304]. Several hundred GBq of carbon-11 can be prepared through this reaction on modern biomedical cyclotrons. Radioligands are produced with specific activities typically in the range 180–370 GBq/μmol [305, 306]. With rigorous precautions in production and labeling methodology, radioligands with impressively higher specific activities of up to about 5550 GBq/μmol may be obtained [305]. The chemical form obtained from the cyclotron irradiation may be [^{11}C]carbon dioxide [307] or [^{11}C]methane [308, 309], depending on whether the nitrogen gas target is doped with oxygen or hydrogen, respectively (Fig. 16). Radiochemistry aimed at preparing ^{11}C-labeled radioligands must begin with either of these two primary cyclotron-produced radioactive species, which may if required be readily interconverted on-line after cyclotron production [310, 311]. [^{11}C]Methane has no direct labeling utility, whereas [^{11}C]carbon dioxide has considerable reactivity that may be exploited to introduce a variety of labeled functional groups into radiotracers, including carboxyl, symmetrical and unsymmetrical urea groups, and carbamate groups [312]. Although alkyl and aryl carboxyl functions may be directly labeled with [^{11}C]carbon dioxide through reactions with for example Grignard reagents [312] or boronates [313], compounds with carboxyl groups are seldom effective PET radioligands for brain imaging because of their poor abilities to cross the BBB. Nonetheless, such ^{11}C-labeled carboxylic acids can generally be obtained rapidly in high yields, affording opportunities for onward conversion to other labeled compounds such as [^{11}C]amides [312, 313]. [^{11}C]*N*-Methylation has been achieved by direct

Author Manuscript Author Manuscript Author Manuscript Author Manuscript

[^{11}C]carboxylation of silanamines followed by reduction to prepare, for example, the D_1 receptor radioligand [^{11}C]SCH 23390 (Fig. 17) [314]. This method has not gained traction because of the general storage instability of the silanamines. In a recent adaptation, it has been shown that [^{11}C]carbon dioxide may be used to achieve [^{11}C]*N*-methylation reactions in two-steps [315]. This is an example of a recent drive towards more directly exploiting readily accessible [^{11}C]carbon dioxide in new labeling procedures for diverse functional groups [312], such as for labeling ureas [316] and carbamates [317] (Fig. 18). A major practical consideration in such direct uses of [^{11}C]carbon dioxide is to avoid carrier dilution by adventitious ingress of atmospheric carbon dioxide and reaction with precursor preceding or during the labeling reaction. Notwithstanding recent progress on advancing the utility of [^{11}C]carbon dioxide for direct labeling, primary cyclotron-produced ^{11}C-labeled precursors are still usually transformed into secondary labeling agents preceding any late-stage labeling reactions.

By far the most widely applied secondary labeling agent is [^{11}C]methyl iodide [318]. This labeling agent has direct utility for attaching a [^{11}C]methyl group to carbon in aryl rings or alkyl chains, or to heteroatoms, such oxygen in phenols and carboxylic acids, sulfur in thiophenols, and nitrogen in amines and amides (Fig. 19). For several years the production of [^{11}C]methyl iodide was based on reduction of cyclotron-produced [^{11}C]carbon dioxide with lithium aluminum hydride followed by treatment of the adduct with hydroiodic acid [319]. This so-called ‘wet procedure’ is especially prone to carrier dilution from the reaction of LAH reagent with any ingress of atmospheric carbon dioxide [320–322]. Methods for producing [^{11}C]methyl iodide by direct high temperature iodination of cyclotron-produced [^{11}C]methane have now been developed [323, 324]. One procedure involves several rapid recycles of unreacted [^{11}C]methane for iodination [324] and delivers [^{11}C]methyl iodide rapidly in high yield and in high specific activity. This method has become generally preferred [325, 326]. Many of the labeling reactions with [^{11}C]methyl iodide can be performed effectively at room temperature in a procedure, often dubbed the ‘loop method’, in which the labeling agent is passed into narrow bore stainless steel tubing that has been precoated with a small amount of desmethyl precursor [327, 328]. Desmethyl precursors are best prepared de novo rather than by demethylation of the target non-radioactive ligand because even trace impurities of non-demethylated compound may cause carrier dilution in the labeling reaction.

[^{11}C]Methyl iodide may be converted ‘on-line’ and efficiently into the more reactive ^{11}C-methylating agent, [^{11}C]methyl triflate by passage over heated silver triflate [329]. A much higher-yielding route to [^{11}C] methyl triflate is *via* [^{11}C]methyl bromide that has been produced from [^{11}C]methane [330]. [^{11}C]Methyl triflate has similar scope to [^{11}C]methyl iodide for labeling at heteroatoms but with lower reaction center selectivity. The use of [^{11}C]methyl triflate in place of [^{11}C]methyl iodide has been noted to improve the practical yields of various PET radioligands [331, 332].

Carbonyl functions appear frequently in small molecule drug-like structures as, for example, in esters and amides. One approach to labeling esters and amides in their carbonyl functions is through the use of ^{11}C-labeled acid chlorides. [^{11}C]Acid chlorides may be prepared in good yield from reactions of cyclotron-produced [^{11}C]carbon dioxide with an

Author Manuscript Author Manuscript Author Manuscript Author Manuscript

organometallic reagent, such as a Grignard reagent, followed by chlorination with a reagent such as phthaloyl dichloride, oxalyl chloride or thionyl chloride [333, 334] (Fig. 20). Volatile [^{11}C]acid chlorides are readily separated from reaction mixtures for subsequent reaction, as in the preparation of [^{11}C]cyclopropanecarbonyl chloride for the radiosynthesis of the opiate receptor radioligand, [^{11}C]diprenorphine [333]. Less volatile [^{11}C]acid chlorides may be produced and used in situ, such as [^{11}C]cyclohexanecarbonyl chloride for the production of the 5-HT$_{1A}$ receptor radioligand, [*carbonyl*-^{11}C]WAY-100635 [335, 336]. In the latter case, the labeling agent may be produced conveniently in a narrow polypropylene tube to which it adheres and is made available for reaction with the amine precursor [336]. As already indicated, strenuous precautions are needed to avoid excessive carrier dilution in reactions of [^{11}C]carbon dioxide with the Grignard reagent. For example, a commercial source of reagent may become unacceptably contaminated with carbon dioxide, and it may therefore need to be made freshly in-house with strict precautions against ingress of atmospheric carbon dioxide.

Carbon monoxide, although generally considered to be quite inert, shows rich chemistry in transition metal-mediated insertion reactions that may generate a variety of compound types, including ketones, acids, esters and amides. [^{11}C]Carbon monoxide may be produced on-line in high yield by passage of [^{11}C]carbon dioxide over heated zinc [337] or molybdenum [337, 338]. A major obstacle to the early application of [^{11}C]carbon monoxide to producing radiotracers was its low solubility in organic solvents. Various approaches have been adopted to surmount this obstacle, including the use of a high-pressure autoclave [339], transient and reversible trapping of the [^{11}C]carbon monoxide in solution [340], and even the generation of the [^{11}C]carbon monoxide from [^{11}C]carbon dioxide in solution [341]. A recent method uses xenon to carry [^{11}C]carbon monoxide efficiently into organic solution at room temperature and low pressure [342]. These advances have opened up the possibility to use [^{11}C]carbon monoxide to label a vast array of carbonyl-containing structural motifs (Fig. 21), often in high yields and without the need for protection-deprotection schemes [343–345]. Moreover, the achieved specific activities are generally very high as there is low risk for contamination of reactions by environmental carbon monoxide. [^{11}C]Carbon monoxide is now increasingly applied to producing PET radioligands (*e.g.* [^{11}C]FIMX) [346].

Another widely produced labeling agent is [^{11}C] hydrogen cyanide, which is especially useful for preparing aryl [^{11}C]nitriles from transition metal-promoted reactions with aryl halides [347] (Fig. 22), including PET radioligands for CB$_1$ receptors (*e.g.* [^{11}C]SD5024) [147] and mGluR5 receptors (*e.g.* [^{11}C]SP203 [348]). [^{11}C]Hydrogen cyanide is prepared by treating [^{11}C]methane with ammonia gas over heated platinum [147]. Experience has shown that radioligands produced from [^{11}C]hydrogen cyanide generally have lower specific activity than expected from the specific activity of the [^{11}C]methane precursor. A recent study has employed a micro-ion selective electrode to measure the specific activity of [^{11}C]cyanide [349].

Methods are available for preparing a myriad of other secondary labeling agents of as yet less utility and popularity than those mentioned above, including [^{11}C]formaldehyde [350, 351], higher [^{11}C]alkyl halides [352, 353], [^{11}C]nitroalkanes [354], [^{11}C]acetone [355],

Author Manuscript Author Manuscript Author Manuscript Author Manuscript

[^{11}C]phosgene [356–359], and [^{11}C]benzyl halides [360–362]. Readers are directed to the pertinent literature [350–362] for more details on such methods.

14.2. Fluorine-18

Although many methods are known for producing fluorine-18, the ^{18}O(p,n)^{18}F reaction on ^{18}O-enriched water has become almost universally applied, because of its high yield of up to several hundred GBq from modern biomedical cyclotrons [363]. The fluorine-18 is obtained in a single chemical form, namely [^{18}F]fluoride ion, at very high NCA specific activity. The [^{18}F]fluoride ion becomes an increasingly reactive nucleophile as water of hydration is removed [296]. In all labeling procedures, care is required to maintain high specific activity by avoiding carrier dilution from materials that may come into contact with the [^{18}F]fluoride ion, especially for example Teflon tubing [364]. With such precautions, specific activities of radiotracers are typically of the order of 180–370 GBq/μmol at end of synthesis, typically 1 to 2 half-lives after radionuclide production.

Classical aliphatic nucleophilic substitution reactions (notionally S_N1-type) on, for example alkyl bromides or tosylates, may be used to label some radioligands directly, such as [^{18}F]fallypride [365], [^{18}F]FBR [106], and [^{18}F]SP203 [165] (structures shown in Table 4). Aromatic nucleophilic substitutions in homoarenes (notionally S_NAr-type) can usually be achieved on substrates bearing good leaving groups (*e.g.* Br, NO_2, Me_3N^+) in ortho or para orientation to a strong electron-withdrawing group (*e.g.,* CO, NO_2, CN). The earlier mentioned radioligand [^{18}F]XB-1 (Table 4) is an example produced by such a process [159]. For some radioligands, such as [^{18}F]FPEB (Table 4), this type of procedure can also be adequately effective with a nitrile group in meta orientation [366]. Substituted [^{18}F]fluoropyridines may also be obtained from [^{18}F]fluoride ion, by displacement of good leaving groups (Br, NO_2, Me_3N^+). Activation by an electron-withdrawing group is generally needed for introducing [^{18}F]fluoride ion into the meta position, but not usually for ortho or para position. These nucleophilic substitution reactions have been extensively reviewed [367, 368].

Over the last two decades, the introduction of hypervalent iodine precursors, such as diaryliodonium salts [369, 370] and aryl ylides [371, 372], has expanded the chemical space that can be labeled with [^{18}F]fluoride ion to include electron-rich aromatic rings, as recently reviewed [373–375] (Fig. 23). [^{18}F]Flumazenil [376] and [^{18}F]FIMX [107] are notable examples of radioligands that have been produced regularly from such hypervalent precursors.

More recently, progress has been made in achieving aryl ring radiofluorination through copper-mediated reactions on substrates, such as diaryliodonium salts [377], aryl boronic acids [378], and aryl boronate esters [379] (Fig. 24). These labeling reactions have wider scope than classical S_NAr reactions, as they are readily applicable to labeling both electron-rich and electron-deficient arenes, irrespective of substitution patterns. The synthetic accessibility of stable arylboron precursors is also attractive.

Direct methods for labeling with [^{18}F]fluoride ion have not always been applicable or preferred. Hence, several methods have been developed for converting [^{18}F]fluoride ion

Author Manuscript Author Manuscript Author Manuscript Author Manuscript

efficiently into secondary labeling agents, particularly electrophilic agents. Prominent examples are [^{18}F]dideuterated fluoromethyl bromide and higher functionalized [^{18}F]fluoroalkanes, such as [^{18}F]2-fluoroethyl tosylate [380] and bromide [381], and ring radiofluorinated benzaldehydes and benzyl halides [382] (Fig. 25).

Many structural motifs that are common in small drug-like molecules have until recently been neglected as possible sites for introduction of a positron-emitter, because of the perceived difficulty of doing so at an NCA level of specific activity. A recent drive in fluorine-18 radiochemistry is now to open up methods for labeling such structural motifs. For example, significant progress has been made in developing methods for labeling alkyl [383] and aryl trifluoromethyl groups [384–387] (Fig. 26).

CONCLUSION

The development of reversibly binding PET radio-ligands for brain imaging poses enormous challenges to chemists and other scientists, and is vulnerable to many factors that may cause failure at any stage. A strong appreciation of the many considerations that are important to such PET radioligand development, as outlined in this article, will hopefully aid chemists to avoid the most obvious pitfalls and to maximize their chances of success. Considerable success is indeed possible as evidenced by the now widespread use of many useful PET radioligands.

Supplementary Material

Refer to Web version on PubMed Central for supplementary material.

Acknowledgments

This work was supported by the Intramural Research Program of the National Institutes of Health (NIMH; ZIA MH002793). The author is grateful to Dr. Shuiyu Lu (NIMH) for critical reading of the manuscript. The author is also grateful to numerous coauthors for their contributions to research cited by the author in this article.

References

1. Imming P, Sinning C, Meyer A. Drugs, their targets and the nature and number of drug targets. Nature Rev. 2007; 5:821–834.
2. Heiss WD, Herholz K. Brain receptor imaging. J Nucl Med. 2006; 47:302–312. [PubMed: 16455637]
3. Politis M, Piccini P. Positron emission tomography imaging in neurological disorders. J Neurol. 2012; 259:1769–1780. [PubMed: 22297461]
4. Savitz JB, Drevets WC. Neuroreceptor imaging in depression. Neurobiol Dis. 2013; 52:49–65. [PubMed: 22691454]
5. Hargreaves RJ. The role of molecular imaging in drug discovery and development. Clin Pharmacol Ther. 2008; 83:349–353. [PubMed: 18167503]
6. Farde L. The advantage of using positron emission tomography in drug research. Trends Neurosci. 1996; 19:211–214. [PubMed: 8761953]
7. Matthews PM, Rabiner EA, Passchier J, Gunn RN. Positron emission tomography molecular imaging for drug development. Br J Clin Pharmacol. 2011; 73:175–186.
8. Piel M, Vernaleken I, Rösch F. Positron emission tomography in CNS drug discovery and drug monitoring. J Med Chem. 2014; 57:9232–9258. [PubMed: 25144329]

Author Manuscript Author Manuscript Author Manuscript Author Manuscript

9. Kung MP, Stevenson DA, Plössl K, Meegalla SK, Beckwith A, Essman WD, Mu M, Lucki I, Kung HF. [^{99m}Tc]TRODAT-1: a novel technetium-99m complex as a dopamine transporter imaging agent. Eur J Nucl Med. 1997; 24:372–380. [PubMed: 9096087]
10. Guo Y, Chen X, Jia H, Ji X, Liu B. Synthesis and biological evaluation of one novel technetium-99m-labeled nitroquipazine derivative as an imaging agent for serotonin transporter. Appl Radiat Isot. 2008; 66:1804–1809. [PubMed: 18684634]
11. Pike VW. Positron-emitting radioligands for studies *in vivo* - probes for human psychopharmacology. J Psychopharmacology. 1993; 7:139–158.
12. Kegeles LS, Mann JJ. *In vivo* imaging of neurotransmitter systems using radiolabeled receptor ligands. Neuropsychopharmacology. 1997; 17:293–307. [PubMed: 9348545]
13. Halldin C, Gulyás B, Langer O, Farde L. Brain radioligands - state of the art and new trends. Q J Nucl Med. 2001; 45:139–152. [PubMed: 11476163]
14. Laruelle M, Slifstein M, Huang Y. Relationships between radiotracer properties and image quality in molecular imaging of the brain with positron emission tomography. Mol Imaging Biol. 2003; 5:363–375. [PubMed: 14667491]
15. Wong DF, Pomper MG. Predicting the success of a radiopharmaceutical for *in vivo* imaging of central nervous system neuroreceptor systems. Mol Imaging Biol. 2003; 5:350–362. [PubMed: 14667490]
16. Eckelman WC, Kilbourn MR, Mathis CA. Discussion of targeting proteins *in vivo: in vitro* guidelines. Nucl Med Biol. 2006; 33:449–451. [PubMed: 16720235]
17. Patel S, Gibson R. *In vivo* site-directed radiotracers: a mini-review. Nucl Med Biol. 2008; 35:805–815. [PubMed: 19026942]
18. van de Bittner GC, Ricq EL, Hooker JM. A philosophy of CNS radiotracer design. Acc Chem Res. 2014; 47:3127–3134. [PubMed: 25272291]
19. Brust P, van den Hoff J, Steinbach J. Development of ^{18}F-labeled radiotracers for neuroreceptor imaging with positron emission tomography. Neurosci Bull. 2014; 30:777–811. [PubMed: 25172118]
20. Varnäs K, Varrone A, Farde L. Modeling of PET data in CNS drug discovery and development. J Pharmokinet Pharmacodyn. 2013; 40:267–279.
21. Gunn RN, Slifstein M, Searle GE, Price JC. Quantitative imaging of protein targets in the human brain with PET. Phys Med Biol. 2015; 60:R363–R411. [PubMed: 26513176]
22. Mintun MA, Raichle ME, Kilbourn MR, Wooten GF, Welch MJ. A quantitative model for the *in vivo* assessment of drug binding sites with positron emission tomography. Ann Neurol. 1984; 15:217–227. [PubMed: 6609679]
23. Innis RB, Cunningham VJ, Delforge J, Fujita M, Gjedde A, Gunn RN, Holden J, Houle S, Huang SC, Ichise M, Iida H, Ito H, Kimura Y, Koeppe RA, Knudsen GM, Knuuti J, Lammertsma AA, Laruelle M, Logan J, Maguire RP, Mintun MA, Morris ED, Parsey R, Price JC, Slifstein M, Soss V, Suhara T, Votaw JR, Wong DF, Carson RE. Consensus nomenclature for *in vivo* imaging of reversibly binding radioligands. J Cereb Blood Flow Metab. 2007; 27:1533–1539. [PubMed: 17519979]
24. Zanotti-Fregonara P, Hines CS, Zoghbi SS, Liow J-S, Zhang Y, Pike VW, Drevets WC, Mallinger AG, Zarate CA Jr, Fujita M, Innis RB. Population-based input function and image-derived input function for [^{11}C](*R*)-rolipram PET imaging: methodology, validation and application to the study of major depressive disorder. NeuroImage. 2012; 63:1532–1541. [PubMed: 22906792]
25. Lammertsma AA, Hume SP. Simplified reference tissue model for PET receptor studies. NeuroImage. 1996; 4:153–158. [PubMed: 9345505]
26. Gunn RN, Lammertsma AA, Hume SP, Cunningham VJ. Parametric imaging of ligand-receptor binding in PET using a simplified reference region model. NeuroImage. 1997; 6:279–287. [PubMed: 9417971]
27. Logan J, Fowler JS, Volkow ND, Wolf AP, Dewey SL, Schlyer DJ, MacGregor RR, Hitzemann R, Bendriem B, Gatley SJ, Christman DR. Graphical analysis of reversible radioligand binding from time-activity measurements applied to [*N*-^{11}C-methyl]-(−)-cocaine PET studies in human subjects. J Cereb Blood Flow Metab. 1990; 10:740–747. [PubMed: 2384545]

Author Manuscript Author Manuscript Author Manuscript Author Manuscript

28. Logan J, Fowler JS, Volkow ND, Wang GJ, Ding YS, Alexoff DL. Distribution volume ratios without blood sampling from graphical analysis of PET data. J Cereb Blood Flow Metab. 1996; 16:834–840. [PubMed: 8784228]
29. Logan J. Graphical analysis of PET data applied to reversible and irreversible tracers. Nucl Med Biol. 2000; 27:661–670. [PubMed: 11091109]
30. Itoh T, Abe K, Zoghbi SS, Inoue O, Hong J, Imaizumo M, Pike VW, Innis RB, Fujita M. PET measurement of the *in vivo* affinity of ^{11}C-(*R*)-rolipram and the density of its target, phosphodiesterase-4, in the brains of conscious and anaesthetized rats. J Nucl Med. 2009; 50:749–756. [PubMed: 19372471]
31. Farde L, Ginovart N, Itoh H, Lundkvist C, Pike VW, McCarron JA, Halldin C. PET-characterisation of [*carbonyl*-^{11}C]WAY-100635 binding to 5-HT_{1A} receptors in the primate brain. Psychopharmacology. 1997; 133:196–202. [PubMed: 9342787]
32. Farde L, Hall H, Ehrin E, Sedvall G. Quantitative analysis of D_2 receptor binding in the living human brain by PET. Science. 1986; 231:258–261. [PubMed: 2867601]
33. Sadzot B, Price JC, Mayberg HS, Douglass KH, Dannals RF, Lever JR, Ravert HT, Wilson AA, Wagner HN Jr, Feldman MA, Frost JJ. Quantification of human opiate receptor concentration and affinity using high and low specific activity [^{11}C]diprenorphine and positron emission tomography. J Cereb Blood Flow Metab. 1991; 11:204–219. [PubMed: 1847703]
34. Abadie P, Baron JC, Bissserbe JC, Boulenger JP, Rioux P, Travère JM, Barré L, Petit-Taboué C, Zarifan E. Central benzodiazepine receptors in human brain: estimation of regional B_{max} and K_D values with positron emission tomography. Eur J Pharmacol. 1992; 213:107–115. [PubMed: 1323469]
35. Delforge J, Spelle L, Bendriem B, Samson Y, Syrota A. Parametric images of benzodiazepine receptor concentration using a partial-saturation injection. J Cereb Blood Flow Metab. 1997; 17:343–355. [PubMed: 9119907]
36. Shrestha S, Hirvonen J, Hines CS, Henter I, Svenningsson P, Pike VW, Innis RB. Serotonin-1A receptors in major depression quantified using PET: controversies, confounds, and recommendations. NeuroImage. 2012; 59:3243–3251. [PubMed: 22155042]
37. Mathis CA, Mason NS, Lopresti BJ, Klunk WE. Development of positron emission tomography β-amyloid plaque imaging agents. Semin Nucl Med. 2012; 42:423–432. [PubMed: 23026364]
38. Kung HF. The β-amyloid hypothesis in Alzheimer's disease: seeing is believing. ACS Med Chem Lett. 2012; 3:265–267. [PubMed: 24936237]
39. Owen DRJ, Matthews PM. Imaging brain microglial activation using positron emission tomography and translocator protein-specific radioligands. Int Rev Neurobiol. 2011; 101:19–39. [PubMed: 22050847]
40. Kreisl WC, Mbeo G, Fujita M, Zoghbi SS, Pike VW, Innis RB, McArthur JC. Stroke incidentally identified using improved positron emission tomography for microglial activation. Arch Neurol. 2009; 66:1288–1289. [PubMed: 19822787]
41. Hirvonen J, Kreisl WC, Fujita M, Dustin I, Khan O, Appel S, Zhang Y, Morse C, Pike VW, Innis RB, Theodore WH. Increased *in vivo* expression of an inflammatory marker in temporal lobe epilepsy. J Nucl Med. 2012; 53:234–240. [PubMed: 22238156]
42. Kreisl WC, Lyoo CH, McGwier M, Snow J, Jenko KJ, Corona W, Morse CL, Zoghbi SS, Pike VW, McMahon FJ, Turner RS, Innis RB. Biomarkers Consortium PET Radioligand Project Team. PET radioligand binding to translocator protein correlates with severity of Alzheimer's disease and may mark conversion from mild cognitive impairment. Brain. 2013; 136:2228–2238. [PubMed: 23775979]
43. Kreisl WC, Fujita M, Fujimura Y, Kimura N, Jenko KJ, Kannan P, Hong J, Morse CL, Zoghbi SS, Gladding RL, Jacobson S, Oh U, Pike VW, Innis RB. Comparison of [^{11}C]-(*R*)-PK 11195 and [^{11}C]PBR28, two radioligands for translocator protein (18kDa) in human and monkey: implications for positron emission tomographic imaging of this inflammation biomarker. NeuroImage. 2010; 49:2024–2932.
44. Owen DR, Yeo AJ, Gunn RN, Song K, Wadsworth G, Lewis A, Rhodes C, Pulford DJ, Bennacef I, Parker CA, St Jean PL, Cardon LR, Mooser VE, Matthews PM, Rabiner EA, Rubio JP. An 18-kDa

Author Manuscript Author Manuscript Author Manuscript Author Manuscript

translocator protein (TSPO) polymorphism explains differences in binding affinity of the PET radioligand PBR28. J Cereb Blood Flow Metab. 2012; 32:1–5. [PubMed: 22008728]

45. Kreisl WC, Jenko KJ, Hines CS, Lyoo CH, Corona W, Morse CL, Zoghbi SS, Hyde T, Kleinman JE, Pike VW, McMahon FJ, Innis RB. Biomarkers Consortium PET Radioligand Project Team. A genetic polymorphism for translocator protein 18 kDa affects both *in vitro* and *in vivo* radioligand binding in human brain to this putative biomarker of neuroinflammation. J Cereb Blood Flow Metab. 2013; 33:53–58. [PubMed: 22968319]
46. Owen DR, Howell OW, Tang SP, Wells SA, Bennacef I, Bergstrom BM, Gunn RN, Rabiner EA, Wilkins MR, Reynolds R, Matthews PM, Parker CA. Two binding sites for [^{3}H]PBR28 in human brain: implications for TSPO PET imaging of neuroinflammation. J Cereb Blood Flow Metab. 2010; 30:1608–1618. [PubMed: 20424634]
47. Owen DRJ, Gunn RN, Rabiner EA, Bennacef I, Fujita M, Kreisl WC, Innis RB, Pike VW, Reynolds R, Matthews PM, Parker CA. Mixed-affinity binding in humans with 18-kDa translocator protein ligands. J Nucl Med. 2011; 52:24–32. [PubMed: 21149489]
48. Pike VW, Taliani S, Lohith TG, Owen DRJ, Pugliesi I, Da Pozzo E, Hong J, Zoghbi SS, Gunn RN, Parker CA, Rabiner EA, Fujita M, Innis RB, Martini C, Da Settimo F. Evaluation of novel N^1-methyl-2-phenylindol-3-ylglyoxylamides as a new chemotype of 18 kDa translocator protein-selective ligand suitable for the development of positron emission tomography radioligands. J Med Chem. 2011; 54:366–373. [PubMed: 21133364]
49. Mizrahi R, Rusjan PM, Kennedy J, Pollock B, Mulsant B, Suridjan I, De Luca V, Wilson AA, Houle S. Translocator protein (18 kDa) polymorphism (rs 6971) explains in-vivo brain binding affinity of the PET radioligand [^{18}F]-FEPPA. J Cereb Blood Flow Metab. 2012; 32:968–972. [PubMed: 22472607]
50. Willeit M, Praschak-Rieder N. Imaging the effects of genetic polymorphisms on radioligand binding in the living human brain: a review on genetic neuroreceptor imaging of monoaminergic systems in psychiatry. NeuroImage. 2010; 53:878–892. [PubMed: 20399868]
51. Hall H, Halldin C, Farde L, Sedvall G. Whole hemisphere autoradiography of the postmortem human brain. Nucl Med Biol. 1998; 25:715–719. [PubMed: 9863555]
52. Varnäs K, Halldin C, Hall H. Autoradiographic distribution of serotonin transporters and receptor subtypes in human brain. Human Brain Mapping. 2004; 22:246–260. [PubMed: 15195291]
53. Långström B, Andrén PE, Lindhe Ö, Svedberg M, Hall H. *In vitro* imaging techniques in neurodegenerative diseases. Mol Imaging Biol. 2007; 9:161–175. [PubMed: 17318669]
54. Svedberg MM, Hall H, Hellstrom-Lindahl E, Estrada S, Guan Z, Nordberg A, Långström B. [^{11}C]PIB-amyloid binding and levels of Aβ40 and Aβ42 in postmortem brain tissue from Alzheimer patients. Neurochem Int. 2009; 54:347–357. [PubMed: 19162107]
55. Gulyás B, Brockschnieder D, Nag S, Pavlova E, Kasá P, Beliczai Z, Légrádi A, Gulya K, Thiele A, Dyrks T, Halldin C. The norepinephrine transporter (NET) radioligand (*S,S*)-[^{18}F]FMeNER-D_2 shows significant decreases in NET density in the human brain in Alzheimer's disease: a post mortem autoradiographic study. Neurochem Int. 2010; 56:789–798. [PubMed: 20211213]
56. Young, AB., Frey, KA., Agranoff, BW. Positron Emission Tomography and Autoradiography: Principles and Applications for the Brain and Heart. In: Phelps, ME.Mazziotta, JC., Schelbert, HR., editors. *In Vitro* and *In Vivo*. Vol. Ch 2. Raven Press; New York: 1986. p. 73-111.
57. Banay-Schwartz M, Kenessey A, DeGuzman T, Lajtham A, Palkovits M. Protein content of various regions of rat brain and adult and aging human brain. Age. 1992; 15:51–54.
58. Marutle A, Warpmann U, Bogdanovic N, Nordberg A. Regional distribution of subtypes of nicotinic receptors in human brain and effect of aging studied with (+)-[^{3}H]epibatidine. Brain Res. 1998; 801:143–149. [PubMed: 9729344]
59. Sihver W, Gillberg PG, Nordberg A. Laminar distribution of nicotinic receptor subtypes in human cerebral cortex as determined by [^{3}H](−)nicotine, [^{3}H]cytosine and [^{3}H]epibatidine *in vitro* autoradiography. Neuroscience. 1998; 85:1121–1133. [PubMed: 9681951]
60. Cumming P. Absolute abundances and affinity states of dopamine receptors in mammalian brain: a review. Synapse. 2011; 65:892–909. [PubMed: 21308799]

Author Manuscript Author Manuscript Author Manuscript Author Manuscript

61. Burnett PWJ, Eastwood SL, Harrison PJ. [^{3}H]WAY-100635 for 5-HT$_{1A}$ receptor autoradiography in human brain: a comparison with [^{3}H]8-OH-DPAT and demonstration of increased binding in the frontal cortex in schizophrenia. Neurochem Int. 1997; 30:565–574. [PubMed: 9152998]
62. Reynolds GP, Mason SL, Meldrum A, De Keczer S, Parnes H, Eglen RM, Wong EHF. 5-Hydroxytryptamine (5-HT)$_4$ receptors in post mortem human brain tissue: distribution, pharmacology and effects of neurodegenerative diseases. Br J Pharmacol. 1995; 114:993–998. [PubMed: 7780656]
63. Arranz B, Rosel P, San L, Sarro S, Navarro MA, Marcusson J. Characterization of the 5-HT$_4$ binding site in human brain. J Neural Transm. 1998; 105:575–586. [PubMed: 9826103]
64. Hirst WD, Minton JAL, Bromidge SM, Moss SF, Latter AJ, Riley GR, Routledge C, Middlemiss DN, Price GW. Characterization of [^{125}I]-SB-258585 binding to human recombinant and native 5-HT$_6$ receptors in rat, pig and human brain tissue. Br J Pharmacol. 2000; 130:1597–1605. [PubMed: 10928963]
65. Gündish D, Koren AO, Horti AG, Pavlova OA, Kimes AS, Muhkin AG, London ED. *In vitro* characterization of 6-[^{18}F]fluoro-A-85380, a high affinity ligand for $\alpha_4\beta_2$ nicotinic acetylcholine receptors. Synapse. 2005; 55:89–87. [PubMed: 15529332]
66. Svedberg MM, Hall H, Hellström-Lindahal E, Estrada S, Guan Z, Nordberg A, Långström B. [^{11}C]PIB-amyloid binding and levels of Aβ40 and Aβ42 in postmortem brain tissue form Alzheimer patients. Neurochem Int. 2009; 54:347–357. [PubMed: 19162107]
67. Kopp J, Hall H, Persson AM, Sedvall G. Temperature dependence of [^{3}H]Ro-15–1788 binding to benzodiazepine receptors in human post mortem brain homogenates. J Neurochem. 1990; 55:1310–1315. [PubMed: 2168936]
68. Hall H, Litton J-E, Halldin C, Kopp J, Sedvall G. Studies on the binding of [^{3}H]flumazenil and [^{3}H]sarmazenil in post-mortem human brain. Human Psychopharmacology. 1992; 7:367–377.
69. Jenko KJ, Hirvonen J, Henter IO, Anderson KB, Zoghbi SS, Hyde TM, Soboslay AD, Innis RB, Kleinman JE. Binding of a tritiated inverse agonist to cannabinoid CB$_1$ receptors is increased in patients with schizophrenia. Schizophrenia Res. 2012; 141:185–188.
70. Montague DM, Lawler CP, Mailman RB, Gilmore JH. Developmental regulation of the dopamine D$_1$ receptor in human caudate and putamen. Neuropsychopharmacology. 1999; 21:641–649. [PubMed: 10516960]
71. Hall G, Wedel I, Halldin C, Kopp J, Farde L. Comparison of the *in vitro* receptor binding properties of *N*[^{3}H]methylspiperone and [^{3}H]raclopride to rat and human brain membranes. J Neurochem. 1990; 55:2048–2057. [PubMed: 1977888]
72. Tang SW, Helmeste DM, Fang H, Li M, Vu R, Bunney W Jr, Potkin S, Jones EG. Differential labeling of dopamine and sigma sites by [^{3}H]nemonapride and [^{3}H]raclopide in postmortem human brains. Brain Res. 1997; 765:7–12. [PubMed: 9310388]
73. Staley JK, Basile M, Flynn DD, Mash DC. Visualizing dopamine and serotonin transporters in the human brain with the potent cocaine analog [^{125}I]RTI-55: *in vitro* binding and autoradiographic characterization. J Neurochem. 1994; 62:549–556. [PubMed: 8294917]
74. Herdon HJ, Roberts JC, Coulton S, Porter RA. Pharmacological characterization of the GlyT-1 glycine transporter using two novel radioligands. Neuropharmacology. 2010; 59:558–565. [PubMed: 20691713]
75. Patel S, Hamill T, Connolly B, Jagoda E, Li W, Gibson RE. Species differences in mGluR5 binding sites in mammalian central nervous system determined using *in vitro* binding with [^{18}F]F-PEB. Nucl Med Biol. 2007; 34:1009–1017. [PubMed: 17998106]
76. Pfeiffer A, Pasi A, Mehraein P, Herz A. Opiate receptor binding sites in human brain. Brain Res. 1982; 248:87–96. [PubMed: 6289997]
77. Dean B, Scarr E, Pavey G, Copolov D. Studies on serotonergic markers in the human hippocampus: changes in subjects with bipolar disorder. J Affect Disord. 2003; 75:65–69. [PubMed: 12781352]
78. Griffante C, Carletti R, Andreetta F, Corsi M. [^{3}H]GR205171 displays similar NK$_1$ receptor binding profile in gerbil and human brain. Br J Pharmacol. 2006; 148:39–45. [PubMed: 16501582]

Author Manuscript Author Manuscript Author Manuscript Author Manuscript

79. Rao VLR, Butterworth RF. Characterization of binding sites for the $_3$ receptor ligands [^{3}H]PK11195 and [^{3}H]RO5–4864 in human brain. Eur J Pharmacol. 1997; 340:89–99. [PubMed: 9527511]
80. Fujita M, Imaizumi M, Zoghbi SS, Fujimura Y, Farris AG, Suhara T, Hong J, Pike VW, Innis RB. Kinetic analysis in healthy humans of a novel positron emission tomography radioligand to image the peripheral benzodiazepine receptor, a potential biomarker for inflammation. NeuroImage. 2008; 40:43–52. [PubMed: 18093844]
81. Bylund DB, Teows ML. Radioligand binding methods - practical guide and tips. Am J Physiol. 1993; 265:L421–L429. [PubMed: 8238529]
82. Cai L, Innis RB, Pike VW. Radioligand development for PET imaging of β-amyloid (Aβ) - current status. Curr Med Chem. 2007; 14:19–52. [PubMed: 17266566]
83. Keen, M. Methods in Molecular Biology. Vol. 106. Humana Press; Totowa, NJ: 1999.
84. Noguchi J, Zhang M-R, Yanamoto K, Nakao R, Suzuki K. *In vitro* binding of [^{11}C]raclopride with ultrahigh specific activity in rat brain determined by homogenate assay and autoradiography. Nucl Med Biol. 2008; 35:19–27. [PubMed: 18158939]
85. Harada R, Okamura N, Furumoto S, Tago T, Maruyama M, Higuchi M, Yoshikawa T, Arai H, Iwata R, Kudo Y, Yanai K. Comparison of the binding characteristics of [^{18}F]THK-523 and other amyloid imaging tracers to Alzheimer's disease pathology. Eur J Nucl Med Mol Imaging. 2013; 40:125–132. [PubMed: 23100049]
86. Cheng Y-C, Prusoff WH. Relationship between the inhibition constant (*K*i) and the concentration of inhibitor which causes 50 per cent inhibition (I_{50}) of an enzymatic reaction. Biochem Pharmacol. 1973; 22:3099–3108. [PubMed: 4202581]
87. Hulme EC, Trevethick MA. Ligand binding assays at equilibrium: validation and interpretation. Br J Pharmacol. 2010; 161:1219–1237. [PubMed: 20132208]
88. Slifstein M, Hwang D-R, Huang Y, Guo N-N, Sudo Y, Narendran R, Talbot P, Laruelle M. *In vivo* affinity of [^{18}F]fallypride for striatal and extrastriatal dopamine D_2 receptors in nonhuman primates. Psychopharmacology. 2004; 175:274–286. [PubMed: 15024551]
89. Strange PG. Use of the GTPγS ([^{35}S]GTPγS and Eu-GTPγS) binding assay for analysis of ligand potency and efficacy at G protein-coupled receptors. Br J Pharmacol. 2010; 161:1238–1249. [PubMed: 20662841]
90. Zhang R, Xie X. Tools for GPCR drug discovery. Acta Pharmacologica Sinica. 2012; 33:372–384. [PubMed: 22266728]
91. de Jong LAA, Uges DRA, Franke JP, Bischoff R. Receptor-ligand binding assays: technologies and applications. J Chromatogr B. 2005; 829:1–25.
92. Olsson H, Halldin C, Swahn C-G, Farde L. Quantification of [^{11}C]FLB 457 binding to extrastriatal dopamine receptors in the human brain. J Cereb Blood Flow Metab. 1999; 19:1164–1173. [PubMed: 10532641]
93. Horti AG, Villemagne VL. The quest for Eldorado: development of radioligands for *in vivo* imaging of nicotinic acetylcholine receptors in human brain. Curr Radiopharm Des. 2006; 12:3877–3900.
94. Delforge J, Spelle L, Bendriem B, Samson Y, Bottlaender M, Papageorgiou S, Syrota A. Quantitation of benzodiazepine receptors in human brain using the partial saturation method. J Nucl Med. 1996; 37:5–11. [PubMed: 8544001]
95. Karlsson MD, Farde L, Halldin C, Sedvall G. PET study of D_1 dopamine receptor binding in neuroleptic-naïve patients with schizophrenia. Am J Psychiatry. 2002; 159:761–767. [PubMed: 11986129]
96. Farde L, Wiesel F-X, Stone-Elander S, Halldin C, Nordstrom A-L, Hall H, Sedvall G. D_2 dopamine receptors in neuroleptic-naïve schizophrenic patients. Arch Gen Psychiatry. 1990; 47:213–219. [PubMed: 1968328]
97. Hietala J, Någren K, Lehikoinen P, Ruotsalainen U, Syvälahati E. Measurement of striatal D_2 dopamine receptor density and affinity with [^{11}C]-raclopride *in vivo*: a test-retest analysis. J Cereb Blood Flow Metab. 1999; 19:210–217. [PubMed: 10027776]

Author Manuscript Author Manuscript Author Manuscript Author Manuscript

98. Suhara T, Sudo Y, Okauchi T, Maeda J, Kawabe K, Suzuki K, Okubo Y, Nakashima Y, Ito H, Tanada S, Halldin C, Farde L. Extrastriatal dopamine D_2 receptor density and affinity in the human brain measured by 3D PET. Int J Neuropsychopharmacology. 1999; 2:734–782.

99. Guo Q, Brady M, Gunn RN. A biomathematical modeling approach to central nervous system radioligand discovery and development. J Nucl Med. 2009; 50:1715–1723. [PubMed: 19759115]

100. Pike VW. PET radiotracers: crossing the blood-brain barrier and surviving metabolism. Trends Pharmacol Sci. 2009; 30:431–440. [PubMed: 19616318]

101. Slifstein M, Kegeles LS, Gonzales R, Frankle WG, Xu X, Laruelle M, Abi-Dargham A. [^{11}C]NNC 112 selectivity for dopamine D_1 and serotonin 5-HT_{2A} receptors: a PET study in healthy human subjects. J Cereb Blood Flow Metab. 2007; 27:1733–1741. [PubMed: 17311076]

102. Huang Y, Zheng M-Q, Gerdes JM. Development of effective PET and SPECT imaging agents for the serotonin transporter: has a twenty-year journey reached its destination? Curr Top Med Chem. 2010; 10:1499–1526. [PubMed: 20583995]

103. Schafer KN, Kim S, Matzavinos A, Kuret J. Selectivity requirements for diagnostic imaging of neurofibrillary lesions in Alzheimer's disease: a simulation study. NeuroI-mage. 2012; 60:1724–1733.

104. Donohue SR, Dannals RF, Halldin C, Pike VW. *N*-(4-Cyanotetrahydro-2*H*-pyran-4-yl) and *N*-(1-cyanocyclohexyl) derivatives of 1,5-diarylpyrazole-3-carboxamides showing high affinity for 18 kDa translocator protein and/or cannabinoid receptors. J Med Chem. 2011; 54:2961–2970. [PubMed: 21428406]

105. Briard E, Zoghbi SS, Imaizumi M, Gourley JP, Shetty HU, Hong J, Cropley V, Fujita M, Innis RB, Pike VW. Synthesis and evaluation in monkey of two sensitive ^{11}C-labeled aryloxyanilide ligands for imaging brain peripheral benzodiazepine receptors. in vivo J Med Chem. 2008; 51:17–30.

106. Briard E, Zoghbi SS, Siméon FG, Imaizumi M, Gourley JP, Shetty HU, Lu SY, Fujita M, Innis RB, Pike VW. Single-step high-yield radiosynthesis and evaluation of a sensitive, ^{18}F-labeled ligand for imaging brain peripheral benzodiazepine receptors with PET. J Med Chem. 2009; 52:688–699. [PubMed: 19119848]

107. Xu R, Zanotti-Fregonara P, Zoghbi SS, Gladding RL, Woock AE, Innis RB, Pike VW. Synthesis and evaluation in monkey of [^{18}F]4-fluoro-*N*-methyl-*N*-(4-(6-(methyl-annino)pyrimidin-4-yl)thiazol-2-yl)benzamide ([^{18}F] FIMX): a promising radioligand for PET imaging of brain metabotropic glutamate receptor 1 (mGluR1). J Med Chem. 2013; 56:9146–9155. [PubMed: 24147864]

108. Pike VW, Halldin C, Crouzel C, Barré L, Nutt DJ, Osman S, Shah F, Turton DR, Waters SL. Radioligands for PET studies of central benzodiazepine receptors and PK (peripheral benzodiazepine) binding sites - current status. Nucl Med Biol. 1993; 20:503–525. [PubMed: 8389223]

109. López-Romero B, Evrard G, Durant F, Sevrin M, George P. Molecular structure and stereoelectronic properties of sarmazenil - a weak inverse agonist at the omega modulatory sites (benzodiazepine receptors): comparison with bretazenil and flumazenil. Bioorg Med Chem. 1998; 6:1745–1757. [PubMed: 9839004]

110. Kenakin T. Efficacy as a vector: the relative prevalence and paucity of inverse agonism. Mol Pharmacol. 2004; 65:2–11. [PubMed: 14722230]

111. Park PS-H. Ensemble of G-protein-coupled receptor active states. Curr Med Chem. 2012; 19:1146–1154. [PubMed: 22300048]

112. Assié M-B, Cosi C, Koek W. Correlation between low/high affinity ratios for 5-HT_{1A} receptors and intrinsic activity. Eur J Pharmacol. 1999; 386:97–103. [PubMed: 10611469]

113. Watson J, Collin L, Ho M, Riley G, Scott C, Selkirk JV, Price GW. 5-HT_{1A} receptor agonist-antagonist binding affinity difference as a measure of intrinsic activity in recombinant and native tissue systems. Br J Pharmacol. 2000; 130:1108–1114. [PubMed: 10882396]

114. Fitzgerald LW, Conklin DS, Krause CM, Marshall A, Patterson JP, Tran DP, Iyer G, Kostich WA, Largent BL, Hartig PR. High affinity agonist binding correlates with efficacy (intrinsic activity) at the human serotonin 5-HT_{2A} and 5-HT_{2C} receptors: evidence favouring the ternary complex and two-state models of agonist action. J Neurochem. 1999; 72:2127–2134. [PubMed: 10217294]

Author Manuscript Author Manuscript Author Manuscript Author Manuscript

115. Kearn CS, Greenberg MJ, DiCamelli R, Kurzawa K, Hlllard CJ. Relationship between ligand affinities for the cerebellar cannabinoid receptor CB1 and the induction of GDP/GTP exchange. J Neurochem. 1999; 72:2379–2387. [PubMed: 10349847]
116. Lahti RA, Figur LM, Piercey MF, Rupple PL, Evans DL. Intrinsic activity determinations at the dopamine D_2 guanine nucleotide-binding protein-coupled receptor: utilization of receptor state binding affinities. Mol Pharmacol. 1992; 42:432–438. [PubMed: 1357542]
117. Kobilka BK, Deupi X. Conformational complexity of G-protein-coupled receptors. Trends Pharm Sci. 2007; 28:397–406. [PubMed: 17629961]
118. Rosenbaum DM, Rasmussen SGF, Kobilka BK. The structure and function of G-protein-coupled receptors. Nature. 2009; 459:356–363. [PubMed: 19458711]
119. Deupi X, Kobilka BK. Energy landscapes as a tool to integrate GPCR structure, dynamics and function. Physiology. 2010; 25:293–303. [PubMed: 20940434]
120. Pike VW, Halldin C, Wikström HV. Radioligands for the study of brain 5-HT_{1A} receptors *in vivo*. Prog Med Chem. 2001; 38:189–247. [PubMed: 11774795]
121. Pike VW, McCarron JA, Lammerstma AA, Hume SP, Poole K, Grasby PM, Malizia A, Cliffe IA, Fletcher A, Bench C. First delineation of 5-HT_{1A} receptors in human brain with PET and [^{11}C]WAY-100635. Eur J Pharmacol. 1995; 283:R1–R3. [PubMed: 7498295]
122. Pike VW, McCarron JA, Lammertsma AA, Osman S, Hume SP, Sargent PA, Bench CJ, Cliffe IA, Fletcher A, Grasby PM. Exquisite delineation of 5-HT_{1A} receptors in human brain with PET and [*carbonyl*-^{11}C]WAY-100635. Eur J Pharmacol. 1996; 301:R5–R7. [PubMed: 8773468]
123. Farde L, Ito H, Swahn C-G, Pike VW, Halldin C. Quantitative analyses of carbonyl-carbon-11 WAY-100635 binding to central 5-hydroxytryptamine-1A receptors in man. J Nucl Med. 1998; 39:1965–1971. [PubMed: 9829590]
124. Gunn RN, Sargent PA, Bench CJ, Rabiner EA, Osman S, Pike VW, Hume SP, Grasby PM, Lammertsma AA. Tracer kinetic modeling of the 5-HT_{1A} receptor ligand [*carbony*l-^{11}C]WAY-100635 for PET. Neuro-Image. 1998; 8:426–440. [PubMed: 9811559]
125. Kumar JSD, Prabhakaran J, Majo VJ, Milak MS, Hsiung SC, Tamir H, Simpson NR, van Heertum RL, Mann JJ, Parsey RV. Synthesis and *in vivo* evaluation of a novel 5-HT_{1A} receptor agonist radioligand [*O-methyl*-^{11}C]2-(4-(4-(2-methoxyphenyl)piperazin-1-yl)butyl)-4-methyl-1,2,4-triazine-3, 5(2*H*,4*H*)dione in nonhuman primates. Eur J Nucl Med Mol Imaging. 2007; 34:1050–1060. [PubMed: 17221184]
126. Choi JY, Lyoo CH, Kim JS, Kim KM, Kang JH, Choi S-H, Kim J-J, Ryu YH. ^{18}F-Mefway PET imaging of serotonin 1A receptors in humans: a comparison with ^{18}F-FCWAY. PloS One. 2015; 10(4):e0121342. [PubMed: 25830772]
127. McCarron JA, Zoghbi SS, Shetty HU, Vermeulen ES, Wikström HV, Ichise M, Yasuno F, Halldin C, Innis RB, Pike VW. Synthesis and evaluation of [^{11}C](*R*)-WAY in monkey - a new and simply labeled antagonist radioligand for imaging brain 5-HT_{1A} receptors with PET. Eur J Nucl Med Mol Imaging. 2007; 34:1670–1682. [PubMed: 17579853]
128. Gozlan H, Thibault S, Laporte A-M, Lima L, Hamon M. The selective 5-HT_{1A} antagonist radioligand [^{3}H]WAY-100635 labels both G protein coupled and free 5-HT_{1A} receptors in rat brain membranes. Eur J Pharmacol. 1995; 288:173–186. [PubMed: 7720779]
129. Milak MS, DeLorenzo C, Zanderigo F, Prabhakaran J, Kumar JSD, Majo VJ, Mann JJ, Parsey RV. *In vivo* quantification of human serotonin 1A receptor using ^{11}C-CUMI-101, an agonist PET radiotracer. J Nucl Med. 2010; 51:1892–1900. [PubMed: 21098796]
130. Hendry N, Christie I, Rabiner EA, Laruelle M, Watson J. *In vitro* assessment of the agonist properties of the novel 5-HT_{1A} receptor ligand, CUMI-101 (MMP), in rat brain tissue. Nucl Med Biol. 2011; 38:273–277. [PubMed: 21315283]
131. Shrestha SS, Liow J-S, Lu S, Jenko K, Gladding RL, Svenningsson P, Morse CL, Zoghbi SS, Pike VW, Innis RB. ^{11}C-CUMI-101: a PET radioligand, behaves as a serotonin 1A receptor antagonist and also binds to α_1 adrenoceptors in brain. J Nucl Med. 2014; 55:141–146. [PubMed: 24385311]
132. Finnema SJ, Bang-Andersen B, Wikström HV, Halldin C. Current state of agonist radioligands for imaging brain dopamine D_2/D_3 receptors *in vivo* with positron emission tomography. Curr Top Med Chem. 2010; 10:1477–1498. [PubMed: 20583987]

Author Manuscript Author Manuscript Author Manuscript Author Manuscript

133. Seneca N, Finnema SJ, Farde L, Gulyas B, Wikström HV, Halldin C, Innis RB. Effect of amphetamine on dopamineD2 receptor binding in nonhuman primate brain: a comparison of the agonist radioligand [^{11}C]MNPA and antagonist [^{11}C]raclopride. Synapse. 2006; 59:260–269. [PubMed: 16416444]

134. Skinbjerg M, Sibley DR, Javitch JA, Abi-Dargham A. Imaging the high-affinity state of the dopamine D_2 receptor *in vivo*: fact or fiction? Biochem Pharmacol. 2011; 83:193–198. [PubMed: 21945484]

135. van Wieringen JP, Booij J, Shalgunov V, Elsinga P, Michel MC. Agonist high-and low-affinity states of dopamine D_2 receptors: methods of detection and clinical implications. Naunyn-Schmiederberg's Arch Pharmacol. 2013; 386:135–154.

136. Narendran R, Hwang DR, Slifstein M, Huang Y, Ekelund J, Guillin O, Scher E, Martinez D, Laruelle M. Measurement of the proportion of D_2 receptors configured in site of high affinity for agonist *in vivo*; a positron emission tomography study using [^{11}C]*N*-propyl-norapomorphine ([^{11}C]NPA) with the D_2 antagonist radiotracer [^{11}C]-raclopride. J Pharmacol Exp Ther. 2005; 315:80–90. [PubMed: 16014571]

137. Ginovart N, Galineau L, Willeit M, Mizrahi R, Bloomfield PM, Seeman P, Houle S, Kapur S, Wilson AA. Binding characteristics and sensitivity to endogenous dopamine of [^{11}C]-(+)-PHNO, a new agonist radiotracer for imaging the high-affinity state of the D_2 receptors *in vivo* using positron emission tomography. J Neurochem. 2006; 97:1089–1103. [PubMed: 16606355]

138. Seeman P. Dopamine agonist radioligand binds to both D2high and D2low receptors, explaining why alterations in D2high are not detected in human brain scans. Synapse. 2012; 66:88–93. [PubMed: 21954082]

139. Frost JJ, Douglass K, Mayberg H, Dannals RF, Links J, Wilson A, Ravert H, Wagner HN. Multicom-partmental analysis of C-11 carfentanil binding to opiate receptors in man by positron emission tomography. J Nucl Med. 1986; 27:1027–1027.

140. Terry GE, Hirvonen J, Liow JS, Zoghbi SS, Gladding R, Tauscher JT, Schaus JM, Phebus L, Felder CC, Morse C, Donohue SR, Pike VW, Halldin C, Innis RB. Imaging and quantitation of cannabinoid CB_1 receptors in human and monkey brains using F-18-labeled inverse agonist radioligands. J Nucl Med. 2010; 51:112–120. [PubMed: 20008988]

141. Inoue O, Suhara T, Itoh T, Kobayashi K, Suzuki K, Tateno Y. *In vivo* binding of [^{11}C]Ro15–4513 in human brain measured with PET. Neurosci Lett. 1992; 145:133–136. [PubMed: 1465208]

142. Highfield Nickols H, Conn PJ. Development of allosteric modulators of GPCRs for treatment. Neurobiol Dis. 2014; 61:55–71. [PubMed: 24076101]

143. Melancon BJ, Hopkins CR, Wood MR, Emmitte MR, Emmitte KA, Niswender CM, Christopoulos A, Conn PJ, Lindsley CW. Allosteric modulation of seven transmembrane spanning receptors: theory, practice, and opportunities for central nervous system drug discovery. J Med Chem. 2012; 55:1445–1464. [PubMed: 22148748]

144. Mu L, Schubiger PA, Ametamey SM. Radioligands for the PET imaging of metabotropic glutamate receptor subtype 5 (mGluR5). Curr Top Med Chem. 2010; 10:1558–1568. [PubMed: 20583985]

145. Zanotti-Fregonara P, Zhang Y, Jenko JJ, Gladding RL, Zoghbi SS, Fujita M, Sbardella G, Castellano S, Taliani S, Martini C, Innis RB, Da Settimo F, Pike VW. Synthesis and evaluation of translocator 18 kDa protein (TSPO) positron emission tomography (PET) radioligands with low binding sensitivity to human single nucleotide polymorphism rs6971. ACS Chem Neurosci. 2014; 5:963–971. [PubMed: 25123416]

146. Ikawa M, Lohith TG, Jenko KJ, Shrestha SS, Telu S, Zoghbi SS, Fujita M, Pike VW, Innis RB. [^{11}C]ER176, a radioligand for TSPO, is sensitive to a genetic polymorphism *in vivo* but not *in vitro*. (Submitted).

147. Tsujikawa T, Zoghbi SS, Hong J, Donohue SR, Jenko KJ, Gladding RL, Halldin C, Pike VW, Innis RB, Fujita M. *In vitro* and *in vivo* evaluation of ^{11}C-SD5024, a novel PET radioligand for human brain imaging of cannabinoid CB_1 receptors. NeuroImage. 2014; 84:733–741. [PubMed: 24076222]

148. Imaizumi M, Briard E, Zoghbi SS, Gourley JP, Hong J, Fujimura Y, Pike VW, Innis RB, Fujita M. Brain and whole-body imaging in nonhuman primates of [^{11}C]PBR28, a promising PET

Author Manuscript Author Manuscript Author Manuscript Author Manuscript

radioligand for peripheral benzodiazepine receptors. NeuroImage. 2008; 39:1289–1298. [PubMed: 18024084]

149. Hines CS, Fujita M, Zoghbi SS, Kim JS, Quezado Z, Herscovitch P, Milao N, Ferraris Araneta MD, Morse C, Pike VW, Labovsky J, Innis RB. Propofol decreases *in vivo* binding of ^{11}C-PBR28 to translocator protein (18 kDa) in the human brain. J Nucl Med. 2013; 54:64–69. [PubMed: 23148296]
150. Dickstein LP, Zoghbi SS, Fujimura Y, Imaizumi M, Zhang Y, Pike VW, Innis RB, Fujita M. Comparison of ^{18}F-labeled and ^{11}C-labeled aryloxyanilide analogs to measure translocator protein in human brain using positron emission tomography. Eur J Nucl Med Mol Imaging. 2011; 38:352–357. [PubMed: 21085954]
151. Imaizumi M, Briard E, Zoghbi SS, Gourley JP, Hong J, Musachio JL, Gladding R, Pike VW, Innis RB, Fujita M. Kinetic evaluation in nonhuman primates of two new PET ligands for peripheral benzodiazepine receptors in brain. Synapse. 2007; 61:595–605. [PubMed: 17455247]
152. Lohith TG, Xu R, Tsujikawa T, Morse CL, Anderson KB, Gladding RL, Zoghbi SS, Fujita M, Innis RB, Pike VW. Evaluation in monkey of two candidate PET radioligands, [^{11}C]RX-1 and [^{18}F]RX-2, for imaging brain 5-HT$_4$ receptors. Synapse. 2014; 68:613–623.
153. Fujimura Y, Zoghbi SS, Siméon FG, Taku A, Pike VW, Innis RB, Fujita M. Quantification of translocator protein (18 kDa) in the human brain with PET and a novel radioligand, ^{18}F-PBR06. J Nucl Med. 2009; 50:1047–1053. [PubMed: 19525468]
154. Yasuno F, Zoghbi SS, McCarron JA, Hong J, Ichise M, Brown AK, Gladding RL, Bacher JD, Pike VW, Innis RB. Quantification of serotonin 5-HT$_{1A}$ receptors in monkey brain with [^{11}C](*R*)-(−)-RWAY. Synapse. 2006; 60:510–520. [PubMed: 16952161]
155. Shrestha SS, Nelson EE, Liow JS, Gladding R, Lyoo CH, Noble PL, Morse C, Henter ID, Kruger J, Zhang B, Suomi SJ, Svenningsson P, Pike VW, Winslow JT, Leibenluft E, Pine DS, Innis RB. Fluoxetine administered to juvenile monkeys: effects on the serotonin transporter and behavior. Am J Psychiatry. 2014; 171:323–331. [PubMed: 24480874]
156. Zhang X-Y, Yasuno F, Zoghbi SS, Liow J-S, Hong J, McCarron JA, Pike VW, Innis RB. Quantification of serotonin receptors in human with [^{11}C](*R*)-(−)-RWAY: radiometabolite(s) likely confound brain measurements. Synapse. 2007; 61:469–477. [PubMed: 17415792]
157. Fujita M, Hines CS, Zoghbi SS, Mallinger AG, Dickstein LP, Liow JS, Zhang Y, Pike VW, Drevets WC, Innis RB, Zarate CA Jr. Downregulation of brain phosphodiesterase type IV measured with ^{11}C-(*R*)-rolipram positron emission tomography in major depressive disorder. Biol Psychiatry. 2012; 72:548–554. [PubMed: 22677471]
158. Zanotti-Fregonara P, Zoghbi SS, Liow JS, Luong E, Boellaard R, Gladding RL, Pike VW, Innis RB, Fujita M. Kinetic analysis in human brain of [^{11}C](*R*)-rolipram, a positron emission tomographic radioligand to image phosphodiesterase 4: a retest study and use of an image-derived input function. NeuroImage. 2011; 54:1903–1909. [PubMed: 21034834]
159. Bao X, Lu S, Liow J-S, Zoghbi SS, Jenko KJ, Clark DT, Gladding RL, Innis RB, Pike VW. Radiosynthesis and evaluation of an ^{18}F-labeled positron emission tomography radioligand for brain histamine subtype-3 receptors based on a non-imidazole 2-aminoethylbenzofuran chemotype. J Med Chem. 2012; 55:2406–2415. [PubMed: 22313227]
160. Pike VW, Rash KS, Chen Z, Pedregal C, Statnick MA, Kimura Y, Hong J, Zoghbi SS, Fujita M, Toledo MA, Diaz N, Gackenheimer SL, Tauscher JT, Barth VN, Innis RB. Synthesis and evaluation of radioligands for imaging brain nociceptin/orphanin FQ peptide (NOP) receptors with positron emission tomography. J Med Chem. 2011; 54:2687–2700. [PubMed: 21438532]
161. Kimura Y, Fujita M, Hong J, Lohith TG, Gladding RL, Zoghbi SS, Tauscher JA, Rash KS, Chen Z, Pedregal C, Barth VN, Pike VW, Innis RB. Brain and whole-body imaging in rhesus monkeys of ^{11}C-NOP-1A, a promising PET radioligand for nociceptin/orphanin FQ peptide (NOP) receptors. J Nucl Med. 2011; 52:1638–1645. [PubMed: 21880575]
162. Lohith TG, Zoghbi SS, Morse CL, Araneta MF, Barth VN, Goebl NA, Tauscher JT, Pike VW, Innis RB, Fujita M. Brain and whole-body imaging of nociceptin/orphanin FQ peptide receptor in humans using the PET ligand ^{11}C-NOP-1A. J Nucl Med. 2012; 53:385–392. [PubMed: 22312136]
163. Lohith TG, Zoghbi SS, Morse CL, Ferraris Araneta MD, Barth VN, Goebl NA, Tauscher JT, Pike VW, Innis RB, Fujita M. Retest imaging of [^{11}C]NOP-1A binding to nociceptin/orphanin FQ

Author Manuscript Author Manuscript Author Manuscript Author Manuscript

peptide (NOP) receptors in the brain of healthy humans. NeuroImage. 2014; 87:89–95. [PubMed: 24225488]

164. Yasuno F, Brown AK, Zoghbi SS, Krushinski JH, Chernet E, Tauscher J, Schaus JM, Phebus LA, Chesterfield AK, Felder CC, Gladding RL, Hong J, Halldin C, Pike VW, Innis RB. The PET radioligand [^{11}C]MePPEP binds reversibly and with high specific signal to cannabinoid CB_1 receptors in nonhuman primate brain. Neuropsychopharmacology. 2008; 33:259–269. [PubMed: 17392732]
165. Siméon FG, Brown AK, Zoghbi SS, Patterson VM, Innis RB, Pike VW. Synthesis and simple ^{18}F-labeling of 3-fluoro-5-(2-(2-(fluoromethyl)thiazol-4-yl)ethynyl) benzonitrile as a high affinity radioligand for imaging monkey brain metabotropic glutamate subtype-5 receptors with positron emission tomography. J Med Chem. 2007; 50:3256–3266. [PubMed: 17571866]
166. Brown AK, Kimura Y, Zoghbi SS, Siméon FG, Liow JS, Kreisl WC, Taku A, Fujita M, Pike VW, Innis RB. Metabotropic glutamate subtype 5 receptors are quantified in the human brain with a novel radioligand for PET. J Nucl Med. 2008; 49:2042–2048. [PubMed: 19038998]
167. Zoghbi SS, Shetty HU, Ichise M, Fujita M, Imaizumi M, Liow JS, Shah J, Musachio JL, Pike VW, Innis RB. PET Imaging of the dopamine transporter with ^{18}F-FECNT: a polar radiometabolite confounds brain radioligand measurements. J Nucl Med. 2006; 47:520–527. [PubMed: 16513622]
168. Hansch, C., Leo, A. Substituent Constants for Correlation Analysis in Chemistry and Biology. 1. Wiley-Interscience; New York: 1979.
169. van de Waterbeemd H, Camenish G, Folkers G, Chretien JR, Raevsky OA. Estimation of blood-brain barrier crossing of drugs using molecular size and shape, and H-bonding descriptors. J Drug Targeting. 1998; 6:151–165.
170. Lipinski CA, Lombardo F, Dominy BW, Feeney PJ. Experimental and computational approaches to estimate solubility and permeability in drug discovery and development settings. Adv Drug Deliv Rev. 1997; 23:3–26.
171. Kelder J, Grootenhuis PDJ, Byada DM, Delbressine LPC, Ploemen JP. Polar molecular surface as a dominating determinant for oral absorption and brain penetration of drugs. Pharm Res. 1999; 16:1514–1519. [PubMed: 10554091]
172. Norinder U, Haeberlein M. Computational approaches to the prediction of the blood-brain distribution. Adv Drug Delivery Rev. 2002; 54:291–313.
173. Hitchock SA, Pennington LD. Structure-brain exposure relationships. J Med Chem. 2006; 49:7559–7583. [PubMed: 17181137]
174. Gleeson MP. Generation of a set of simple, interpretable ADMET rules of thumb. J Med Chem. 2008; 51:817–834. [PubMed: 18232648]
175. Zhang L, Villabos A, Beck EM, Bocan T, Chappie TA, Chen L, Grimwood S, Heck SD, Helal CJ, Hou X, Humphrey JM, Lu J, Skaddan MB, McCarthy TJ, Verhoest PR, Wager TT, Zasadny K. Design and selection parameters to accelerate the discovery of novel central nervous system positron emission tomography (PET) ligand and their application in the development of a novel phosphodiesterase 2A PET ligand. J Med Chem. 2013; 56:4568–4579. [PubMed: 23651455]
176. Zoghbi SS, Anderson KB, Jenko KJ, Luckenbaugh DA, Innis RB, Pike VW. On quantitative relationships between drug-like compound lipophilicity and plasma free fraction in monkey and human. J Pharm Sci. 2012; 101:1028–1039. [PubMed: 22170327]
177. Abbot NJ, Chugani DC, Zaharchuk G, Rosen BR, Lo EH. Delivery of imaging agents into brain. Adv Drug Deliv Rev. 1999; 37:253–277. [PubMed: 10837739]
178. Waterhouse RN. Determination of lipophilicity and its use as a predictor of blood-brain barrier penetration of molecular imaging targets. Mol Imaging Biol. 2003; 5:376–389. [PubMed: 14667492]
179. Rankovic Z. CNS drug design: balancing physicochemical properties for optimal brain exposure. J Med Chem. 2015; 58:2584–2608. [PubMed: 25494650]
180. Ertl P, Rohde B, Selzer P. Fast calculation of molecular polar surface area as a sum of fragment-based contributions and its application to the prediction of drug transport properties. J Med Chem. 2000; 43:3714–3717. [PubMed: 11020286]

Author Manuscript Author Manuscript Author Manuscript Author Manuscript

181. Clark DE. Rapid calculation of polar molecular surface area and its application to the prediction of transport phenomena. 2. Prediction of blood-brain barrier penetration. J Pharm Sci. 1999; 88:815–821. [PubMed: 10430548]

182. Rishton GM, LaBonte K, Williams AJ, Kassa K, Kolanov E. Computational approaches to the prediction of blood-brain barrier permeability: a comparative analysis of central nervous system drugs versus secretase inhibitors for Alzheimer's disease. Curr Opin Drug Disc Dev. 2006; 9:303–313.

183. Gerebtzoff G, Seelig A. In silico prediction of blood-brain barrier permeation using the calculated molecular cross-sectional area as main parameter. J Chem Inf Model. 2006; 46:2638–2650. [PubMed: 17125204]

184. Adenot M, Lahana R. Blood-brain barrier permeation models: discriminating between potential CNS and non-CNS drugs including P-glycoprotein substrates. J Comput Inf Comput Sci. 2004; 44:239–248.

185. Hammarlund-Udenaes M, Fridén M, Syvänen S, Gupta A. On the rate and extent of drug delivery to the brain. Pharm Res. 2007; 25:1737–1750. [PubMed: 18058202]

186. Deo AK, Theil FP, Nicolas JM. Confounding parameters in preclinical assessment of blood-brain barrier permeation: an overview with emphasis on species differences and effect of disease states. Mol Pharmaceutics. 2013; 10:1581–1595.

187. [Last accessed 01/19/2016] ACD/Labs data sheet. Available from: http://www.acd-labs.com/download/docs/datasheets/datasheet_bbb.pdf

188. Stieger B, Gao B. Drug transporters in the central nervous system. Clin Pharmacokinet. 2015; 54:225–242. [PubMed: 25647629]

189. Xia CQ, Xiao G, Liu N, Pimprale S, Fox L, Patten CJ, Crespi CL, Miwa G, Gan LS. Comparison of species differences of P-glycoproteins in beagle dog, rhesus monkey, and human using ATPase activity assays. Mol Pharm. 2006; 3:78–86. [PubMed: 16686372]

190. Syvänen S, Lindhe O, Palner M, Kornum BR, Rahman O, Långström B, Knudsen GM, Hammarlund-Udenaes M. Species differences in blood-brain barrier transport of three positron emission tomography radio-ligands with emphasis on P-glycoprotein transport. Drug Metab Dispos. 2009; 37:635–643. [PubMed: 19047468]

191. Doze P, van Waarde A, Elsinga PH, Hendrikse NH, Vaalburg W. Enhanced cerebral uptake of receptor ligands by modulation of P-glycoprotein function in the blood-brain-barrier. Synapse. 2000; 36:66–74. [PubMed: 10700027]

192. Liow J-S, Hu S, Hall MD, Hines CS, Zoghbi SS, Shetty U, Pike VW, Kreisl WC, Herscovitch P, Gottesman MM, Theodore WH, Innis RB. ^{18}F-FCWAY, a serotonin 1A receptor radioligand, is a substrate for efflux transporters at the human blood-brain barrier. J Nucl Med. (In press).

193. Elsinga PH, Hendrikse NH, Bart J, van Waarde A, Vaalburg W. Positron emission tomography studies on binding of central nervous system drugs and P-glycoprotein function in the rodent brain. Mol Imaging Biol. 2005; 7:37–44. [PubMed: 15912274]

194. Tournier N, Cisternino S, Peyronneau MA, Goutal S, Dollé F, Schermann M, Bottlaender M, Saba W, Valette H. Discrepancies in the P-glycoprotein-mediated transport of [^{18}F]MPPF: a pharmacokinetic study in mice and non-human primates. Pharm Res. 2012; 29:2468–2476. [PubMed: 22644589]

195. Passchier J, van Waarde A, Doze P, Elsinga PH, Vaalburg W. Influence of P-glycoprotein on brain uptake of [^{18}F]MPPF in rats. Eur J Pharmacol. 2000; 407:273–280. [PubMed: 11068023]

196. Laćan G, Plenevaux A, Rubins DJ, Way BM, Defraiteur C, Lemaire C, Aerts J, Luxen A, Cherry SR, Melega WP. Cyclosporine, a P-glycoprotein modulator, increases ^{18}F]MPPF uptake in rat brain and peripheral tissues: microPET and ex vivo studies. Eur J Nucl Med Mol Imaging. 2008; 35:2256–2266. [PubMed: 18604533]

197. Tournier N, Valette H, Peyronneau M-A, Saba W, Goutla S, Kuhnast B, Dollé F, Scherrmann J-M, Cisternino S, Bottlaender M. Transport of selected PET radiotracers by human P-glycoprotein (ABCB1) and breast cancer resistance protein (ABCG2): an *in vitro* screening. J Nucl Med. 2011; 52:415–423. [PubMed: 21321274]

198. Liow J-S, Lu S, McCarron JA, Hong J, Musachio JL, Pike VW, Innis RB, Zoghbi SS. Effect of a P-glycoprotein inhibitor, cyclosporin A, on the disposition in rodent brain and blood of the 5-

Author Manuscript Author Manuscript Author Manuscript Author Manuscript

HT_{1A} receptor radioligand, [^{11}C](*R*) (−)-RWAY. Synapse. 2007; 61:96–105. [PubMed: 17117422]

199. Kroll T, Elmenhorst D, Matusch A, Celik AA, Wedekind F, Weisshaupt A, Beer S, Bauer A. [^{18}F]Altanserin and small animal PET: impact of multidrug efflux transporters on ligand brain uptake and subsequent quantification of 5-HT_{2A} receptor densities in the rat brain. Nucl Med Biol. 2014; 41:1–9. [PubMed: 24120220]
200. Schmitt U, Lee DE, Herth MM, Pile M, Buchholz H-G, Roesch F, Himeke C, Lueddens H, Debus F. P-glycoprotein influence on the brain uptake of a 5-HT_{2A} ligand: [^{18}F]MH.HZ. Neuropsychobiology. 2011; 63:183–190. [PubMed: 21304228]
201. Ishiwata K, Kawamura K, Yanai K, Hendrikse NH. *In vivo* evaluation of P-glycoprotein modulation of 8 PET radioligands used clinically. J Nucl Med. 2007; 48:81–87. [PubMed: 17204702]
202. Syvänen S, Labots M, Tagawa Y, Eriksson J, Windhorst AD, Lammertsma AA, de Lange EC, Voskuyl RA. Altered $GABA_A$ receptor density and unaltered blood brain barrier transport in a kainite model of epilepsy: an *in vivo* study using [^{11}C]flumazenil and PET. J Nucl Med. 2012; 53:1974–1983. [PubMed: 23143088]
203. Terry G, Liow JS, Chernet E, Zoghbi SS, Phebus L, Felder CC, Tauscher J, Schaus JM, Pike VW, Halldin C, Innis RB. Positron emission tomography imaging using an inverse agonist radioligand to assess cannabinoid CB_1 receptors in rodents. NeuroImage. 2008; 41:690–698. [PubMed: 18456516]
204. Piel M, Schmitt U, Bausbacher N, Buchholz H-G, Gründer G, Hiemke C, Rösch F. Evaluation of P-glycoprotein (abcb1a/b) modulation of [^{18}F]fallypride in microPET imaging studies. Neuropharmacology. 2014; 84:152–158. [PubMed: 23994301]
205. Hosten B, Boisgard R, Jacob A, Goutal S, Saubamea B, Dollé F, Scherrmann J-M, Cisternino S, Tournier N. [^{11}C]Befloxatone brain kinetics is not influenced by Bcrp function at the blood-brain barrier: a PET study using Bcrp TGEM knockout rats. Eur J Pharm Sci. 2013; 50:520–525. [PubMed: 23981334]
206. Rupniak NMJ, Fisher A, Boyce S, Clarke D, Pike A, O'Connor D, Watt A. P-glycoprotein efflux reduces the brain concentration of the substance P (NK^1 receptor) antagonists SR 1403433 and GR 205171: a comparative study using mdr1a−/− and mdr1a+/+ mice. Behav Pharmacol. 2003; 14:457–463. [PubMed: 14501258]
207. Kreisl WC, Bhatia R, Morse CL, Woock AE, Zoghbi SS, Shetty HU, Pike VW, Innis RB. Increased permeability-glycoprotein inhibition at the human blood-brain barrier can be safely achieved by performing PET during peak plasma concentrations of tariquidar. J Nucl Med. 2015; 56:82–87. [PubMed: 25500831]
208. Ecker GF, Stockner T, Chiba P. Computational models for prediction of interactions with ABC-transporters. Drug Discov Today. 2008; 13:311–317. [PubMed: 18405843]
209. Demel MA, Kraemer O, Ettmayer P, Haaksma E, Ecker GF. Ensemble rule-based classification of substrates of the human ABC-transporter ABCB1 using simple physiochemical descriptors. Mol Inf. 2010; 29:233–242.
210. Seelig A. A general pattern for substrate recognition by P-glycoprotein. Eur J Biochem. 1998; 251:252–261. [PubMed: 9492291]
211. Seelig A, Gatlik-Landwojtowicz E. Inhibitors of multidrug efflux transporters: their membrane and protein interactions. Mini-Rev Med Chem. 2005; 5:135–151. [PubMed: 15720284]
212. Hitchcock SA. Structural modifications that alter the P-glycoprotein efflux properties of compounds. J Med Chem. 2012; 55:4877–4895. [PubMed: 22506484]
213. Desai PV, Sawada GA, Watson IA, Raub TJ. Integration of in silico and *in vitro* tools for scaffold optimization during drug discovery: predicting P-glycoprotein efflux. Mol Pharm. 2013; 10:1249–1261. [PubMed: 23363443]
214. Didziapetris R, Japertas P, Avdeef A, Petrauskas A. Classification analysis of P-glycoprotein substrate specificity. J Drug Target. 2003; 11:391–406. [PubMed: 15203928]
215. Kalvass JC, Maurer TS. Influence of nonspecific brain and plasma binding on CNS exposure: implications for rational drug discovery. Biopharm Drug Dispos. 2002; 23:327–338. [PubMed: 12415573]

Author Manuscript Author Manuscript Author Manuscript Author Manuscript

216. Summerfield SG, Stevens AJ, Cutler L, del Carmen OM, Hammond P, Tang SP, Hersey A, Spaldinh DJ, Jeffrey P. Improving the *in vitro* prediction of the *in vivo* central nervous system penetration: integrating permeability, P-glycoprotein efflux, and free fractions in blood and brain. J Pharmacol Exp Ther. 2006; 316:1282–1290. [PubMed: 16330496]

217. Gandelman MS, Baldwin RM, Zoghbi SS, Zea-Ponce Y, Innis RB. Evaluation of ultrafiltration for the free-fraction determination of single photon emission computed tomography (SPECT) radiotracers: beta-CIT, IBF, and iomazenil. J Pharm Sci. 1994; 83:1014–1019. [PubMed: 7965658]

218. Gleeson MP. Plasma protein binding affinity and its relationship to molecular structure: and in silico analysis. J Med Chem. 2007; 50:101–112. [PubMed: 17201414]

219. Gunn RN, Summerfield SG, Salinas CA, Read KD, Guo Q, Searle GE, Parker CA, Jeffrey P, Laruelle M. Combining PET biodistribution and equilibrium dialysis assays to assess the free brain concentration and BBB transport of CNS drugs. J Cereb Blood Flow Metab. 2012; 32:874–883. [PubMed: 22274741]

220. Summerfield SG, Lucas AJ, Porter RA, Jeffrey P, Gunn RN, Read KR, Stevens AJ, Metcalf AC, Osuna MC, Kilford PJ, Passchier J, Ruffo AD. Toward an improved prediction of human *in vivo* brain penetration. Xenobiotica. 2008; 38:1518–1535. [PubMed: 18979396]

221. Man ICORPTGOR. Report of the Task Group on Reference Man. Pergamon Press; Oxford: 1975.

222. Andersson JD, Pierson ME, Finnema SJ, Gulyás B, Heys R, Elmore CS, Farde L, Halldin C. Development of a PET radioligand for the central 5-HT_{1B} receptor: radiosynthesis and characterization in cynomolgus monkeys of eight radiolabeled compounds. Nucl Med Biol. 2011; 38:261–272. [PubMed: 21315282]

223. Assmus F, Seelig A, Gobbi L, Borroni E, Glaaentzlin P, Fischer H. Label-free assay for the assessment of non-specific binding of positron emission tomography tracer candidates. Eur J Pharm Sci. 2015; 79:27–35. [PubMed: 26341407]

224. Rosso L, Gee AD, Gould IR. *Ab initio* computational study of positron emission tomography ligands interacting with lipid molecule for the prediction of nonspecific binding. J Comput Chem. 2008; 29:2397–2405. [PubMed: 18442082]

225. Kannan P, Brimacombe KR, Kreisl WC, Liow J-S, Zoghbi SS, Telu S, Zhang Y, Pike VW, Halldin C, Gottesman MM, Innis RB, Hall MD. Lysosomal trapping of a radiolabeled substrate of P-glycoprotein as a mechanism for signal amplification in PET. Proc Natl Acad Sci, USA. 2011; 108:2593–2598. [PubMed: 21262843]

226. Lassen NA, Bartenstein PA, Lammertsma AA, Prevett MC, Turton DR, Luthra SK, Osman S, Bloomfield PM, Jones T, Patsalos PN, O'Connell MT, Duncan JS, Andersen JV. Benzodiazepine receptor quantification *in vivo* in humans using [^{11}C]flumazenil and PET: application of the steady-state principle. J Cereb Blood Flow Metab. 1995; 15:152–165. [PubMed: 7798333]

227. Cunningham VJ, Rabiner EA, Slifstein M, Laruelle M, Gunn RN. Measuring drug occupancy in the absence of a reference region: the Lassen plot re-visited. J Cereb Blood Flow Metab. 2010; 30:46–50. [PubMed: 19738632]

228. Zanotti-Fregonara P, Xu R, Zoghbi SS, Liow J-S, Fujita M, Veronese M, Gladding R, Rallis-Frutos D, Hong J, Pike VW, Innis RB. The positron emission tomographic radioligand ^{18}F-FIMX images and quantifies metabotropic glutamate receptor 1 in proportion to the regional density of its gene transcript in human brain. J Nucl Med. 2016; 57:242–247. [PubMed: 26514176]

229. van Dyck CH, Baldwin RM, Amici LA, Garg PK, Ng CK, Soufer R, Charney DS, Innis RB. PET quantification of 5-HT_{2A} receptors in the human brain: a constant infusion paradigm with [^{18}F]altanserin. J Nucl Med. 2000; 41:234–241. [PubMed: 10688105]

230. Liptrot M, Adams KH, Martiny L, Pinborg LH, Lonsdale MN, Olsen NV, Holm S, Svarer C, Knudsen GM. Cluster analysis in kinetic modelling of the brain: a noninvasive alternative to arterial sampling. Neuroimage. 2004; 21:483–493. [PubMed: 14980551]

231. Lundkvist C, Halldin C, Swahn CG, Ginovart N, Farde L. Different brain radioactivity curves in a PET study with [^{11}C] β-CIT labelled in two different positions. Nucl Med Biol. 1999; 26:343–350. [PubMed: 10382835]

Author Manuscript Author Manuscript Author Manuscript Author Manuscript

232. Tan PZ, Baldwin RM, van Dyck CH, Al-Tikriti M, Roth B, Khan N, Charney DS, Innis RB. Characterization of radioactive metabolites of 5-HT_{2A} receptor PET ligand [^{18}F]altanserin in human and rodent. Nucl Med Biol. 1999; 26:601–608. [PubMed: 10587097]

233. Halldin C, Bjurling P, Stålnacke CG, Jossan SS, Oreland L, Långström B. ^{11}C-Labelling of dimethylphenethylamine in two different positions and biodistribution studies. Appl Radiat Isot. 1989; 40:557–560.

234. Gourand F, Emond P, Bergström JP, Takano A, Gulyás B, Guilloteau D, Barré L, Halldin C. A radiometabolite study of the serotonin transporter PET radioligand [^{11}C[MADAM. Nucl Med Biol. 2014; 41:501–506. [PubMed: 24857865]

235. Shetty HU, Zoghbi SS, Liow JS, Ichise M, Hong J, Musachio JL, Halldin C, Seidel C, Innis RB, Pike VW. Identification and regional distribution in rat brain of radiometabolites of the dopamine transporter PET radioligand [^{11}C]PE2I. Eur J Nucl Med Mol Imaging. 2007; 34:667–678. [PubMed: 17096093]

236. Odano I, Varrone A, Savic I, Ciumas C, Karlsson P, Jucaite A, Halldin C, Farde L. Quantitative PET analyses of regional [^{11}C]PE2I binding to the dopamine transporter — application to juvenile myoclonic epilepsy. Neuroimage. 2012; 59:3582–3593. [PubMed: 22056530]

237. Osman S, Lundkvist C, Pike VW, Halldin C, McCarron JA, Swahn C-G, Ginovart N, Luthra SK, Bench CJ, Grasby PM, Wikström H, Barf T, Cliffe IA, Fletcher A, Farde L. Characterization of the radioactive metabolites of the 5-HT_{1A} receptor radioligand, [*O-methyl*-^{11}C]WAY-100635, in monkey and human plasma by HPLC — comparison of the behaviour of an identified radioactive metabolite with parent radioligand in monkey using PET. Nucl Med Biol. 1996; 23:627–634. [PubMed: 8905828]

238. Osman S, Lundkvist C, Pike VW, Halldin C, McCarron JA, Swahn C-G, Ginovart N, Luthra SK, Bench CJ, Grasby PM, Cliffe IA, Fletcher A, Farde L. Characterisation of the appearance of radioactive metabolites in monkey and human plasma from the 5-HT_{1A} receptor radioligand, [*carbonyl*-^{11}C]WAY-100635 — explanation of high signal in PET and an aid to biomathematical modelling. Nucl Med Biol. 1998; 25:215–223. [PubMed: 9620626]

239. Odano I, Halldin C, Karlsoon P, Varrone P, Airaksinen AJ, Krasikova RN, Farde L. [^{18}F]Flumazenil binding to central benzodiazepine receptor studies by PET - quantitative analysis and comparisons with [^{11}C]flumazenil. Neuroimage. 2009; 45:891–902. [PubMed: 19136064]

240. Peyronneau MA, Saba W, Dollé F, Goutal S, Coulon C, Bottlaender M, Valette H. Difficulties in dopamine transporter radioligand PET analysis: the example of LBT-999 using [^{18}F] and [^{11}C] labelling: part II: metabolism studies. Nucl Med Biol. 2012; 39:347–359. [PubMed: 22154687]

241. Saba W, Peyronneau M-A, Dollé F, Goutal S, Bottlaender M, Valette H. Difficulties in dopamine transporter radioligand analysis: the example of LBT-999 using [^{18}F] and [^{11}C] labelling part I: PET studies. Nucl Med Biol. 2012; 39:227–233. [PubMed: 22033025]

242. Park E, Sullivan JM, Planeta B, Gallezot J-D, Lim K, Lin S-F, Ropchan J, McCarthy TJ, Ding Y-S, Morris ED, Williams WA, Huang Y, Carson RE. Test-retest reproducibility of the metabotropic glutamate receptor 5 ligand [^{18}F]FPEB with bolus plus constant infusion in humans. Eur J Nucl Med Mol Imaging. 2015; 42:1530–1541. [PubMed: 26044120]

243. Ma Y, Lang L, Kiesewetter D, Jagoda E, Eckelman WC. Species differences in metabolites of PET ligands: serotonergic 5-HT_{1A} receptor antagonists 3-*trans*-FCWAY and 3-*cis*-FCWAY. Nucl Med Biol. 2006; 33:1013–1019. [PubMed: 17127175]

244. Schou M, Zoghbi SS, Shetty HU, Shchukin E, Liow J-S, Hong J, Andrée BA, Gulyás B, Farde L, Innis RB, Pike VW, Halldin C. Investigation of the metabolites of (*S*,*S*)-[^{11}C]MeNER in humans, monkeys and rats. Mol Imaging Biol. 2009; 11:23–30. [PubMed: 18800204]

245. Zoghbi SS, Liow JS, Yasuno F, Hong J, Tuan E, Lazarova N, Gladding RL, Pike VW, Innis RB. ^{11}C-Loperamide and its desmethyl radiometabolite are avid substrates for brain permeability-glycoprotein efflux. J Nucl Med. 2008; 49:648–656.

246. Lazarova N, Zoghbi SS, Hong J, Seneca N, Tuan E, Gladding RL, Liow JS, Taku A, Innis RB, Pike VW. Synthesis and evaluation of [*N-methyl*-^{11}C]*N*-des-methyl-loperamide as a new and improved PET radiotracer for imaging P-gp function. J Med Chem. 2008; 51:6034–6043. [PubMed: 18783208]

Author Manuscript Author Manuscript Author Manuscript Author Manuscript

247. Senda M, Brooks DJ, Farrar G, Somer EJ, Paterson CL, Sasaki M, McParland BJ. The clinical safety, biodistribution and internal radiation dosimetry of flumetamol (^{18}F) injection in healthy Japanese adult volunteers. Ann Nucl Med. 2015; 29:627–635. [PubMed: 26044876]

248. Passchier J, van Waarde A, Pieterman RM, Elsinga PH, Pruim J, Hendrikse HN, Willemsen ATM, Vaalburg W. *In vivo* delineation of 5-HT_{1A} receptors in human brain with [^{18}F]MPPF. J Nucl Med. 2000; 41:1830–1835. [PubMed: 11079490]

249. Biver F, Goldman S, Luxen A, Monlcus M, Forestini M, Medlewicz J, Lotstra F. Multicompartmental study of fluorine-18 altanserin binding to brain $5HT_2$ receptors in humans using positron emission tomography. Eur J Nucl Med. 1994; 21:937–946. [PubMed: 7995287]

250. Kessler RM, Seibyl J, Cowan RL, Zald D, Young JS, Ansari MS, Stabin MG. Radiation dosimetry of ^{18}F-FPEB in humans. J Nucl Med. 2014; 55:1119–1121. [PubMed: 24799618]

251. Kimes AS, Horti AG, London ED, Chefer SI, Contoreggi C, Ernst M, Friello P, Koren AO, Kurian V, Matochik JA, Pavlova O, Vaupel DB, Mukhin AG. 2-[^{18}F]FA-85380: PET imaging of brain nicotinic acetylcholine receptors and whole body distribution in humans. FASEB J. 2003; 17:1331–1333. [PubMed: 12759330]

252. Bottlaender M, Valette H, Roumenov D, Dollé F, Coulon C, Ottaviani M, Hinnen F, Ricard M. Biodistribution and radiation dosimetry of ^{18}F-fluoro-A-85380 in healthy volunteers. J Nucl Med. 2003; 44:596–601. [PubMed: 12679405]

253. Joshi AD, Sanabri-Bohorquez S, Bormanns G, Koole M, De Hoon J, van Hecken A, Depre M, De Lepeleire I, Van Laere K, Sur C, Hamill TG. Characterization of the novel GlyT1 PET tracer [^{18}F]MK-6577 in humans. Synapse. 2015; 69:33–40. [PubMed: 25196464]

254. Wong DF, Kuwubara H, Kim J, Braşić JR, Chamroonrat W, Gao Y, Valentine H, Willis W, Mathur A, McCaul ME, Wand G, Gean EG, Dannals RF, Horti AG. PET imaging of high-affinity $\alpha_4\beta_2$ nicotinic acetylcholine receptors in humans with ^{18}F-AZAN, a radioligand with optimal brain kinetics. J Nucl Med. 2013; 54:1308–1314. [PubMed: 23801676]

255. Chien DT, Bahri S, Szardenings AK, Walsh JC, Mu F, Su M-Y, Shankle WR, Elizarov A, Kolb HC. Early clinical PET imaging results with the novel PHF-Tau radioligand [^{18}F]-T807. J Alzheimer's Dis. 2013; 34:457–468. [PubMed: 23234879]

256. Sabri O, Becker G-A, Meyer PM, Hesse S, Wilke S, Graef S, Patt M, Luthardt J, Wagenknecht G, Hoepping A, Smits R, Franke A, Sattler B, Habermann B, Neuhaus P, Fischer S, Tiepolt S, Deuther-Conrad W, Barthel H, Schönknecht P, Brust P. First-in-human quantification study of cerebral $\alpha_4\beta_2$ nicotinic acetylcholine receptors using the novel specific radioligand (−)-[^{18}F]flubatine. NeuroImage. 2015; 118:199–208. [PubMed: 26037057]

257. Ding YS, Fowler JS, Logan J, Wang GJ, Telang F, Garza V, Biegon A, Pareto D, Rooney W, Shea C, Alexoff D, Volkow ND, Vocci F. 6-[^{18}F]Fluoro-A-85380; a new PET tracer for the nicotinic acetylcholine receptor: studies in the human brain and *in vivo* demonstration of specific binding in white matter. Synapse. 2004; 53:184–189. [PubMed: 15236351]

258. Bretin F, Bahri MA, Bernard C, Warnock G, Aerts J, Mestdagh N, Buchanan T, Otoul C, Koestler F, Mievis F, Giacomelli F, Degueldre C, Hustinx R, Luxen A, Seret A, Plenevaux A, Salmon E. Biodistribution and radiation dosimetry for the novel SV2A radiotracer [^{18}F]UCB-H: first-in-human study. Mol Imaging Biol. 2015; 17:557–564. [PubMed: 25595813]

259. Kimura Y, Siméon FG, Zoghbi SS, Zhang Y, Hatazawa J, Pike VW, Innis RB, Fujita M. Biodistribution and radiation dosimetry of a positron emission tomographic ligand, [^{18}F]SP203, to image metabotropic glutamate subtype 5 receptors in humans. Eur J Nucl Med Mol Imaging. 2010; 37:1943–1949. [PubMed: 20585776]

260. Olsson H, Halldin C, Farde L. Differentiation of extrastriatal dopamine D_2 receptor density and affinity in the human brain using PET. Neuroimage. 2004; 22:794–803. [PubMed: 15193608]

261. Takano A, Halldin C, Varrone A, Karlsson P, Sjoholm N, Stubbs JB, Schou M, Airaksinen AJ, Tauscher J, Gulyás B. Biodistribution and radiation dosimetry of the norepenephrine transporter radioligand (*S*,*S*)-[^{18}F]FMeNER-D_2: a human whole body PET study. Eur J Nucl Med Mol Imaging. 2008; 35:630–636. [PubMed: 18000665]

262. Sprague DR, Chin FT, Liow J-S, Fujita M, Burns HD, Hargreaves R, Stubbs JB, Pike VW, Innis RB, Mozley PD. Human biodistribution and radiation dosimetry of the tachykinin NK_1 antagonist radioligand [^{18}F]SPA-RQ: comparison of thin-slice, bisected, and 2-dimensional planar image analysis. J Nucl Med. 2007; 48:100–107. [PubMed: 17204705]

Author Manuscript Author Manuscript Author Manuscript Author Manuscript

263. Hesse S, Brust P, Mäding P, Becker GA, Patt M, Seese A, Sorger D, Zessin J, Meyer PM, Lobsien D, Laudi S, Habermann B, Fuchtner F, Luthardt J, Bresch A, Steinbach J, Sabri O. Imaging of the brain serotonin transporters (SERT) with ^{18}F-labelled fluoromethyl-McN5652 and PET in humans. Eur J Nucl Med Mol Imaging. 2012; 39:1001–1011. [PubMed: 22349718]

264. Arlicot N, Vercouillie J, Ribeiro M-J, Tauber C, Venel Y, Baulieu JL, Maia S, Corcia P, Stabin MG, Reynolds A, Kassiou M, Guilloteau D. Initial evaluation in healthy humans of [^{18}F]DPA-714, a potential PET biomarker for neuroinflammation. Nucl Med Biol. 2012; 39:570–578. [PubMed: 22172392]

265. Barret O, Thomae D, Tavares A, Alagille D, Papin C, Waterhouse R, McCarthy T, Jennings D, Marek K, Russell D, Seibyl J, Tamagnan G. *In vivo* assessment and dosimetry of 2-novel PDE10A PET radiotracers in humans: ^{18}F-MNI-659 and ^{18}F-654. J Nucl Med. 2014; 55:1297–1304. [PubMed: 24898025]

266. Barret O, Hannestad J, Vala C, Alagille D, Tavares A, Laruelle M, Jennings D, Marek K, Russell D, Seibyl J, Tamagnan G. Characterization in humans of ^{18}F-MNI-444, a PET radiotracer for brain adenosine 2A receptors. J Nucl Med. 2015; 56:586–591. [PubMed: 25698783]

267. Burns HD, Van Laere K, Sanabria-Bohórquez S, Hamill TG, Bormans G, Eng W, Gibson R, Ryan C, Connolly B, Patel S, Krause S, Vanko A, Van Hecken A, Dupont P, De Lepeleire I, Rothenberg P, Stoch SA, Cote J, Hagmann WK, Jewell JP, Lin LS, Liu P, Goulet MT, Gottesdiener K, Wagner JA, de Hoon J, Mortelmans L, Fong TM, Hargreaves RJ. [^{18}F]MK-9470, a positron emission tomography (PET) tracer for *in vivo* human PET brain imaging of the cannabinoid-1 receptor. Proc Natl Acad Sci, USA. 2007; 104:9800–9805. [PubMed: 17535893]

268. Petrou M, Frey KA, Kilbourn MR, Scott PJH, Raffel DM, Bohne NI, Müller MLTM, Albin RL, Koeppe RRA. *In vivo* imaging of human cholinergic nerve terminals with (−)-5–^{18}F-fluoroethoxy benzovesamicol: biodistribution, dosimetry, and tracer kinetic analyses. J Nucl Med. 2014; 55:396–404. [PubMed: 24481024]

269. Mizrahi R, Rusjan PM, Vutcu I, Ng A, Wilson AA, Houle S, Bloomfield PM. Whole body distribution and radiation dosimetry in humans of a new PET ligand, [^{18}F]-FEPPA, to image translocator protein (18 kDa). Mol Imaging Biol. 2013; 156:353–359.

270. Villemagne VL, Furumoto S, Fodero-Tavoletti MT, Mulligan RS, Hodges J, Harada R, Yates P, Piguet O, Pejoska S, Doré V, Yanai K, Masters CL, Kudo Y, Rowe CC, Okamura N. *In vivo* evaluation of a novel tau imaging tracer for Alzheimer's disease. Eur J Nucl Med Mol Imaging. 2014; 41:816–826. [PubMed: 24514874]

271. Okumura M, Arakawa R, Ito H, Seki C, Takahashi H, Takano H, Haneda E, Nakao R, Suzuki H, Suzuki K, Okubo Y, Suhara T. Quantitative analysis of NK_1 receptor in the human brain using PET with ^{18}F-FE-SPA-RQ. J Nucl Med. 2008; 49:1749–1755. [PubMed: 18927336]

272. Takano A, Gulyás B, Varrone A, Karlsson P, Sjoholm N, Larsson S, Jonsson C, Odh R, Sparks R, Al Tawil N, Hoffmann A, Zimmermann T, Thiel A, Halldin C. Biodistribution and radiation dosimetry of the 18 kDa translocator protein (TSPO) radioligand [^{18}F]FEDAA1106. Eur J Nucl Med Mol Imaging. 2011; 38:2058–2065. [PubMed: 21732107]

273. Shidahara M, Watabe H, Tashiro M, Okamura N, Furumoto S, Watanuki S, Furukawa K, Arakawa Y, Funaki Y, Iwata R, Gonda K, Kudo Y, Arai H, Ishiwata K, Yanai K. Quantitative kinetic analysis of PET amyloid imaging agents [^{18}F]FACT in human brain. Nucl Med Biol. 2015; 42:734–744. [PubMed: 26093494]

274. Lin JJ, Hsu WC, Hsiao IT, Wey SP, Jin L-W, Skovronsky D, Wai YY, Chang HP, Lo CW, Yao CH, Yen TC, Kung MP. Whole body distribution and brain PET imaging with AV-45, a novel amyloid imaging agent - a pilot study. Nucl Med Biol. 2010; 37:497–508. [PubMed: 20447562]

275. Lin K-J, Weng Y-S, Wey S-P, Hsiao IT, Lu C-S, Skovronsky D, Chang H-P, Kung M-P, Yen T-C. Whole body biodistribution and radiation dosimetry of ^{18}F-FP(+)-DTBZ (^{18}F-AV-133): a novel vesicular monoamine transporter 2 imaging agent. J Nucl Med. 2010; 51:1480–1485. [PubMed: 20720042]

276. Choi JY, Lyoo CH, Kim JS, Kim KM, Kang JH, Choi S-H, Kim J-J, Ryu YH. ^{18}F-Mefway PET imaging of serotonin 1A receptors in humans: a comparison with ^{18}F-FCWAY. PloS One. 2015; doi: 10.1371/journal.pone.0121342

Author Manuscript Author Manuscript Author Manuscript Author Manuscript

277. Hillmer AT, Wooten DW, Bajwa AK, Higgins AT, Lao PJ, Betthauser TJ, Barnhart TE, Rowley HA, Stone CK, Johnson SC, Mukherjee J, Christian BT. First-in-human evaluation of ^{18}F-Mefway, a PET radioligand specific to serotonin-1A receptors. J Nucl Med. 2014; 55:1973–1979. [PubMed: 25453045]

278. Fujimura Y, Kimura Y, Siméon FG, Dickstein LP, Pike VW, Innis RB, Fujita M. Biodistribution and radiation dosimetry in humans of a new PET ligand, ^{18}F-PBR06, to image translocator protein (18 kDa). J Nucl Med. 2010; 51:145–149. [PubMed: 20008980]

279. Nye JA, Votaw JR, Bremner JD, Davis MR, Voll RJ, Camp VM, Goodman MM. Quantification of dopamine transporter density with [^{18}F]FECNT PET in healthy humans. Nucl Med Biol. 2014; 41:217–222. [PubMed: 24533985]

280. van Laere K, Ahmad RU, Hudyan H, Celen S, Dubois K, Schmidt ME, Bormans G, Koole M. Human biodistribution and dosimetry of ^{18}F-JNJ42259152, a radioligand for phosphodiesterase 10A imaging. Eur J Nucl Med Mol Imaging. 2013; 40:254–261. [PubMed: 23160998]

281. Herzog H, Elmenhorst D, Winz O, Bauer A. Biodistribution and radiation dosimetry of the A_1 adenosine receptor ligand ^{18}F-CPFPX determined from whole-body PET. Eur J Nucl Med Mol Imaging. 2008; 35:1499–1506. [PubMed: 18373090]

282. Kazumata K, Dhawan V, Chaly T, Antonini A, Margouleff C, Belakhlef A, Neumeyer J, Eidelberg D. Dopamine transporter imaging with fluorine-18-FPCIT and PET. J Nucl Med. 1998; 39:1521–1530. [PubMed: 9744335]

283. Varonne A, Stepanov V, Nakao R, Gulyás B, Emond P, Deloye JB, Vercouillie J, Stabin MG, Jonsson C, Guilloteau D, Halldin C. Imaging of the striatal and extrastriatal dopamine transporter with ^{18}F-LBT-999: quantification, biodistribution, and radiation dosimetry in nonhuman primates. J Nucl Med. 2011; 52:1313–1321. [PubMed: 21764797]

284. Ryu YH, Liow JS, Zoghbi S, Fujita M, Collins J, Tipre D, Sangare J, Hong J, Pike VW, Innis RB. Di-sulfiram inhibits defluorination of ^{18}F-FCWAY, reduces bone radioactivity, and enhances visualization of radioligand binding to serotonin 5-HT_{1A} receptors in human brain. J Nucl Med. 2007; 48:1154–1161. [PubMed: 17574977]

285. Matusch A, Meyer PT, Bier D, Holschbach MH, Woitalla D, Elmenhorst D, Winz OH, Zilles K, Bauer A. Metabolism of the A1 adenosine receptor PET ligand [^{18}F]CPFPX by CYP1A2: implications for bolus/infusion studies. Nucl Med Biol. 2006; 33:891–898. [PubMed: 17045169]

286. Palner M, McCormick P, Parkes J, Knudsen GM, Wilson AA. Systemic catechol-O-methyl transferase inhibition enable the D1 agonist radiotracer *R*-[^{11}C]SKF 82957. Nucl Med Biol. 2010; 37:837–843. [PubMed: 20870159]

287. Sorger D, Scheunemann M, Grossmann U, Fischer S, Vercouillie J, Hiller A, Wenzel B, Roghani A, Schliebs R, Brust P, Sabri O, Steinbach J. A new ^{18}F-labeled fluoroacetylmorpholino derivative of vesamicol for neuroimaging of the vesicular acetylcholine transporter. Nucl Med Biol. 2008; 35:185–195. [PubMed: 18312828]

288. Miller PW, Long NJ, Villar R, Gee AD. Synthesis of ^{11}C, ^{18}F, ^{15}O and ^{13}N radiolabels for positron emission tomography. Angew Chem Int Ed. 2008; 47:8998–9033.

289. Ferrieri, RA. Handbook of Radiopharmaceuticals. Welch, MJ., Redvanly, CS., editors. Vol. Ch 75. Wiley & Sons Ltd; Chichester: 2003. p. 229-282.

290. Antoni, G., Kihlberg, T., Långström, B. Handbook of Radiopharmaceuticals. Welch, MJ., Redvanly, CS., editors. Vol. Ch 5. Wiley & Sons Ltd; Chichester: 2003. p. 141-194.

291. Allard M, Fouquet E, James D, Szlosek-Pinaud M. State of the art in ^{11}C-labeled radiotracers synthesis. Curr Med Chem. 2008; 15:235–277. [PubMed: 18288983]

292. Henriksen, G. Munich Molecular Imaging Handbook Series. Vol. 1. Scintomics Print Media and Publishing; Fürstenfeldbruck: 2010. p. 75-101.Ch. 2

293. Itsenko O, Gomez-Vallejo V, Jacek JL, Kozirowski J. On ^{11}C chemistry reviews - surveying and filling the gaps. Curr Org Chem. 2013; 17:2067–2096.

294. Snyder, SE., Kilbourn, MR. Handbook of Radiopharmaceuticals. Welch, MJ., Redvanly, CS., editors. Vol. Ch 6. Wiley & Sons Ltd; Chichester: 2003. p. 195-227.

295. Schirrmacher R, Wangler C, Schirrmacher E. Recent developments and trends in F-18-radiochemistry: syntheses and applications. Mini-Rev Org Chem. 2007; 4:317–329.

Author Manuscript Author Manuscript Author Manuscript Author Manuscript

296. Cai L, Lu S, Pike VW. Chemistry with [^{18}F]fluoride ion. Eur J Org Chem. 2008; 2008(17):2853–2873.

297. Schirrmacher, R., Wängler, C., Schirrmacher, E. Munich Molecular Imaging Handbook Series. Vol. 1. Scintomics Print Media and Publishing; Fürstenfeldbruck: 2010. p. 5-73.Ch. 1

298. Cole E, Stewart M, Littich R, Hoareau R, Scott PJH. Radiosyntheses using fluorine-18: the art and science of late stage fluorination. Curr Topics Med Chem. 2014; 14:875–900.

299. Brooks AF, Topczewski JJ, Ichiishi N, Sanford MS, Scott PJH. Late-stage [^{18}F]fluorination: new solutions to old problems. Chem Sci. 2014; 5:4545–4553. [PubMed: 25379166]

300. Jacobson O, Kiesewetter DO, Chen X. Fluorine-18 radiochemistry, labeling strategies and synthetic routes. Bioconjugate Chem. 2015; 26:1–18.

301. Madsen K, Marner L, Haahr M, Gillings N, Knudsen GM. Mass dose effects and *in vivo* affinity in brain PET receptor studies - a study of cerebral 5-HT_4 receptor binding with [^{11}C]SB2017145. Nucl Med Biol. 2011; 38:1085–1091. [PubMed: 21831646]

302. Hume SP, Gunn RN, Jones T. Pharmacological constraints associated with positron emission tomographic scanning of small laboratory animals. Eur J Nucl Med. 1998; 25:173–176. [PubMed: 9473266]

303. Jagoda EM, Vaquero JJ, Seidel J, Green MV, Eckelman WC. Experiment assessment of mass effects in the rat: implications for small animal PET imaging. Nucl Med Biol. 2004; 31:771–779. [PubMed: 15246368]

304. Finn RD, Wolf AP. Cyclotron production of ^{11}C-carbon dioxide from a nitrogen gas target. J Nucl Med. 1972; 13:429–430.

305. Gómez-Vallejo, V., Gaja, V., Koziorowski, J., Lllop, J. Positron Emission Tomography — Current Clinical and Research Aspects. Hsieh, C-H., editor. Vol. Ch 7. Rijeka: InTech; 2012. p. 183-210.

306. Lapi SE, Welch MJ. A historical perspective on the specific activity of radiopharmaceuticals: what have we learned in the 35 years of the ISRC. Nucl Med Biol. 2013; 40:314–320. [PubMed: 23357081]

307. Suzuki K, Yamazaki T, Sasaki M, Kubodera A. Specific activity of [^{11}C]CO_2 in a N_2 gas target: effect of irradiation dose, irradiation history, oxygen content and beam energy. Radiochim Acta. 2000; 88:211–215.

308. Buckley K, Huser J, Jivan S, Chun K, Ruth T. ^{11}C-Methane production in small volume, high pressure gas targets. Radiochim Acta. 2000; 88:201–205.

309. Andersson J, Truong P, Halldin C. In-target produced [^{11}C]methane: increased specific radioactivity. Appl Radiat Isot. 2009; 67:106–110. [PubMed: 19013077]

310. Christman DR, Finn RD, Karlstrom KI, Wolf AP. The production of ultra high activity ^{11}C-labeled hydrogen cyanide, carbon dioxide, carbon monoxide and methane via the ^{14}N(p,α)^{11}C reaction, (XV). Int J Appl Radiat Isot. 1975; 26:435–442.

311. Landais P, Finn R. On-line preparation of [^{11}C]carbon dioxide from [^{11}C]methane. Appl Radiat Isot. 1989; 40:265–266.

312. Rotstein BH, Liang SH, Holland JP, Collier TL, Hooker JM, Wilson AA, Vasdev N. $^{11}CO_2$ fixation: a renaissance in PET radiochemistry. Chem Commun. 2013; 49:5621–5629.

313. Riss PJ, Lu S, Telu F, Aigbirhio FI, Pike VW. Cu-catalyzed conversion of boronates into ^{11}C-labeled carboxylic acids. Angew Chem Int Ed. 2012; 51:2698–2702.

314. Ram S, Ehrenkaufer RE, Spicer LD. Synthesis of the labeled D1 receptor antagonist SCH 23390 using [^{11}C]carbon dioxide. Appl Radiat Isot. 1989; 40:425–427.

315. Liger F, Eijsbouts T, Cadarossanesaib F, Tourvieille C, Le Bars D, Billard T. Direct [^{11}C]Methylation of amines from [^{11}C]CO_2 for the synthesis of PET radiotracers. Eur J Org Chem. 2015:6434–6438.

316. Dheere AKH, Yusuf N, Gee A. Rapid and efficient synthesis of [^{11}C]ureas via the incorporation of [^{11}C]CO_2 into aliphatic and aromatic amines. Chem Commun. 2013; 49:8193–8195.

317. Hooker JM, Reibel AT, Hill SM, Schueller MJ, Fowler JS. One-pot, direct incorporation of [^{11}C]CO_2 into carbamates. Angew Chem Int Ed. 2009; 48:3482–3485.

Author Manuscript Author Manuscript Author Manuscript Author Manuscript

318. Wuest, F., Berntd, M., Kiess, T. PET Chemistry the Driving Force in Molecular Imaging. Schubiger, PA.Lehmann, L., Friebe, M., editors. Vol. Ch 7. Springer; NewYork: 2007. p. 183-214.

319. Marazano C, Maziere M, Berger G, Comar D. Synthesis of methyl iodide-^{11}C and formaldehyde ^{11}C. Int J Appl Radiat Isot. 1977; 28:49–52. [PubMed: 558171]

320. Crouzel C, Långström B, Pike VW, Coenen HH. Recommendations for a practical production of [^{11}C]methyl iodide. Appl Radiat Isot. 1987; 38:601–603.

321. Iwata R, Ido T, Ujiie A, Takahashi T, Ishiwata K, Hatano K, Sugahara M. Comparative study of specific activity of [^{11}C]methyl iodide: a search for the source of carrier carbon. Appl Radiat Isot. 1988; 39:1–7.

322. Gomez-Vallejo V, Llop J. Specific activity of $^{11}CH_3I$ synthesized by the wet method; main sources of no-radioactive carbon. Appl Radiat Isot. 2008; 67:111–114. [PubMed: 19004631]

323. Link JM, Krohn KA, Clark JC. Production of [^{11}C]CH_3I by single pass reaction of [^{11}C]CH_4 with I_2. Nucl Med Biol. 1997; 24:93–97. [PubMed: 9080480]

324. Larsen P, Ulin J, Dahlstrom K, Jensen M. Synthesis of C-11 iodomethane by iodination of C-11 methane. Appl Radiat Isot. 1997; 48:153–157.

325. Kniess T, Rode K, Wuest F. Practical experiences with the synthesis of [^{11}C]CH_3I through gas phase iodination reaction using a TRACERlab FX(C) synthesis module. Appl Radiat Isot. 2008; 66:482–488. [PubMed: 17683943]

326. Sandell J, Langer O, Larsen P, Dollé F, Vaufrey F, Demphel S, Crouzel C, Halldin C. Improved specific radioactivity of the PET radioligand [^{11}C]FLB 457 by use of the GE medical systems PETtrace MeIMicroLab. J Label Compd Radiopharm. 2000; 43:331–338.

327. Wilson AA, Garcia AA, Jin LL, Houle SS. Radiotracer synthesis from [^{11}C]iodomethane: a remarkably simple captive solvent method. Nucl Med Biol. 2000; 27:529–532. [PubMed: 11056365]

328. Wilson AA, Garcia A, Houle S, Vasdev N. Utility of commercial radiosynthetic modules in captive solvent [^{11}C]-methylation reactions. J Label Compd Radiopharm. 2009; 52:490–492.

329. Jewett DM. A simple synthesis of [^{11}C]methyl triflate. Int J Rad Appl Instrum [A]. 1992; 43:1383–1385.

330. Mock BH, Mulholland GK, Vavrek MT. Convenient gas phase bromination of [^{11}C]methane and production of [^{11}C]methyl triflate. Nucl Med Biol. 1999; 26:467–471. [PubMed: 10382852]

331. Någren K, Muller L, Halldin C, Swahn CG, Lehikoinen P. Improved synthesis of some commonly used PET radioligands by the use of [^{11}C]methyl triflate. Nucl Med Biol. 1995; 22:235–239. [PubMed: 7767319]

332. Lundkvist C, Sandell J, Någren K, Pike VW, Halldin C. Improved syntheses of the PET radioligands, [^{11}C]FLB457, [^{11}C]MDL100907 and [^{11}C]beta-CIT-FE, by the use of [^{11}C]methyl triflate. J Label Compd Radiopharm. 1998; 41:545–556.

333. Luthra SK, Pike VW, Brady F. The preparation of carbon-11 labelled diprenorphine: a new radioligand for the study of the opiate receptor system. in vivo J Chem Soc, Chem Commun. 1985:1423–1425.

334. Luthra SK, Pike VW, Brady F. Preparation of some NCA [1–^{11}C]acid chlorides as labelling agents. J Labelled Comp Radiopharm. 1990; 26:471–476.

335. Hwang D-R, Simpson NR, Montoya J, Mann JJ, Laruelle M. An improved one-pot procedure for the preparation of [^{11}C-*carbonyl*]-WAY100635. Nucl Med Biol. 1999; 26:815–819. [PubMed: 10628562]

336. McCarron JA, Turton DR, Pike VW, Poole KG. Remotely-controlled production of the 5-HT_{1A} receptor radioligand, [*carbonyl*-^{11}C]WAY-100635, via ^{11}C-carboxylation of an immobilized Grignard reagent. J Labelled Comp Radiopharm. 1996; 38:941–953.

337. Dahl K, Itsenko O, Rahman O, Ulin J, Sjöberg C-O, Sandblome P, Larsson LA, Schou M, Halldin C. An evaluation of a high-pressure ^{11}CO carbonylation apparatus. J Labelled Comp Radiopharm. 2015; 58:220–225. [PubMed: 25820685]

338. Zeisler SK, Nader M, Theobald A, Oberdorfer F. Conversion of no-carrier-added [^{11}C]carbon dioxide to [^{11}C]carbon monoxide on molybdenum for the synthesis of ^{11}C-labelled aromatic ketones. Appl Radiat Isot. 1997; 48:1091–1095.

Author Manuscript Author Manuscript Author Manuscript Author Manuscript

339. Kihlberg, T., Långström, B. Method and apparatus for production of [^{11}C]carbon monoxide in labeling synthesis. PCT Int Appl. WO2002/102711. 2002.

340. Kealey S, Miller PW, Long NJ, Plisson C, Martarello L, Gee AD. Copper(I) scorpionate complexes and their application in palladium-mediated [^{11}C]carbonylation reactions. Chem Commun. 2009; 25:3696–698.

341. Taddei C, Bongarzone S, Dheere AKH, Gee AD. [^{11}C]CO_2 to [^{11}C]CO conversion mediated by [^{11}C]silanes: a novel route for [^{11}C]carbonylation reactions. Chem Commun. 2015; 51:11795–11797.

342. Eriksson J, van den Hoek J, Windhorst AD. Transition metal mediated synthesis using [^{11}C]CO at low pressure - a simplified method for ^{11}C-carbonylation. J Labelled Com Radiopharm. 2012; 55:223–228.

343. Långström B, Itsenko O, Rahman O. [^{11}C]Carbon monoxide, a versatile and useful precursor in labelling chemistry for PET ligand development. J Labelled Comp Radiopharm. 2007; 50:794–810.

344. Kealey S, Gee A, Miller PW. Transition metal mediated [^{11}C]carbonylation reactions: recent advances and applications. J Labelled Comp Radiopharm. 2014; 57:195–201. [PubMed: 24425679]

345. Rahman O. [^{11}C]Carbon monoxide in labeling chemistry and positron emission tomography tracer development: scope and limitations. J Labelled Comp Radiopharm. 2015; 58:86–98. [PubMed: 25689679]

346. Hong J, Lu S, Xu R, Liow J-S, Woock AE, Jenko KJ, Gladding RL, Zoghbi SS, Innis RB, Pike VW. [*carbonyl*-^{11}C]4-Fluoro-*N*-methyl-*N*-(4-(6-(methyl-amino) pyrimidin-4-yl)thiazol-2-yl)benzamide ([^{11}C]FIMX) is an effective radioligand for PET imaging of metabotropic glutamate receptor 1 (mGluR1) in monkey brain. Nucl Med Biol. 2015; 42:967–974. [PubMed: 26320813]

347. Andersson Y, Långström B. Transition metal-mediated reactions using [^{11}C]cyanide in synthesis of ^{11}C-labelled aromatic compounds. J Chem Soc Perkin Trans 1. 1994; 1:1395–400.

348. Siméon FG, Liow J-S, Zhang Y, Hong J, Gladding RL, Zoghbi SS, Innis RB, Pike VW. Synthesis and characterization in monkey of [^{11}C]SP203 as a radioligand for imaging brain metabotropic glutamate 5 receptors. Eur J Nucl Med Mol Imaging. 2012; 39:1949–1958. [PubMed: 22885775]

349. Shea C, Alexoff DL, Kim D, Hoque R, Schueller MJ, Fowler JS, Qu W. Total cyanide mass measurement with micro-ion selective electrode for determination of specific activity of carbon-11 cyanide. Appl Radiat Isot. 2015; 102:48–54. [PubMed: 25980658]

350. Berger G, Mazière M, Sastre J, Comar D. Carrier-free ^{11}C formaldehyde; an approach. J Labelled Comp Radio-pharm. 1980; 17:59–71.

351. Hooker JM, Schonberger M, Schieferstein H, Fowler J. A simple and rapid method for the preparation of [^{11}C]formaldehyde. Angew Chem Int Ed. 2008; 47:5989–5992.

352. Slegers G, Sambre J, Goethals P, Vandecasteele C, van Haver D. Synthesis of [1–^{11}C]iodoethane for the preparation of [^{11}C]ethyl labelled radiopharmaceuticals. Appl Radiat Isot. 1986; 37:279–282.

353. Långström B, Antoni G, Gullberg P, Halldin C, Någren K, Rimland A, Svärd H. The synthesis of 1–^{11}C-labeled ethyl propyl, butyl and isobutyl iodides and examples of alkylation reactions. Appl Radiat Isot. 1986; 37:1141–1145.

354. Schoeps KO, Stone-Elander S, Halldin C. On-line synthesis of [^{11}C]nitroalkanes. Appl Radiat Isot. 1989; 40:261–262.

355. Berger G, Mazière M, Prenant C, Comar D. Synthesis of carbon-11 labeled acetone. Int J Appl Radiat Isot. 1980; 31:577–578.

356. Landais P, Crouzel C. A new synthesis of carbon-11 labeled phosgene. Appl Radiat Isot. 1987; 38:297–300.

357. Roeda D, Crouzel C, van Zanten B. The production of ^{11}C-phosgene without added carrier. Radiochem Radioanal Lett. 1978; 33:175–178.

358. Bramoullé Y, Roeda D, Dollé F. A simplified [^{11}C]phosgene synthesis. Tetrahedron Lett. 2010; 51:313–316.

Author Manuscript Author Manuscript Author Manuscript Author Manuscript

359. Roeda D, Dollé F. [^{11}C]Phosgene: a versatile reagent for radioactive carbonyl insertion into medicinal radiotracers for positron emission tomography. Curr Top Med Chem. 2010; 10:1680–1700. [PubMed: 20583989]
360. Halldin C, Långström B. Synthesis of [^{11}C]-labelled aldehydes. Acta Chem Scand B. 1984; 38:1–4.
361. Fasth KJ, Malmborg P, Långström B. Synthesis of some ^{11}C-labeled substituted benzyl iodides. J Labelled Comp Radiopharm. 1989; 26:251–252.
362. Pekosak A, Filp U, Rotteveel L, Poot AJ, Windhorst AD. Improved synthesis and application of [^{11}C]benzyl iodide in positron emission tomography radiotracer production. J Labelled Comp Radiopharm. 2015; 58:342–348. [PubMed: 26031614]
363. Guillaume M, Luxen A, Nebeling B, Argentini M, Clark JC, Pike VW. Recommendations for fluorine-18 production. Appl Radiat Isot. 1991; 42:749–762.
364. Berridge MS, Apana SM, Hersch JM. Teflon radiolysis as the major source of carrier in fluorine-18. J Label Compd Radiopharm. 2009; 52:543–548.
365. Mukherjee J, Yang ZY, Das MK, Brown T. Fluorinated benzamides neuroleptics - III. Development of (*S*)-*N*-{(1-allyl-2-pyrrolidinyl)methyl]-5-(3-[^{18}F]fluoropropyl)-2,3-dimethoxybenzamide as an improved dopamine D-2 receptor tracer. Nucl Med Biol. 1995; 22:283–296. [PubMed: 7627142]
366. Hamill TG, Krause S, Ryan C, Bonnefous C, Goverk S, Seiderts TJ, Cosford ND, Roppe J, Kamenecka T, Patel S, Gibson RE, Sanabria S, Riffel K, Eng W, King C, Yang X, Green MD, Hargreaves R, Burns HD. Synthesis, characterization, and first successful monkey imaging studies of metabotropic glutamate receptor subtype 5 (mGluR5) PET radiotracers. Synapse. 2005; 56:205–216. [PubMed: 15803497]
367. Dollé F. Fluorine-18-labelled fluoropyridines: advances in radiopharmaceutical design. Curr Pharm Des. 2005; 11:3221–3235. [PubMed: 16250851]
368. Xiong H, Hoye AT, Fan K-H, Li X, Clemens J, Horchler CL, Lim NC, Attardo G. Facile route to 2-fluoropyridines via 2-pyridinyltrialkylammonium salts prepared from pyridine *N*-oxides and application to ^{18}F-labeling. Org Lett. 2015; 17:3726–3729. [PubMed: 26193373]
369. Pike VW, Aigbirhio FI. Reactions of cyclotron-produced [^{18}F]fluoride with diaryliodonium salts - a novel single-step route to no-carrier-added [^{18}F]fluoroarenes. J Chem Soc, Chem Commun. 1995:2215–2216.
370. Chun JH, Lu S, Lee YS, Pike VW. Fast and high yield microreactor syntheses of ortho substituted [^{18}F]fluoro-arenes from reactions of [^{18}F]fluoride ion with diaryliodonium salts. J Org Chem. 2010; 75:3332–3338. [PubMed: 20361793]
371. Satyamurthy, N., Barrio, JR. No-carrier-added nucleophilic [F-18]fluorination of aromatic compounds. WO2010/117435 A2. Date: 2010; October 14th
372. Rotstein BH, Stephenson NA, Vasdev N, Liang SH. Spirocyclic hypervalent iodine(III)-mediated radiofluorination of non-activated and hindered aromatics. Nat Commun. 2014; 5:1–7.
373. Yusubov MS, Svitch DY, Larkina MS, Zhdankin VV. Applications of iodonium salts and iodonium ylides as precursors for nucleophilic fluorination in positron emission tomography. Arkivoc. 2013; (i):364–395.
374. Kovac M, Mavel S, Anderluh M. ^{18}F-Labeled aryl-tracers through direct introduction of [^{18}F]fluoride into electron-rich arenes. Curr Org Chem. 2013; 17:2921–2935.
375. Tredwell M, Gouverneur V. ^{18}F Labeling of arenes. Angew Chem Int Ed. 2012; 51:11426–11437.
376. Moon BS, Park JH, Lee HJ, Lee BC, Kim SE. Routine production of [^{18}F]flumazenil from iodonium tosylate using a sample pretreatment method: a 2.5-year production report. Mol Imaging Biol. 2014; 16:619–625. [PubMed: 24788440]
377. Ichiishi N, Brooks AF, Topczewski J, Rodnick ME, Sanford MS, Scott PJH. Copper-catalyzed [^{18}F]fluorination of (mesityl)(aryl)iodonium salts. Org Lett. 2014; 16:3224–3227. [PubMed: 24890658]
378. Mossine AV, Brooks AF, Makaravage KJ, Miller JM, Ichiishi N, Sanford MS, Scott PJH. Synthesis of [^{18}F]arenes via the copper-mediated [^{18}F]fluorination of boronic acids. Org Lett. 2015; 17:5780–5783. [PubMed: 26568457]

Author Manuscript Author Manuscript Author Manuscript Author Manuscript

379. Tredwell M, Preshlock S, Taylor NJ, Gruber S, Huiban M, Passchier J, Mercier J, Genicot C, Gouverneur V. A general copper-mediated nucleophilic F-18 fluorination of arenes. Angew Chem Int Ed. 2014; 53:7751–7755.

380. Kniess T, Laube M, Brust P, Steinbach J. 2-[^{18}F]Fluoroethyl tosylate - a versatile tool for building ^{18}F-based radiotracers for positron emission tomography. Med Chem Comm. 2015; 6:1714–1754.

381. Zhang MR, Suzuki K. [^{18}F]Fluoroalkyl agents: synthesis, reactivity and application for development of PET ligands in molecular imaging. Curr Top Med Chem. 2007; 7:1817–1828. [PubMed: 17979790]

382. Wuest, F. PET Chemistry - The Driving Force in Molecular Imaging. Schubiger, PA.Lehmann, L., Friebe, M., editors. Vol. Ch 3. Springer; New York: 2007. p. 52-78.

383. Riss PJ, Aigbirhio FI. A simple, rapid procedure for nucleophilic radiosynthesis of aliphatic [^{18}F]trifluoromethyl groups. Chem Commun. 2011; 47:11873–11875.

384. van der Born D, Herscheid JDM, Orru RVA, Vugts DJ. Efficient synthesis of [^{18}F]trifluoromethane and its application in the synthesis of PET tracers. Chem Commun. 2013; 49:4018–4020.

385. Huiban M, Tredwell M, Mizuta S. A broadly applicable [^{18}F]trifluoromethylation of aryl and heteroaryl iodides for PET imaging. Nat Chem. 2013; 5:941–944. [PubMed: 24153372]

386. Lien VT, Riss PJ. Radiosynthesis of [^{18}F]trifluoroalkyl groups: scope and limitations. BioMed Res Int. 2014; 2014:380124.doi: 10.1155/2014/380124 [PubMed: 25110676]

387. Ruehl T, Rafique W, Lien VT, Riss P. Cu(I)-mediated ^{18}F-trifluoromethylation of arenes. Chem Commun. 2014; 50:6056–6059.

Author Manuscript Author Manuscript Author Manuscript Author Manuscript

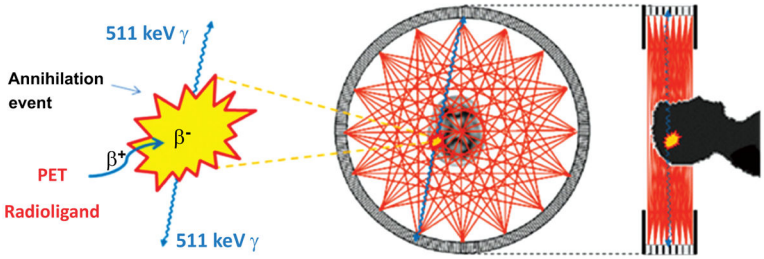

Fig. (1).

Physical basis of PET brain imaging. A PET radioligand that has entered brain after intravenous administration emits a positron. This positron loses kinetic energy over a short distance of a few millimeters before combining with an electron to form positronium, which then annihilates to produce two 511 keV γ-rays that are emitted in almost exactly opposite directions. The PET camera has several adjacent rings of sensitive γ-ray detectors that record all such coincident arrivals of paired γ-rays. Lines between pairs of simultaneously activated detectors cover the positions of positron annihilation events from which PET scans can be reconstructed to *measure* the distribution of radioactivity in three dimensions. Rapid sequences of scans are recorded to provide regional kinetic information over a few half-lives of the radioligand label (*i.e.*; ^{11}C or ^{18}F). The detection of coincident γ-ray arrivals amounts to 'electronic collimation', and dispenses with the need for 'physical collimation' which would otherwise diminish detection sensitivity as in SPECT.

Author Manuscript Author Manuscript Author Manuscript Author Manuscript

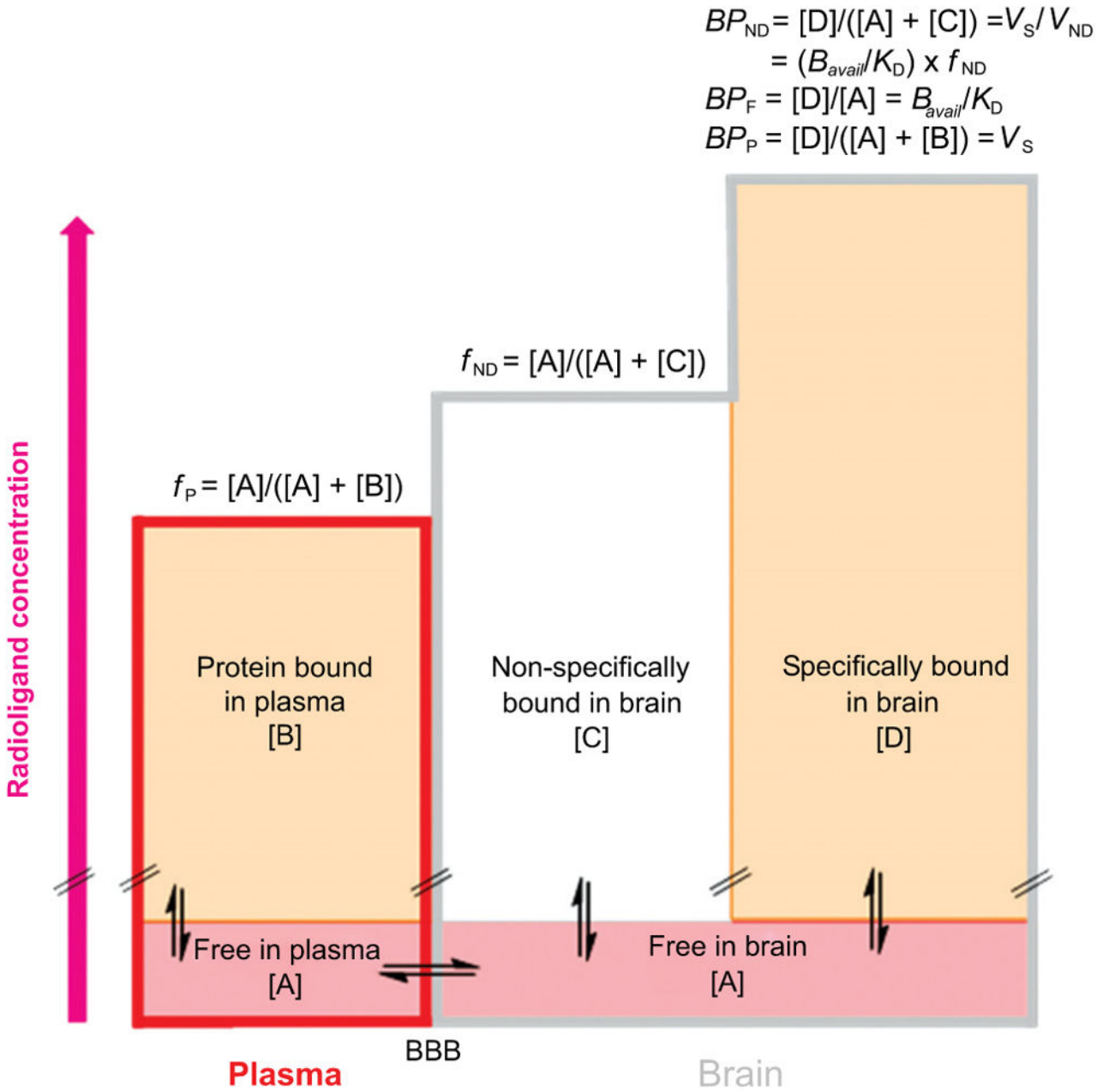

Fig. (2).

Graphical representation of the distribution of a PET radioligand between plasma and 2 tissues in brain *at equilibrium*. The height of each rectangle represents radioligand concentration. The free concentration of radioligand in plasma and brain is assumed to be the same and equal to **[A]**, because of assumed free unhindered bidirectional passive diffusion across the BBB. The plasma free fraction of radioligand, $f_{P,}$ is the ratio of free radioligand concentration **[A]** to total radioligand concentration in plasma *i.e.*; free **[A]** plus protein bound **[B]**. Similarly, the brain free fraction of a radioligand, $f_{ND,}$ is the ratio of free radioligand concentration **[A]** to the sum of free **[A]** and nonspecifically bound **[C]**

radioligand concentrations in brain. **[D]** Represents the specifically bound concentration of radioligand in brain. Some mathematical relationships of *binding potentials* to other parameters are shown above the right column.

Author Manuscript Author Manuscript Author Manuscript Author Manuscript

Author Manuscript Author Manuscript Author Manuscript Author Manuscript

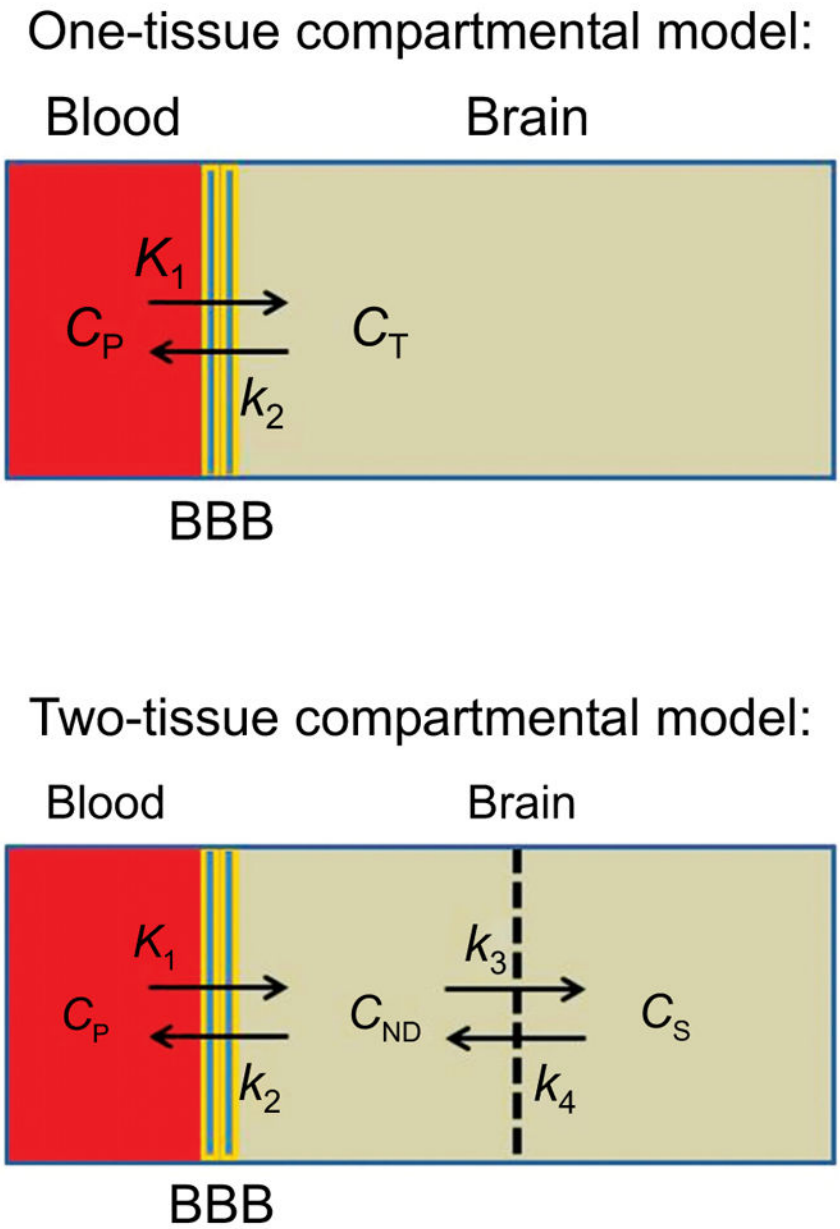

Fig. (3).

One and two tissue compartmental models that are frequently used as a basis for quantification of PET radioligand behavior: (C_P, plasma radioligand concentration; C_T, brain tissue radioligand concentration; C_{ND}, nonspecific plus free radioligand concentration; C_S, specific radioligand concentration).

Author Manuscript Author Manuscript Author Manuscript Author Manuscript

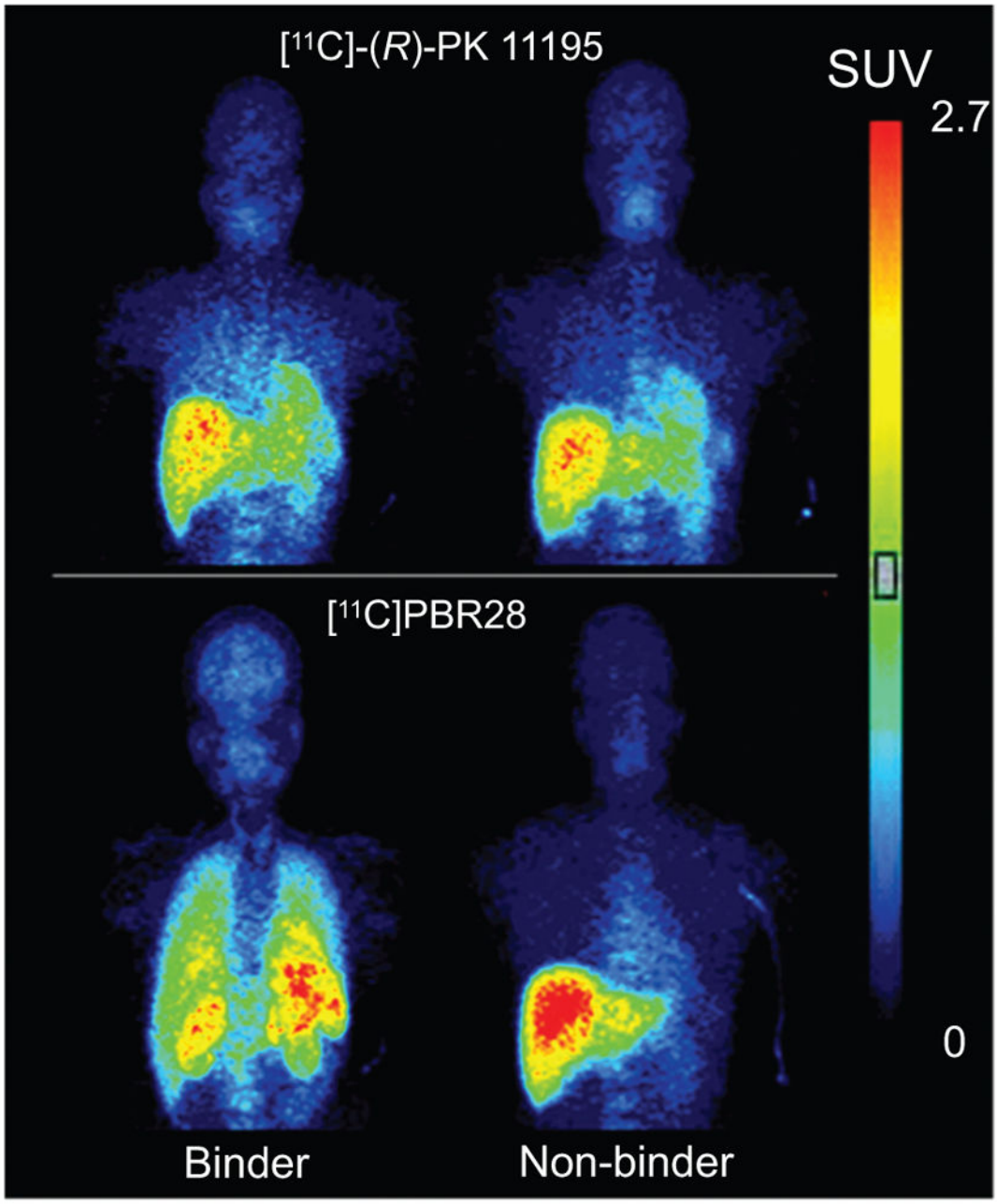

Fig. (4).

Imaging of TSPO in brain and body organs under baseline conditions in PBR28 binders (HABs) and non-binders (LABs) with the prototypical radioligand [^{11}C](*R*)-PK11195 and with the later generation radioligand [^{11}C] PBR28. From Kreisl *et al.* [43], with permission. Unlike [^{11}C](*R*)-PK11195, [^{11}C]PBR28 shows no TSPO-specific binding in brain or periphery of non-binder.

Author Manuscript Author Manuscript Author Manuscript Author Manuscript

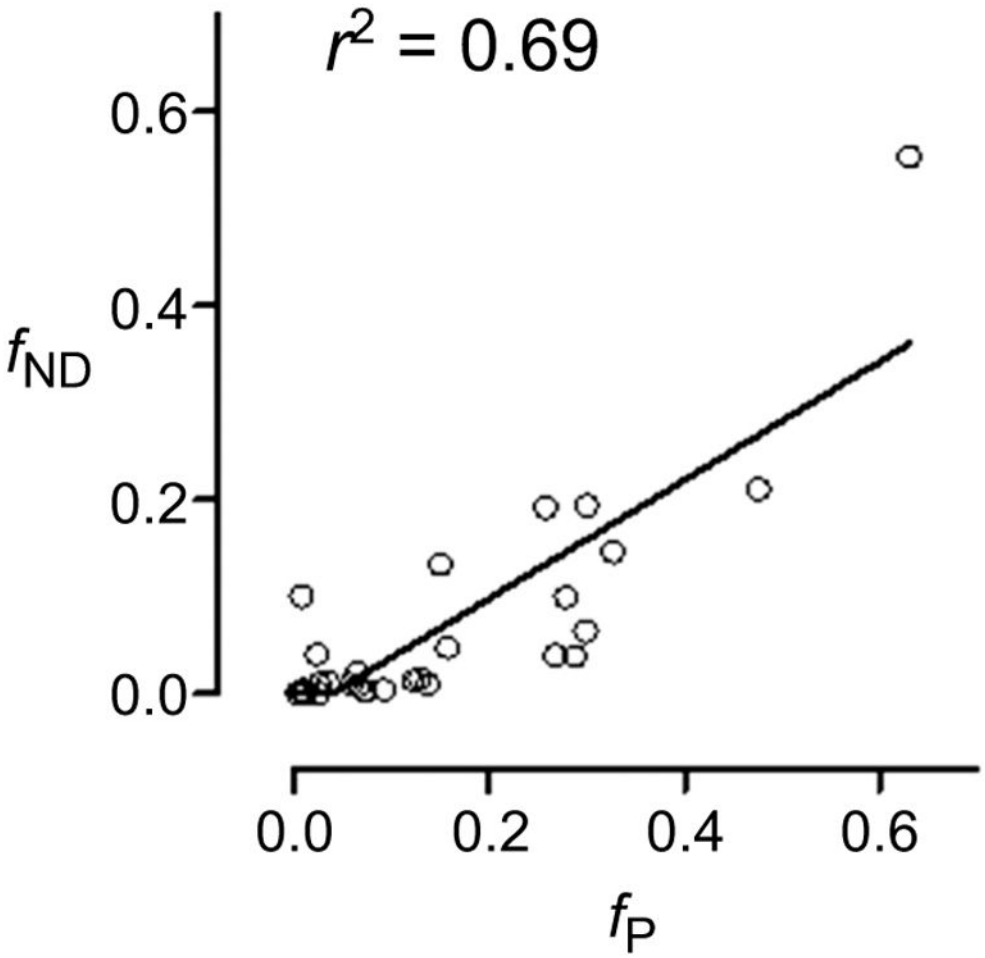

Fig. (5).

Plot of f_{ND} *versus* f_P for 28 ligands in pig. Data are sourced from from Guo *et al.* [99]. Although the plot shows a quite strong linear correlation, slope is far from unity, and differences between parameters can be large for many ligands.

Author Manuscript Author Manuscript Author Manuscript Author Manuscript

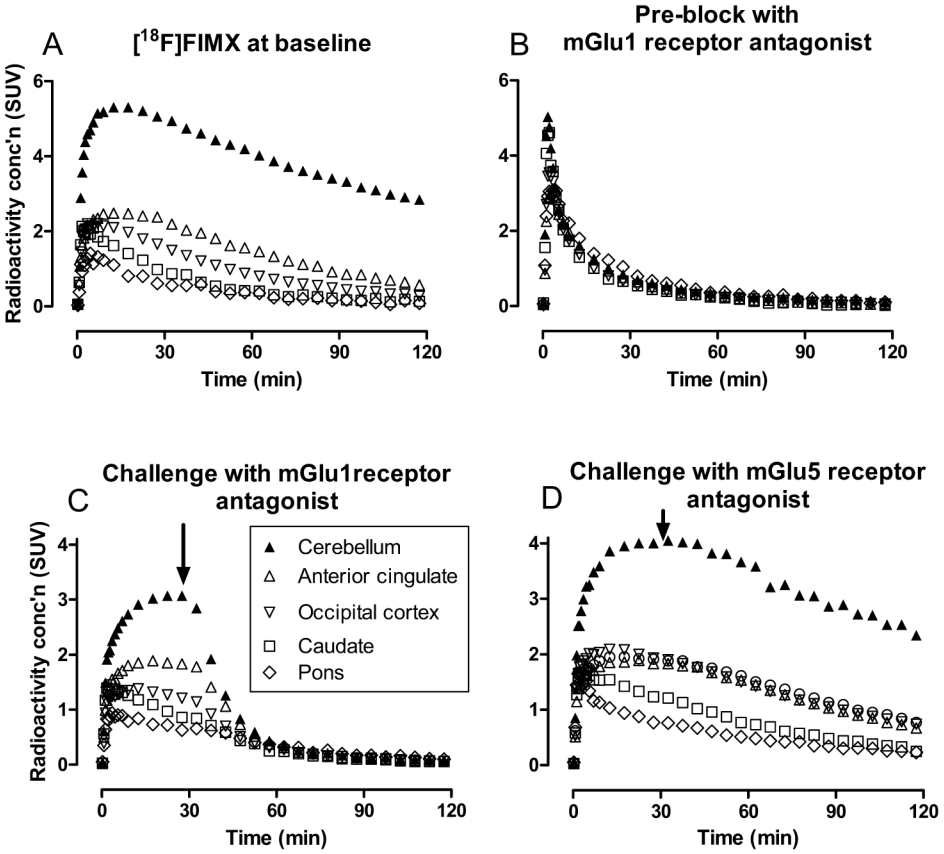

Fig. (6).

PET Time-activity curves in monkey brain regions after administration of [^{18}F]FIMX. **(A)** At baseline; **(B)** after pre-block with a selective mGlu1 receptor antagonist; **(C)** at baseline with challenge from an mGlu1 receptor antagonist at 27.5 min; and **(D)** at baseline with challenge from an mGlu5 receptor antagonist at 27.5 min. (Adapted from [107]). The experiments show that [^{18}F]FIMX has high specific binding to mGlu1 receptors at baseline.

Author Manuscript Author Manuscript Author Manuscript Author Manuscript

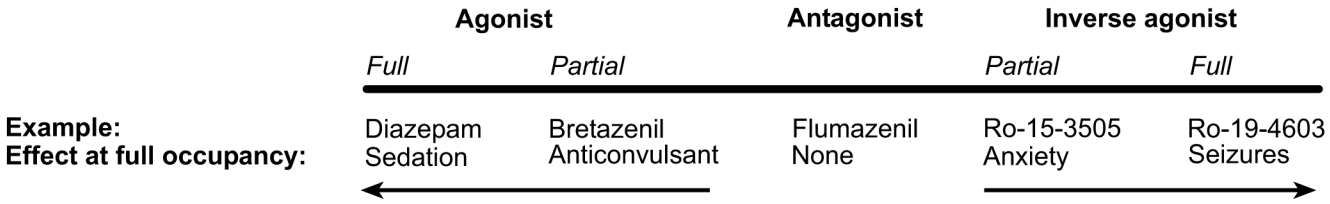

Fig. (7).
Illustration of the spectrum of ligand efficacy with ligands for benzodiazepine receptors.

Author Manuscript Author Manuscript Author Manuscript Author Manuscript

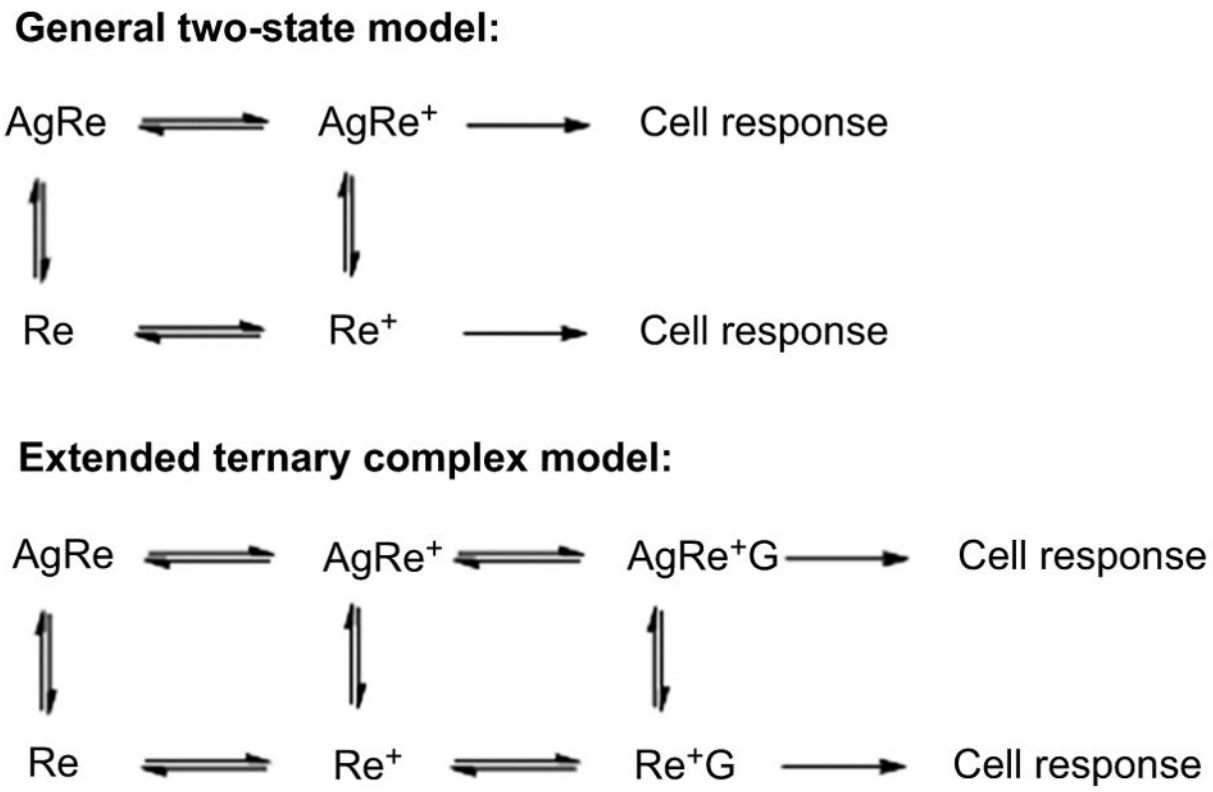

Fig. (8).
The general two-state and extended ternary complex models of GPCR function induced by an agonist. Ag is agonist, Re is receptor, Re* is receptor in activated state, and G is a G-protein.

Author Manuscript Author Manuscript Author Manuscript Author Manuscript

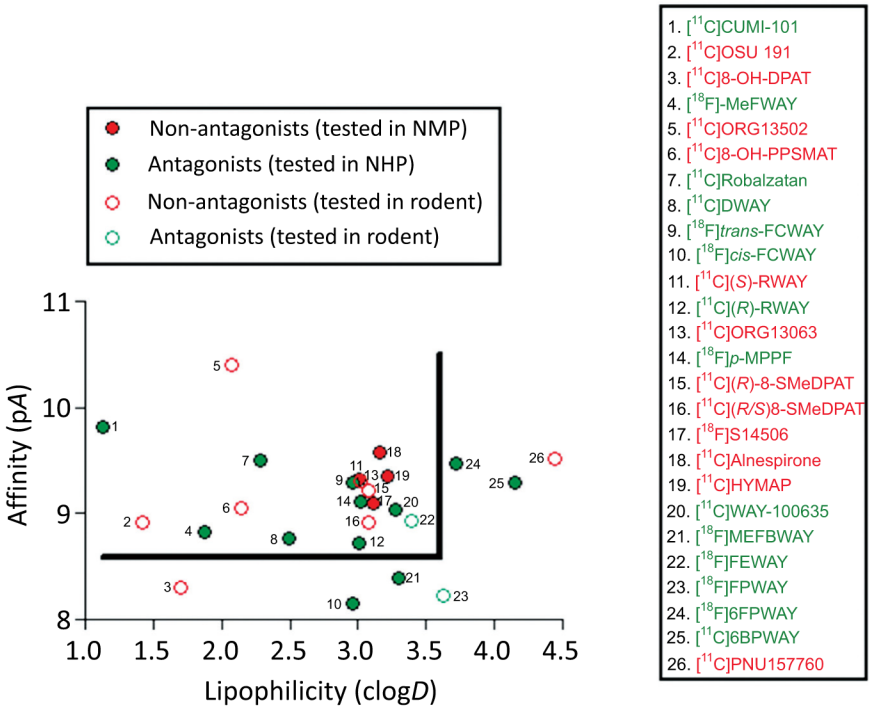

Fig. (9).

Plot of affinity (p*A) versus* computed lipophilicity (clogD) for antagonist and non-antagonist radioligands for brain 5-HT_{1A} receptors. All 26 radioligands have been tested in monkey (solid symbols) or in rat (open symbols). Antagonists shown by green solid symbols and within the top left-hand sector bounded by the line gave strong performance in monkey, whereas agonist radioligands (solid red symbols) with similar affinity and lipophilicity give small or negligible signals. Similarly agonists perform poorly in rat (open red circles). Radioligands 1 (originally classed as an agonist), 4, 7, 8, 9, 14 and 20 have been used in human studies. The plot indicates that high affinity, moderate lipophilicity and antagonist pharmacology are desirable properties for obtaining sensitive radioligands for imaging brain 5-HT_{1A} receptors in animal or human brain. clogD was calculated with Pallas software. Other data are from reference [120], and references therein, except for radioligands 1 [125], 4 [126], 11 [127], and 12 [127].

Author Manuscript Author Manuscript Author Manuscript Author Manuscript

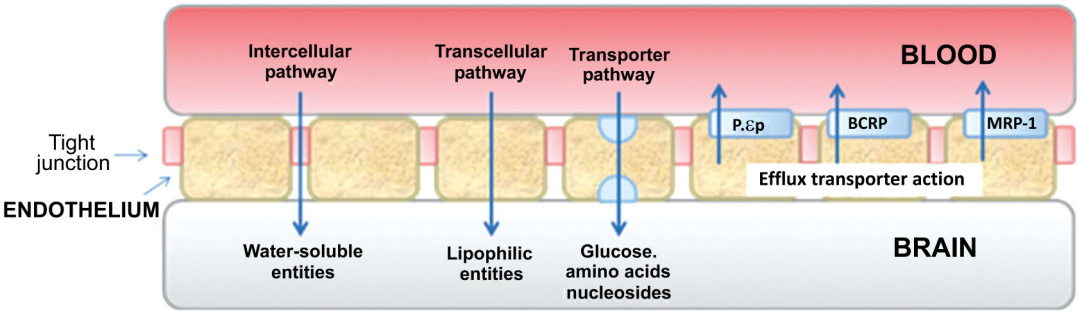

Fig. (10).

Representation of the structure of the BBB showing pathways into brain and major efflux transporters.

Author Manuscript Author Manuscript Author Manuscript Author Manuscript

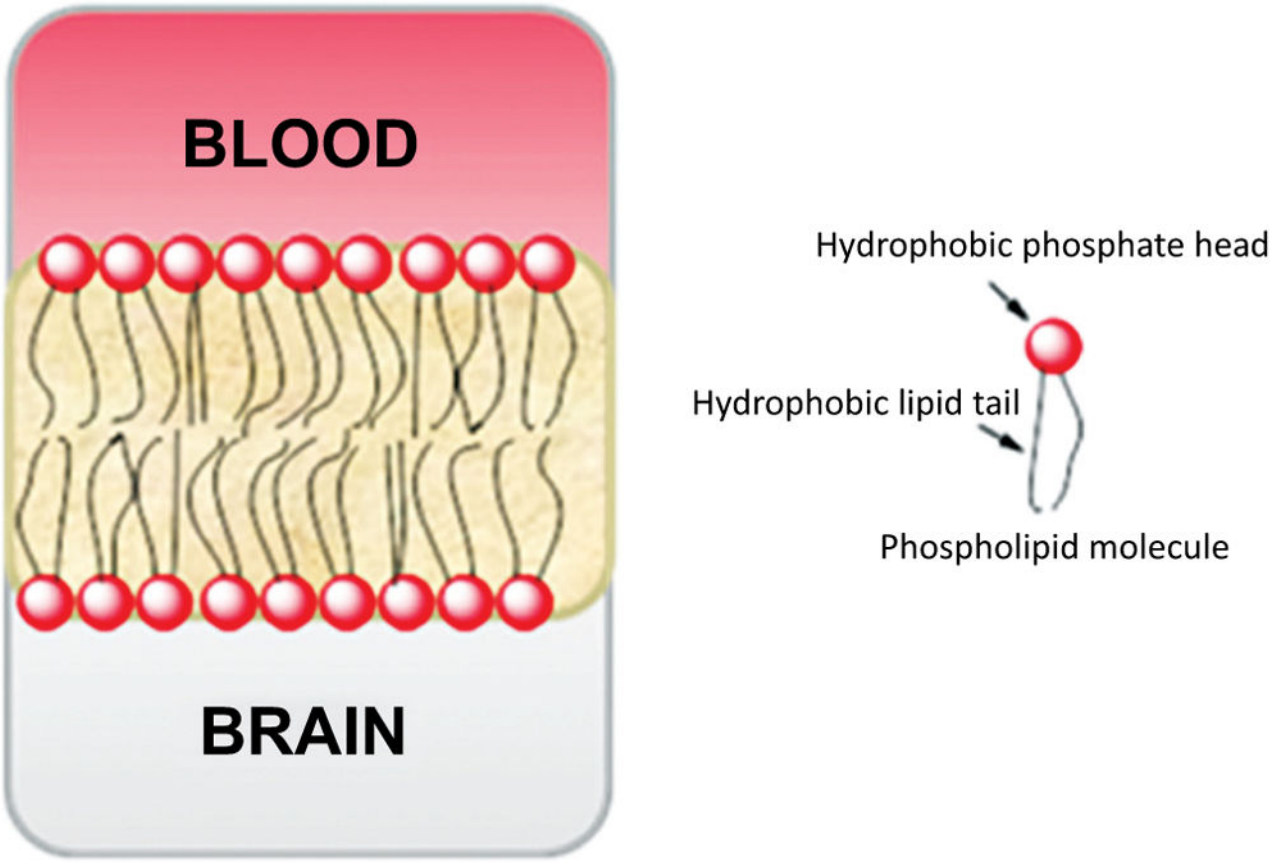

Fig. (11).
Representation of the structure of the phospholipid bilayer at the BBB.

Author Manuscript Author Manuscript Author Manuscript Author Manuscript

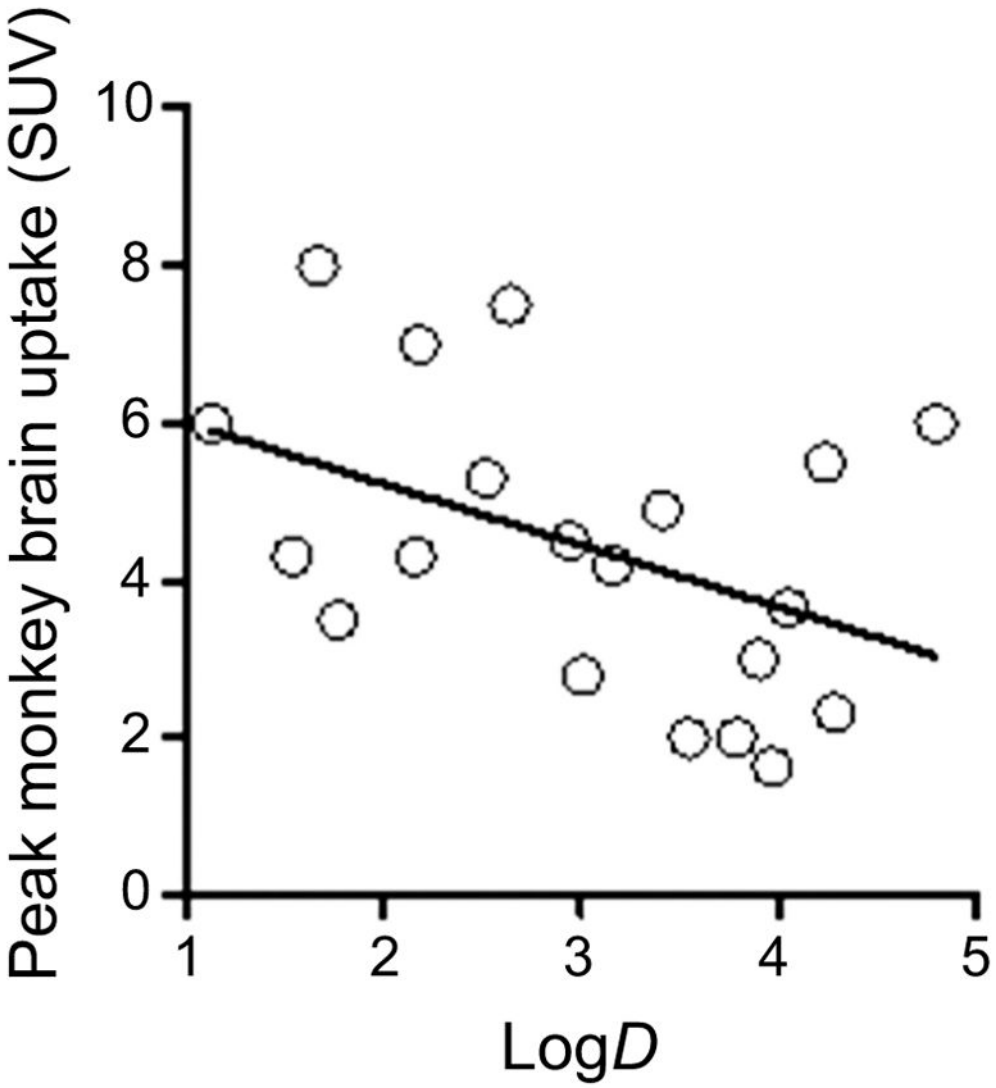

Fig. (12).

Plot of peak radioactivity concentration in rhesus monkey brain (SUV) *versus* radioligand lipophilicity (measured logD) for the 20 radioligands listed in Table 4. Line represents linear fit (r^2 = 0.19).

Author Manuscript Author Manuscript Author Manuscript Author Manuscript

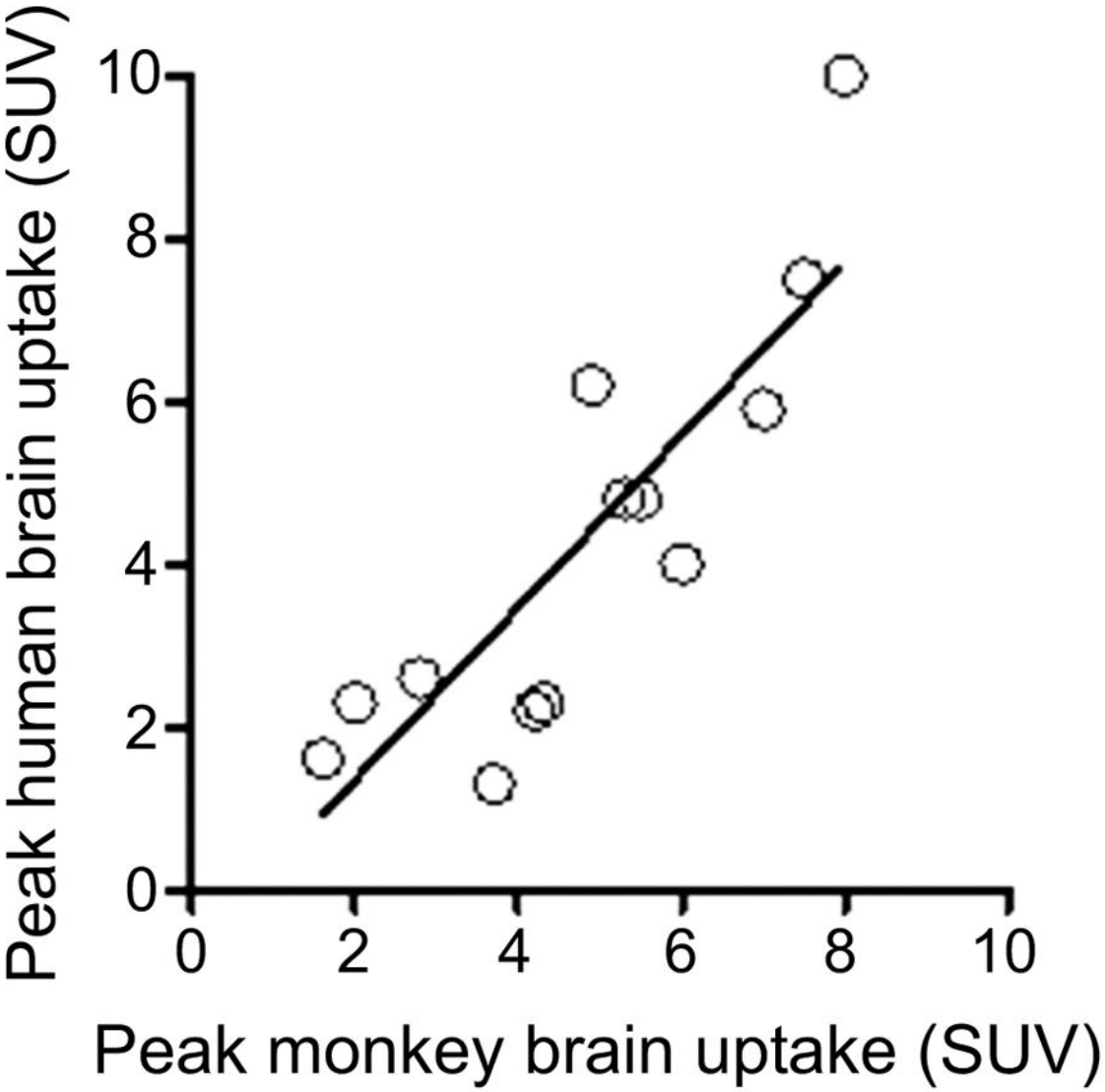

Fig. (13).
Relationship of peak human brain uptake to peak monkey brain uptake (SUV) for 14 radioligands in Table 4. Line represents linear fit (r^2 = 0.74).

Author Manuscript Author Manuscript Author Manuscript Author Manuscript

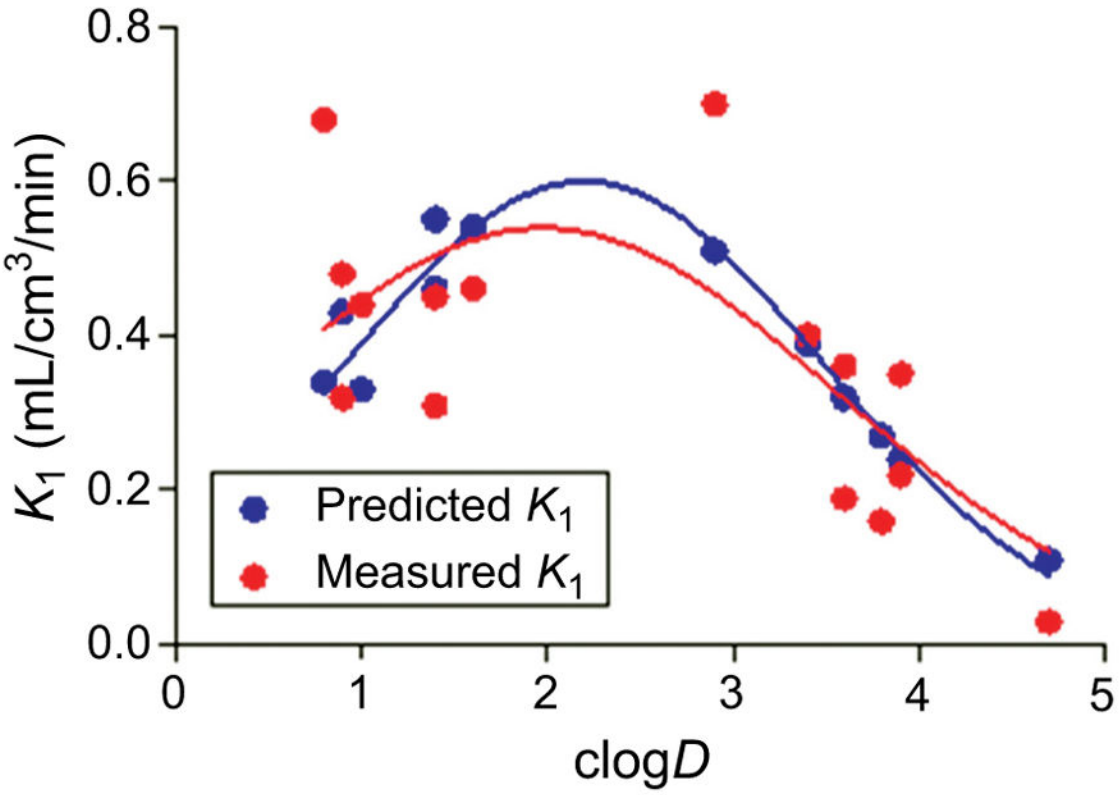

Fig. (14).

Plots of predicted and measured K_1 *versus* lipophilicity (clogD) for 15 ligands in pig. The blue and red lines are Gaussian fits to the predicted and measured data, respectively. (Source data: Guo *et al.* [99]).

Author Manuscript Author Manuscript Author Manuscript Author Manuscript

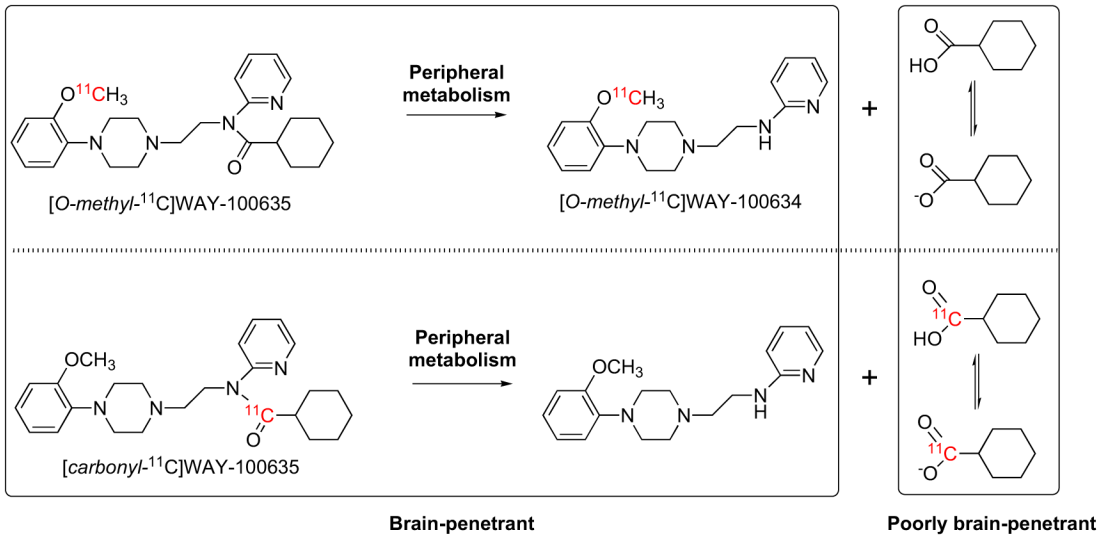

Fig. (15).

Metabolism of [*O-methyl*-^{11}C]WAY-100635 and [*carbonyl*-^{11}C]WAY-100635 in primates. Labeling in the carbonyl position avoids generating the brain-penetrant radioactive amine [*O-methyl*-^{11}C]WAY-100634.

Author Manuscript Author Manuscript Author Manuscript Author Manuscript

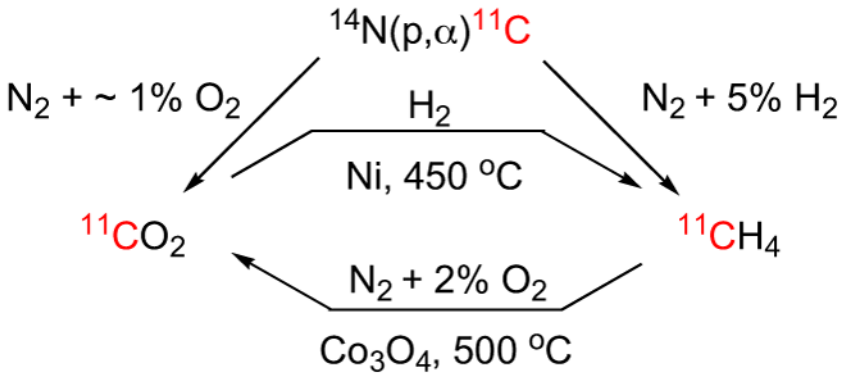

Fig. (16).

Cyclotron methods for preparing [^{11}C]carbon dioxide or [^{11}C]methane, and methods for their on-line intercon-versions.

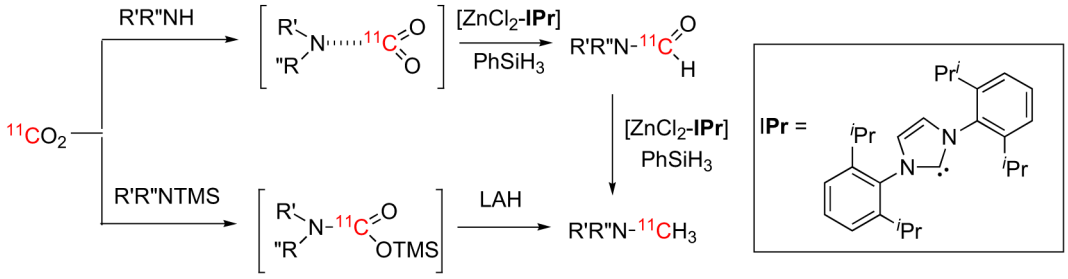

Fig. (17).

Preparation of [*N-methyl*-^{11}C]amines via ^{11}C-carbonylation of amines.

Author Manuscript Author Manuscript Author Manuscript Author Manuscript

Author Manuscript Author Manuscript Author Manuscript Author Manuscript

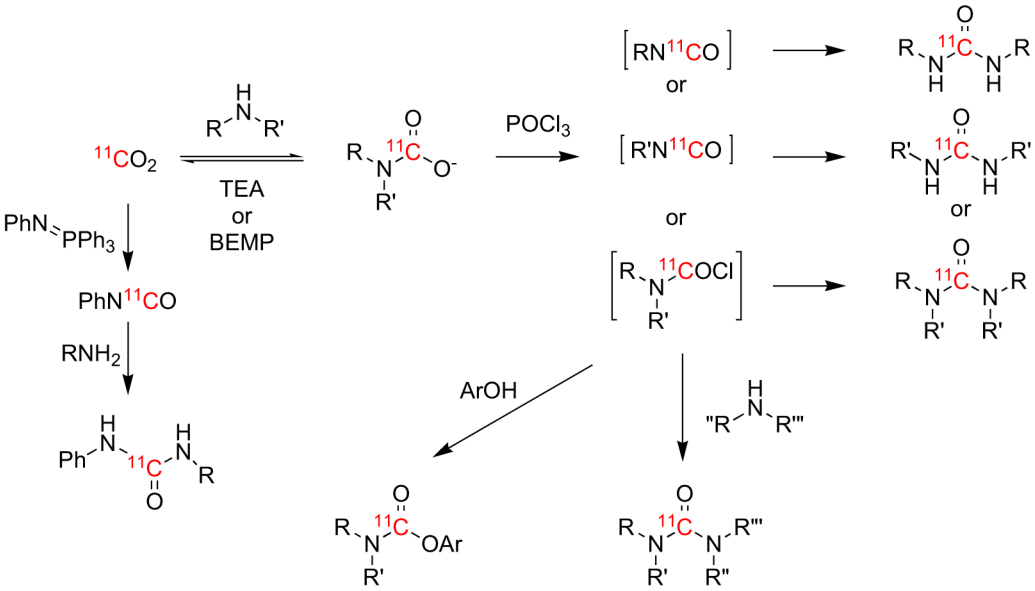

Fig. (18).
Utility of [^{11}C]carbon dioxide for labeling ureas and carbamates.

Author Manuscript Author Manuscript Author Manuscript Author Manuscript

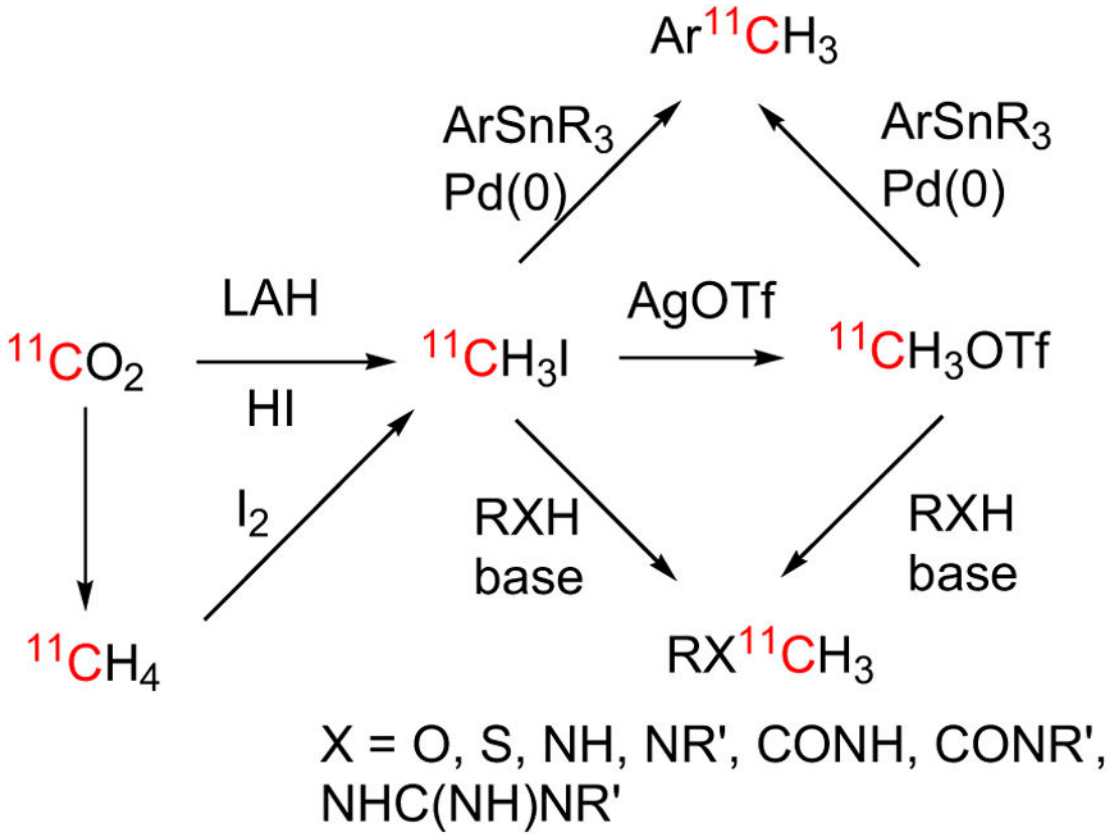

Fig. (19).
Preparation of [^{11}C]methyl iodide and [^{11}C]methyl triflate and utility for radiolabeling various structural motifs.

Author Manuscript Author Manuscript Author Manuscript Author Manuscript

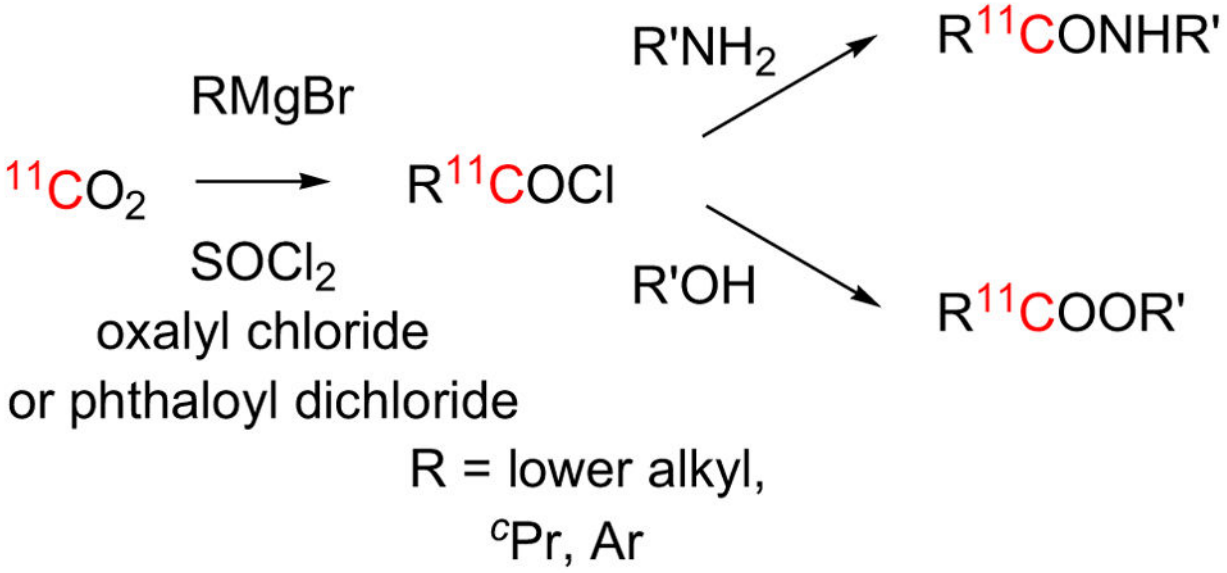

Fig. (20).
Preparation and utility of [^{11}C]acid chlorides.

Author Manuscript Author Manuscript Author Manuscript Author Manuscript

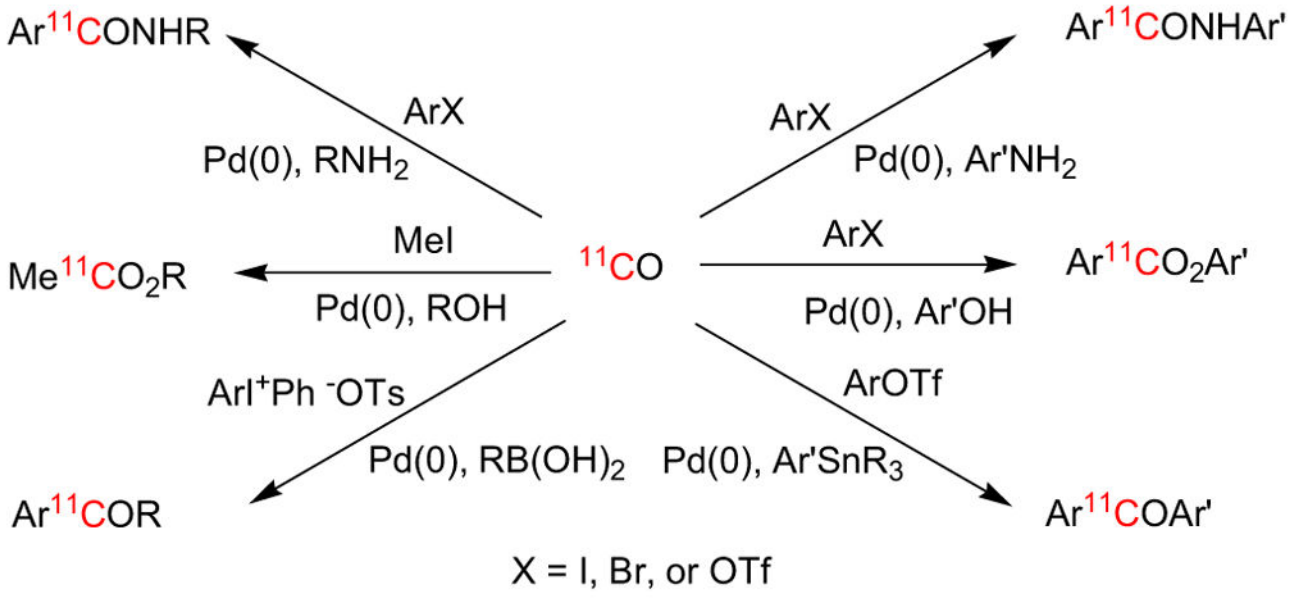

Fig. (21).
Synthesis of ^{11}C-labeled ketones, esters, and amides from [^{11}C]carbon monoxide.

Author Manuscript Author Manuscript Author Manuscript Author Manuscript

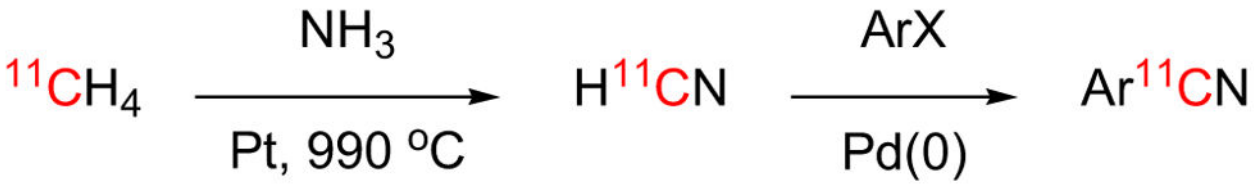

Fig. (22).
Preparation of [^{11}C]hydrogen cyanide and application to prepare [^{11}C]aryl nitriles.

Author Manuscript Author Manuscript Author Manuscript Author Manuscript

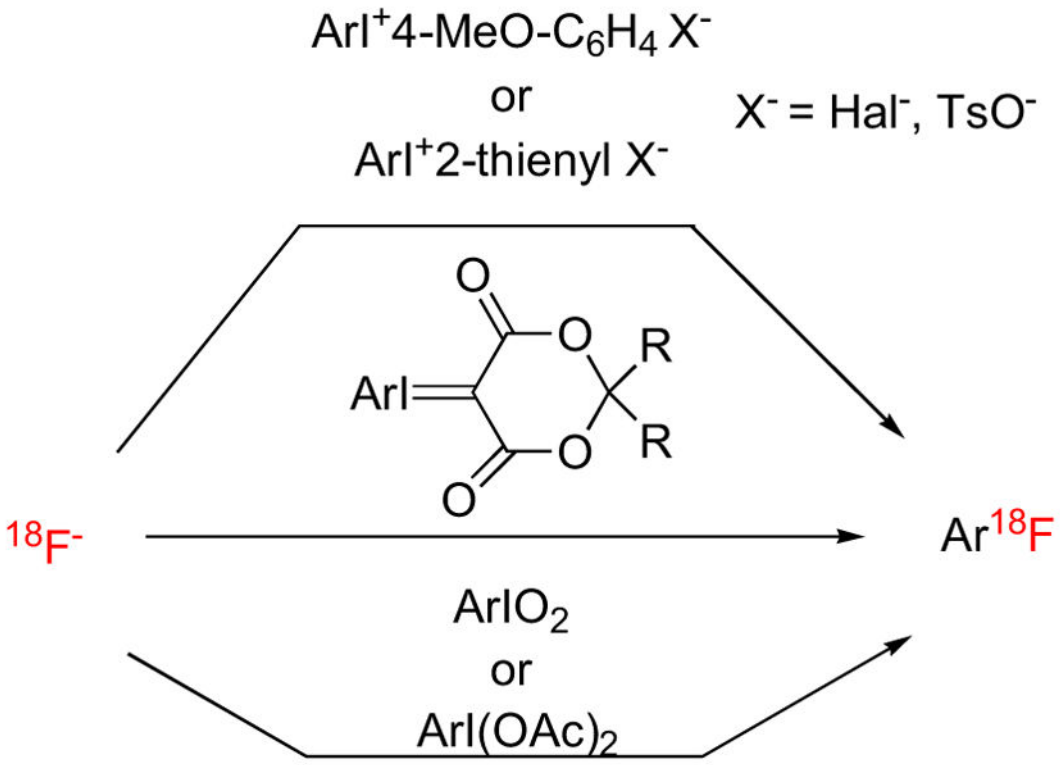

Fig. (23).
Preparation of [^{18}F]aryl fluorides from hypervalent iodine substrates.

Author Manuscript Author Manuscript Author Manuscript Author Manuscript

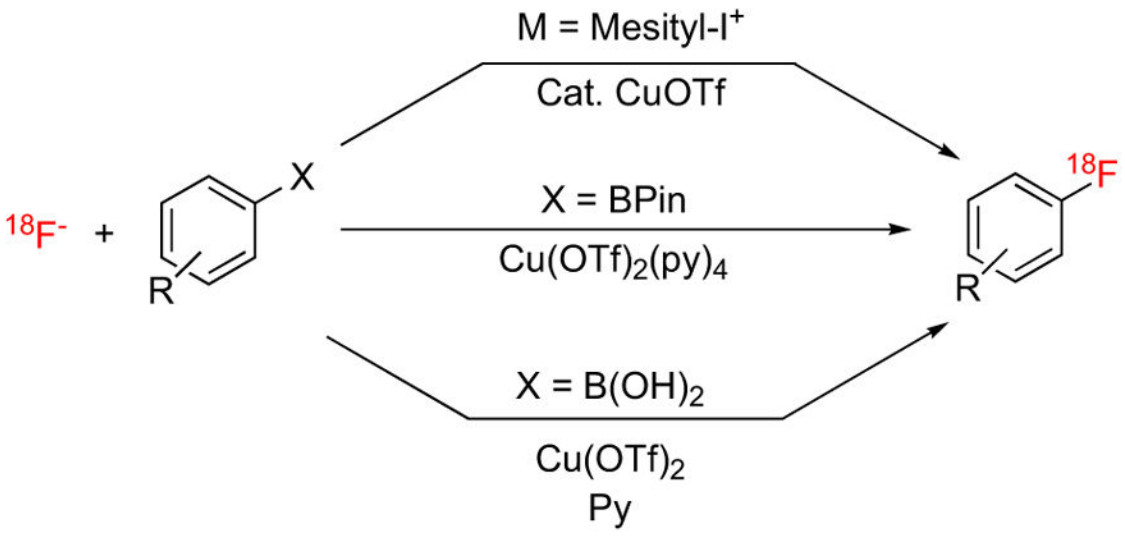

Fig. (24).
Cu-mediated routes to [^{18}F]fluoroarenes from [^{18}F]fluoride ion.

Author Manuscript Author Manuscript Author Manuscript Author Manuscript

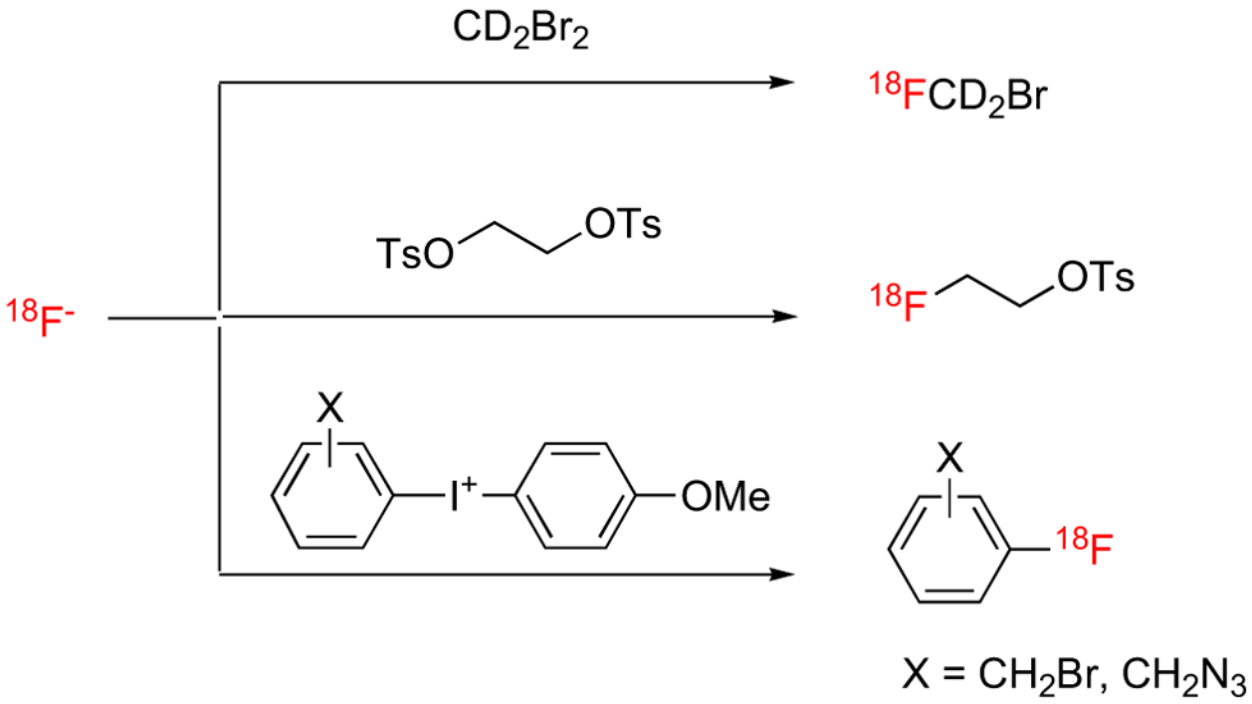

Fig. (25).
Examples of conversions of [^{18}F]fluoride ion into secondary labeling agents.

Author Manuscript Author Manuscript Author Manuscript Author Manuscript

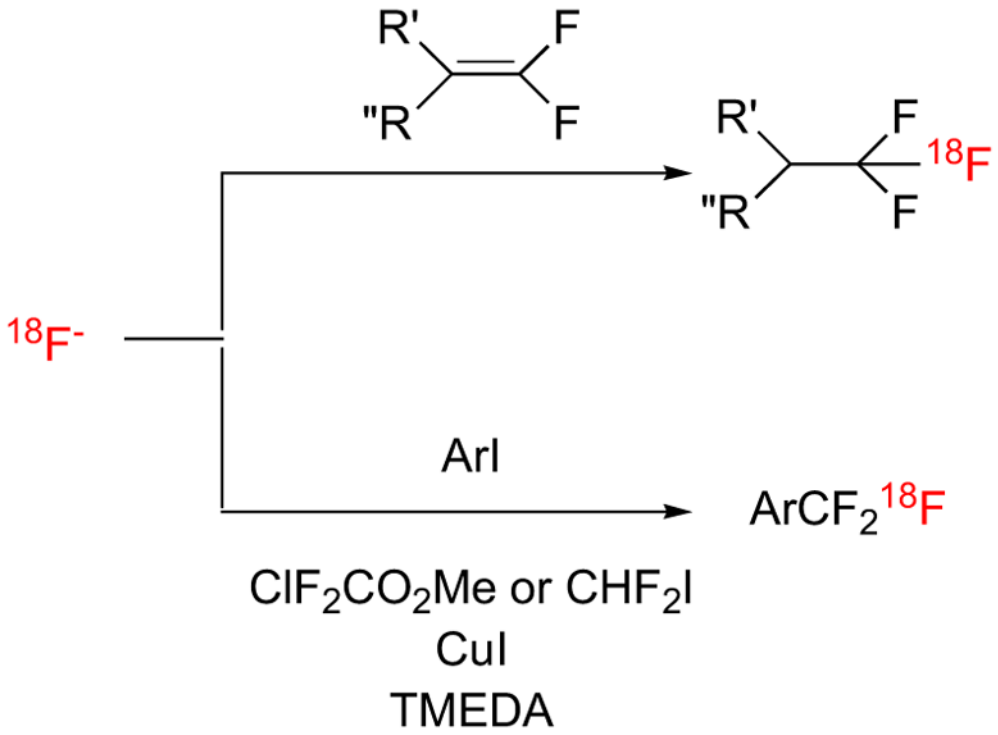

Fig. (26).
Labeling of alkyl and aryl trifluoromethyl groups with [^{18}F]fluoride ion.

Author Manuscript Author Manuscript Author Manuscript Author Manuscript

Table 1

Examples of drugs for treating neuropsychiatric disorders, and their respective protein targets.

Drug	For treating:	Main putative site(s) of action	Type
Alprazolam	Anxiety, Panic disorder	$GABA_A$ Receptor (Bz binding site)	Channel
Amphetamine	ADHD, Narcolepsy	DAT	Transporter
Ariprazole	Psychosis, Depression	D_2, 5-HT_{1A} and other receptors	GPCRs
Buprenorphine	Opiate addiction, Pain	μ-Opiate receptor	GPCR
Duloxetine	Depression, Anxiety	SERT and NET	Transporters
Escitalopram	Depression, Anxiety	SERT	Transporter
Fluoxetine	Depression, Anxiety	SERT	Transporter
Galantamine	Alzheimer's disease	AChE	Enzyme
Lorazepam	Anxiety, Panic disorder	$GABA_A$ receptor (Bz binding site)	Channel
Memantine	Alzheimer's disease	NMDA Receptor	Channel
Methylphenidate	ADHD	DAT	Transporter
Pregabalin	Neuropathic pain, Anxiety	Ca^{2+} channel ($\alpha_2\delta$ subunit)	Channel
Quetiapine	Bipolar disorder, Schizophrenia	D_2, 5-HT_{2A} Receptors, and others	GPCRs
Rasagiline	Parkinson's disease	MAO-B	Enzyme
Risperidone	Schizophrenia, Bipolar disorder	D_2 and 5-HT_2 receptors	GPCRs
Sertraline	Depression, Anxiety, OCD, PTSD, PMDD	SERT	Transporter
Trazodone	Depression, Anxiety	SERT	Transporter
Venlafaxine	Depression, Anxiety	SERT, NET and DAT	Transporters

Author Manuscript Author Manuscript Author Manuscript Author Manuscript

Table 2

B_{max}, K_D, and B_{max}/K_D values determined *in vitro* on normal human brain tissue for some protein targets successfully imaged with PET.

Protein	Brain region	Radioligand[a]	B_{max} (nM)	K_D (nM)	B_{max}/K_D[b]	Reference
5-HT_{1A}	Parahipp. gyrus	**[^{3}H]WAY-100635**	24±2	1.1±0.2	22	[61]
5-HT_4	Caudate	[^{3}H]GR113808	9±2	0.07±0.01	129	[62]
	Caudate	[^{3}H]GR113808	14.9	0.20	75	[63]
5-HT_6	Striatum	[^{125}I]SB-258585	22±4	1.3	17	[64]
$\alpha_4\beta_2$nAChR	Cortex	**6-[^{18}F]fluoro-A-85380**	0.7	0.059	12	[65]
Aβ plaques	Temporal cortex	**[^{11}C]PIB**	28[b]	~2	~ 14	[66]
Bz	Neocortex	**[^{3}H]Flumazenil**	35	6.1	6	[67]
	Temporal cortex	**[^{3}H]Flumazenil**	70±2	2.2±0.1	32	[68]
		[^{3}H]Sarmazenil	54±2	1.9±0.2	29	[68]
CB_1	Frontal cortex	**[^{3}H]MePPEP**	47±17	0.3±0.1	157	[69]
D_1	Caudate	**[^{3}H]SCH23390**	103±17	2.1±0.6	49	[70]
D_2	Putamen	**[^{3}H]Raclopride**[c]	8±1	0.9	9	[71]
	Putamen	**[^{3}H]Raclopride**[d]	9.9±0.9	3.89	3	[71]
	Caudate	**[^{3}H]Raclopride**[e]	24±9	2.5±0.2	10	[72]
DAT	Putamen	**[^{3}H]RTI-55**	52±17	0.10±0.02	520	[73]
GlyT-1	Cortex	**[^{3}H]GSK931145**	57±7	4.5±0.8	13	[74]
mGluR5	Cortex	**[^{18}F]FPEB**	25±6	0.11±0.04	230	[75]
Opiate	Frontal cortex	**[^{3}H]Diprenorphine**	14.8±0.9	0.22± 0.03	67	[76]
NET	Locus coeruleus	**[^{18}F](*S*,*S*)-FMeNER-D_2**	35±3	3.6	10	[55]

Author Manuscript Author Manuscript Author Manuscript Author Manuscript

Protein	Brain region	Radioligand[a]	B_{max} (nM)	K_D (nM)	B_{max}/K_D[b]	Reference
SERT	Hippocampus	[^{3}H]Citalopram	28±4	3.6±0.8	8	[77]
NK_1	Striatum	[^{3}H]GR205171	43±3	0.02	2150	[78]
TSPO	Temporal cortex	**[^{3}H]PK11195**	71±6	2.9±0.5	24	[79]

[a] Ligands shown in bold, when labeled with carbon-11 or fluorine-18, have been used for imaging the target protein with PET.

[b] Rounded to nearest integer.

[c] AD brain

[d] at 23 °C

[e] at 37 °C

Author Manuscript Author Manuscript Author Manuscript Author Manuscript

Table 3

Examples of PET studies determining brain protein density (B_{avail}) and/or radioligand (K_D) affinity in normal human subjects, and the corresponding B_{avail}/K_D values.

Protein	Brain region	Radioligand	B_{avail} from PET (nM)	K_D from PET (nM)	B_{avail}/K_D from PET[a]	Reference
Bz	R. m. t. ctx Occ. ctx.	[^{11}C]Flumazenil	55±12	12±2	5	[34]
		[^{11}C]Flumazenil	89	13.7	7	[94]
D_1	R. caudate	[^{11}C]SCH23390	45±12	22±8	2	[95]
D_2	Putamen	[^{11}C]Raclopride	14±2	3.8±0.6	4	[32]
	R. putamen Striatum	[^{11}C]Raclopride	28± 8	9±2	3	[96]
		[^{11}C]Raclopride	29±4	9±1	3	[97]
D_2	Thalamus	[^{11}C]FLB-457	2.3±0.6	0.7±0.3	3	[98]
Opiate	Thalamus	[^{11}C]Diprenorphine	19±2	0.7±0.2	25	[33]

[a]Rounded to nearest integer.

Author Manuscript Author Manuscript Author Manuscript Author Manuscript

Table 4

20 PET radioligands: peak brain uptakes in monkey and human, and some of their molecular properties.

Radioligand[a]	Structure	Target	Peak monkey brain uptake[b] [SUV]	Peak human brain uptake[b] [SUV]	MWt[c] [Da]	LogD[7.4d]	cLogP	N + O	HBDs[e]	HBAs[f]	PSA[g] [Å^2]	Most basic site[h] pK_a
[^{11}C](*R*)-PK11195	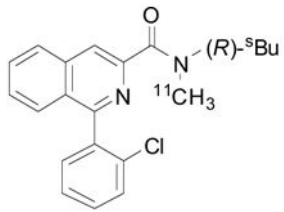	TSPO	1.6 [43]	1.6	353	3.97	4.89	3	0	3	33	3.53
[^{11}C]ER176	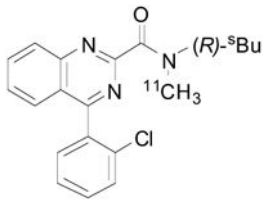	TSPO	2.0 [145]	2.3 [146]	353	3.55 [145]	3.80	4	0	1	45	0.2
[^{11}C]SD5024	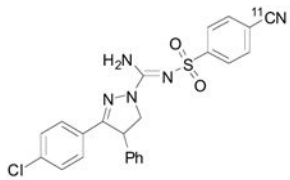	CB_1	2.0 [147]	2.3 [147]	463	3.79 [147]	3.50	7	1	2	112	4.98

Author Manuscript Author Manuscript Author Manuscript Author Manuscript

Radioligand[a]	Structure	Target	Peak monkey brain uptake[b] [SUV]	Peak human brain uptake[b] [SUV]	MWt[c] [Da]	LogD[7.4d]	cLogP	N + O	HBDs[e]	HBAs[f]	PSA[g] [Å^2]	Most basic site[h] pK_a
[^{11}C]IGA-1	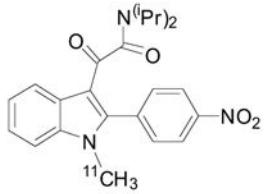	TSPO	2.3 [48]	n.d.	406		3.35	7	0	3	92	NA
[^{11}C]PBR28	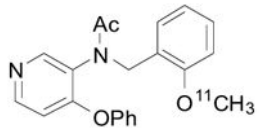	TSPO	2.8 [105, 148]	2.6 [80, 42, 149, 150]	348	3.01	2.56	5	0	5	51	6.58
[^{11}C]PBR01	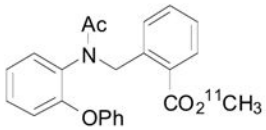	TSPO	3.0 [105, 151]	n.d.	374	3.90	3.05	4	0		56	4.4
[^{11}C]RX-1	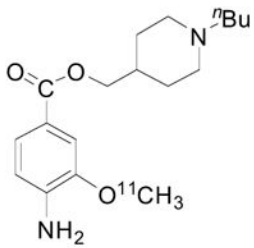	5-HT$_{1A}$	3.5 [152]	n.d.	321	1.77	2.36	5	1	3	65	8.47

Author Manuscript Author Manuscript Author Manuscript Author Manuscript

Radioligand[a]	Structure	Target	Peak monkey brain uptake[b] [SUV]	Peak human brain uptake[b] [SUV]	MWt[c] [Da]	LogD[7.4d]	cLogP	N + O	HBDs[e]	HBAs[f]	PSA[g] [Å^2]	Most basic site[h] pK_a
[^{18}F]FBR	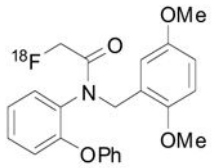	TSPO	3.7 [106]	1.3 [150, 153]	395	4.05	3.58	5	0	5	48	4.99
[^{11}C]RWAY	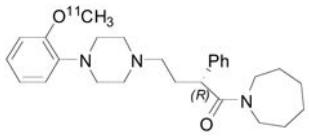	5-HT$_{1A}$	4.2 [127, 154, 155]	2.2 [156]	436	3.16	2.85	5	0	5	36	7.94
[^{11}C](*R*)-rolipram	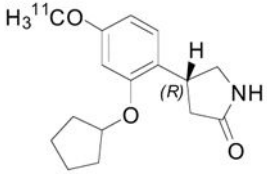	PDE4	4.3	2.3 [157, 158]	275	2.16	2.35	4	1	3	48	7.61
[^{18}F]RX-2	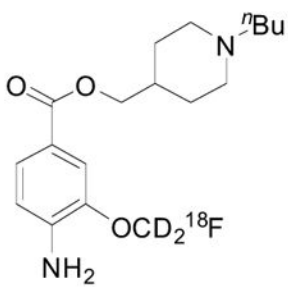	5-HT$_4$	4.31 [152]	n.d.	289	1.54 [152]	1.42	4	1	3	56	8.47

Author Manuscript Author Manuscript Author Manuscript Author Manuscript

Radioligand[a]	Structure	Target	Peak monkey brain uptake[b] [SUV]	Peak human brain uptake[b] [SUV]	MWt[c] [Da]	LogD[7.4d]	cLogP	N + O	HBDs[e]	HBAs[f]	PSA[g] [Å^2]	Most basic site[h] pK$_a$
[^{18}F]XB-1	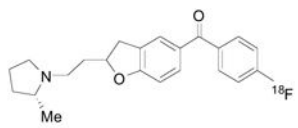	H_3	4.5 [159]	n.d.	351	2.95	4.34	3	0	3	30	9.29
[^{11}C]NOP-1A	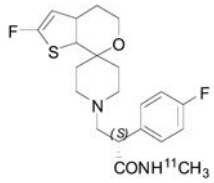	NOP	4.9 [160, 161]	6.2 [162, 163]	408	3.41	3.47	4	1	3	42	7.36
[^{18}F]FIMX	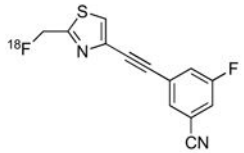	mGlu1	5.3 [107]	4.8	343	2.52 [107]	0.69	7	1	3	69	4.95
[^{18}F]FMPEP-d_2	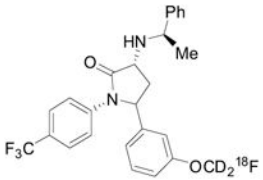	CB_1	5.5 [140]	4.8 [140]	473	4.24	4.99	4	1	3	42	6.86
[^{11}C]MePPEP	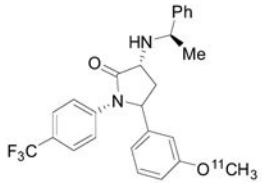	CB_1	6.0 [164]	4.0 [164]	455	4.80	4.87	4	1	3	42	6.86

Author Manuscript Author Manuscript Author Manuscript Author Manuscript

Radioligand[a]	Structure	Target	Peak monkey brain uptake[b] [SUV]	Peak human brain uptake[b] [SUV]	MWt[c] [Da]	LogD[7.4d]	cLogP	N + O	HBDs[e]	HBAs[f]	PSA[g] [Å^2]	Most basic site[h] pK_a
[^{11}C]CUMI-101	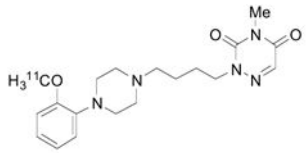	5-HT_{1A}	~ 6 [155]	N.A.	373	1.13	0.55	8	0	8	69	9.13
[^{18}F]SP203	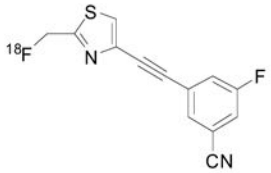	mGlu5	7.0 [165]	5.9 [166]	260	2.18	3.66	2	0	1	37	NA
[^{18}F]FECNT	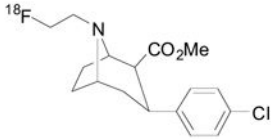	DAT	7.5 [167]	7.5 [167]	325	2.64	3.47	3	0	3	30	6.99
[^{18}F]Fallypride	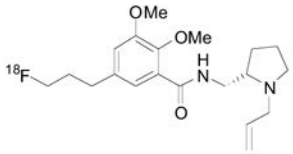	D_2	~ 8.0	~ 10	364		3.33	5	1	4	51	8.70
Criteria:												
[168]							> 1.5 & < 2.7					
[169]					< 450						< 90	
[170]					≤ 400		< 5		≤ 3	≤ 7		
[171]											< 70	

Author Manuscript Author Manuscript Author Manuscript Author Manuscript

Radioligand[a]	Structure	Target	Peak monkey brain uptake[b] [SUV]	Peak human brain uptake[b] [SUV]	MWt[c] [Da]	LogD[7.4d]	cLogP	N + O	HBDs[e]	HBAs[f]	PSA[g] [Å^2]	Most basic site[h] pK_a
[172]								≤ 5				
[172]								> log*P*				
[173]					< 500	2–5	2–5		< 3		< 90	
[174]					< 400		< 4.0					
(MDR + LDR) (I) [175]					< 351	< 2.8	< 4.0		< 2		32–86	< 9.5

[a]Listed in ascending order of peak brain uptake in monkey. Unreferenced values are from the author's laboratory.

[b]Weighted mean of reported values, or of reported range for reported region of highest uptake. Unreferenced values are from the author's laboratory.

[c]For non-labeled compound.

[d]From reference [176], unless otherwise indicated.

[e]Counted as hetero atoms having a lone electron pair.

[f]Counted as electronegative atoms bonded to H.

[g]From ChemDraw.

[h]From Pallas software.

Author Manuscript Author Manuscript Author Manuscript Author Manuscript

Table 5

Reports of P-gp transporter sensitivity for some PET radioligands across species, based on *in vitro* assays and on *in vivo*, mainly PET, studies.

Radioligand	Imaging target	*In vivo* species	*In vitro* species	Substrate (Yes/No)	Reference
[^{11}C]Carazolol	β-AR	M (g)		Yes	[191]
[^{11}C]Carazolol	β-AR	R (pc)		Yes	[191]
[^{18}F]S-1′-fluorocarazolol	β-AR	M (g)		Yes	[191]
[^{18}F]S-1′-fluorocarazolol	β-AR	R (pc)		Yes	[191]
[^{18}F]FCWAY	5-HT$_{1A}$		H (c)	Yes	[192]
[^{18}F]FCWAY	5-HT$_{1A}$	H (pt)		Yes	[192]
[^{18}F]MPPF	5-HT$_{1A}$	M (g)		Yes	[193]
[^{18}F]MPPF	5-HT$_{1A}$	M (g)		Yes	[194]
[^{18}F]MPPF	5-HT$_{1A}$	M (p)		Yes	[194]
[^{18}F]MPPF	5-HT$_{1A}$	R		Yes	[195]
[^{18}F]MPPF	5-HT$_{1A}$	R (pc)		Yes	[193]
[^{18}F]MPPF	5-HT$_{1A}$	R (pc)		Yes	[196]
[^{18}F]MPPF	5-HT$_{1A}$	NHP (pc)		No	[194]
[^{18}F]MPPF	5-HT$_{1A}$		H (c)	No	[197]
[^{11}C]RWAY	5-HT$_{1A}$	M		Yes	[198]
[^{11}C]RWAY	5-HT$_{1A}$	R		Yes	[198]
[^{11}C]RWAY	5-HT$_{2A}$	NHP		No	[154]
[^{11}C]WAY	5-HT$_{1A}$	R (pc)		Yes	[193]
[^{11}C]WAY	5-HT$_{1A}$		H (c)	No	[197]
[^{18}F]Altanserin	5-HT$_{2A}$	R (pc)		Yes	[190]
[^{18}F]Altanserin	5-HT$_{2A}$	R (pc)		Yes	[199]
[^{18}F]Altanserin	5-HT$_{2A}$	GP (pc)		Yes	[190]
[^{18}F]Altanserin	5-HT$_{2A}$	MP (pc)		Yes	[190]
[^{18}F]Altanserin	5-HT$_{2A}$	NHP (pc)		Yes	[190]
[^{18}F]MH-MZ	5-HT$_{2A}$	M (pc)		Yes	[200]

Author Manuscript Author Manuscript Author Manuscript Author Manuscript

Radioligand	Imaging target	*In vivo* species	*In vitro* species	Substrate (Yes/No)	Reference
[^{11}C]PIB	A_β	M (pc)		No	[201]
[^{11}C]PIB	A_β		H (c)	No	[197]
[^{11}C]Flumazenil	Bz	R (pt)		Yes	[202]
[^{11}C]Flumazenil	Bz	M (pc)		Yes	[201]
[^{11}C]Flumazenil	Bz		H (c)	No	[197]
[^{11}C]MePPEP	CB_1	M (g)		No	[203]
[^{11}C]MePPEP	CB_1	NHP (pd)		No	[164]
[^{18}F]Fallypride	D_2/D_3	M (pc)		Yes	[204]
[^{18}F]Fallypride	D_2/D_3	M (g)		Yes	[204]
[^{18}F]Fallypride	D_2/D_3	R (pc)		Yes	[204]
[^{18}F]Fallypride	D_2/D_3		H (c)	No	[197]
[^{11}C]Raclopride	D_2/D_3	M (pc)		No	[201]
[^{11}C]Raclopride	D_2/D_3		H (c)	No	[197]
[^{11}C]Befloxatone	MAO-A	R (c)		No	[205]
[^{11}C]Befloxatone	MAO-A		H (c)	No	[197]
[^{11}C]GR205171	NK_1	M (g)		Yes	[206]
[^{11}C]GR205171	NK_1	R (pc)		Yes	[190]
[^{11}C]GR205171	NK_1	GP (pc)		Yes	[190]
[^{11}C]GR205171	NK_1	NHP (pc)		Yes	[190]
[^{11}C]PK11195	TSPO	M (pc)		No	[201]
[^{11}C]PK11195	TSPO		H (c)	No	[197]

M = Mouse, R = Rat, GP = Guinea pig; MP = mini-pig; NHP = non-human primate; H = Human, c = cell-based assay; g = efflux transporter knockout; pc = pharmacological block of efflux transporter with cyclosporin A; pd = pharmacological block of efflux transporter with DCPQ; pt = pharmacological block of efflux transporter with tariquidar.

Author Manuscript Author Manuscript Author Manuscript Author Manuscript

Table 6

Reports of BCRP transporter sensitivity for some PET radioligands in various species, based on *in vitro* assays and on *in vivo,* mainly PET, studies.

Radioligand	Imaging target	*In vivo* species	*In vitro* species	Substrate (Yes/No)	Reference
[^{18}F]MPPF	5-HT_{1A}	M (g)		No	[194]
[^{18}F]MPPF	5-HT_{1A}		H (c)	No	[197]
[^{11}C]WAY	5-HT_{1A}		H (c)	No	[197]
[^{11}C]PIB	A_{β}		H (c)	No	[197]
[^{11}C]Flumazenil	Bz		H (c)	No	[197]
[^{18}F]Fallypride	D_2/D_3		H (c)	No	[197]
[^{11}C]Raclopride	D_2/D_3		H (c)	No	[197]
[^{11}C]Befloxatone	MAO-A	R (g)		No	[205]
[^{11}C]Befloxatone	MAO-A		H (c)	Yes	[197]
[^{11}C]PK11195	TSPO		H (c)	No	[197]

M = Mouse, R = Rat; H = Human.

c = cell-based assay; g = efflux transporter knockout.

Author Manuscript Author Manuscript Author Manuscript Author Manuscript

Table 7

Examples of labeled sub-structures found in ^{18}F-Labeled PET radioligands studied in humans, and whether noted to be susceptible to radiodefluorination.

Entry	Labeled sub-structure	Radioligand examples	Noted defluorination susceptibility	References
1	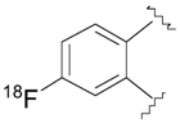	[^{18}F]Flumazenil	No	[239]
2	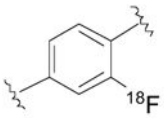	[^{18}F]Flumetamol	No	[247]
3	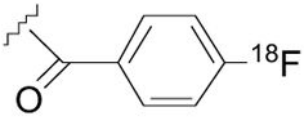	p-[^{18}F]MPPF	No	[248]
4		[^{18}F]FIMX	No	[228]
5		[^{18}F]Altanserin	No	[249]
6	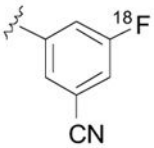	[^{18}F]FPEB	No	[250]
7	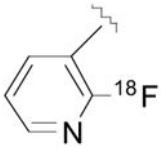	2-[^{18}F]F-A85380	No	[251] [252]
8		[^{18}F]MK-6577	No, but some skull radioactivity uptake	[253]
9	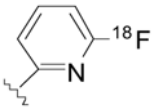	[^{18}F]AZAN	No	[254]
10	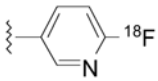	[^{18}F]T807	Negligible	[255]
11		[^{18}F](-)-Flubatine	Negligible	[256]
12		6-[^{18}F]F-A85380	No	[257]
13	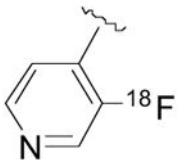	[^{18}F]UCB-H	No	[258]

Author Manuscript Author Manuscript Author Manuscript Author Manuscript

Entry	Labeled sub-structure	Radioligand examples	Noted defluorination susceptibility	References
14	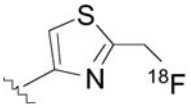	[^{18}F]SP203	Low, but radioactivity uptake in red marrow	[259]
15	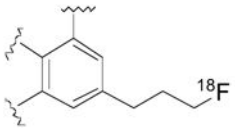	[^{18}F]Fallypride	No	[260]
16	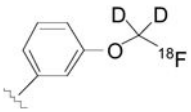	[^{18}F]FMPEP-d_2	Yes	[140]
17	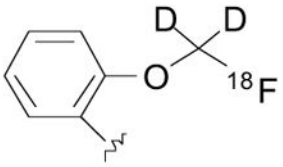	[^{18}F]FMENER-d_2	Yes	[261]
18	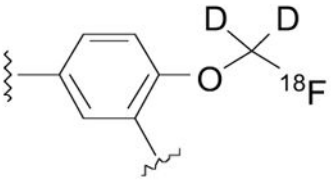	[^{18}F]SPA-RQ	Low, but some radioactivity uptake in red marrow	[262]
19	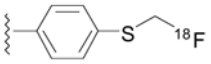	[^{18}F]Fluoromethyl-McN5652	No	[263]
20	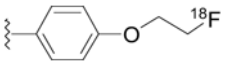	[^{18}F]DPA-714	No but some skull radioactivity uptake - presumed to be in marrow	[264]
21		[^{18}F]MNI-659	No but some skull radioactivity uptake - presumed to be in marrow	[265]
22		[^{18}F]MNI-444	No, but low skull radioactivity uptake	[266]
23		[^{18}F]MK-9470	No	[267]
24	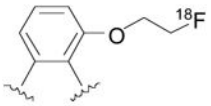	[^{18}F]FEOBV	No	[268]

Author Manuscript Author Manuscript Author Manuscript Author Manuscript

Entry	Labeled sub-structure	Radioligand examples	Noted defluorination susceptibility	References
25	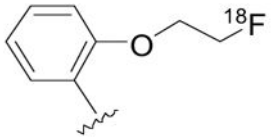	[^{18}F]FEPPA	No	[269]
26	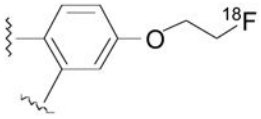	[^{18}F]THK-523	No, but low radioactivity uptake in skull	[270]
27	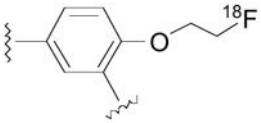	[^{18}F]FESPA-RQ	Yes, but low	[271]
28		[^{18}F]FEDAA1106	No	[272]
29	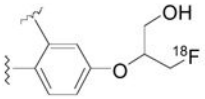	[^{18}F]FACT	No, but low radioactivity uptake in skull	[273]
30	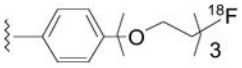	[^{18}F]AV45	No	[274]
31	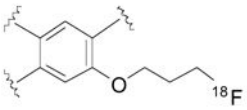	[^{18}F]FP-(+)-DTBZ ([^{18}F]AV-133)	No	[275]
32	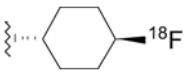	*Trans*-[^{18}F]FCWAY	Yes	[276]
33	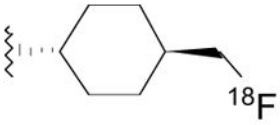	[^{18}F]Mefway	No	[277]
34	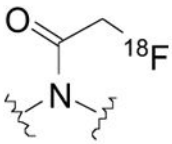	[^{18}F]FBR	Negligible	[278]

Author Manuscript

Entry	Labeled sub-structure	Radioligand examples	Noted defluorination susceptibility	References
35	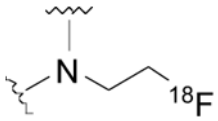	[^{18}F]FECNT	No	[167] [279]
36		[^{18}F]JNJ42259152	No	[280]
37	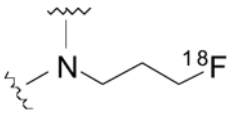	[^{18}F]CPFPX	No	[281]
38		[^{18}F]FPCIT	No	[282]
39	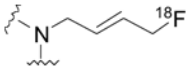	[^{18}F]LBT-999	Yes	[283]